ANUL XLII **1997**

S T U D I A
UNIVERSITATIS BABEŞ-BOLYAI

PHYSICA

1

Editorial Office: 3400 CLUJ-NAPOCA, Gh. Bilaşcu no.24 ♦ Tel. 194315; int. 167

S U M A R - C O N T E N T S - S O M M A I R E

Solid State Physics

Spectroscopy

Theoretical Physics

Physics Education

STUDIA UNIVERSITATIS BABEŞ-BOLYAI, PHYSICA, XLII, 1, 1997

EPR STUDY ON RADIOTHERAPEUTIC GLASSES

S. SIMON[1], I. ARDELEAN[1], D. ENIU[2], V. SIMON[1]

ABSTRACT. Rare-earth aluminium-silicate glasses of $20M_2O_3 \cdot 20Al_2O_3 \cdot 60SiO_2$, (M = Y, Dy) systems were prepared by melts undercooling and activated by neutron irradiation. Besides Y-90 and Dy-165 respectively, no other radioisotopes were induced. The specific gamma activity of yttrium containing sample is about 2.5 times higher than that of dysprosium containing sample. In order to obtain more information about the neighbourhood of the induced radionuclides, important aspect concerning the glass stability in biological environments, the dysprosium sample $20(Dy/Gd)_2O_3 \cdot 20Al_2O_3 \cdot 60SiO_2$ was structural investigated by electron paramagnetic resonance (EPR) of Gd^{3+} ions substituting up to 5 % the dysprosium ions. The sites occupied by rare earth elements are subjected to crystalline fields of strength depending on the heat treatment conditions.

INTRODUCTION

Radiotherapy glasses are radioactive glasses used for in situ beta or gamma irradiation. Aluminium-silicate glasses containing rare earth (RE) cations as Y, Sm, Ho and Dy have the advantage that by neutron activation radioisotopes such as Y-90, Sm-153, Ho-166, Dy-165 can be obtained [1]. The relatively short half lives of these isotopes are important parameters for real time medical treatment. For example, since Y-90 has a half life of 64.1 hours, the radioactivity decays to a negligible level in about 21 days [2, 3]. The rare earth aluminium-silicate glasses are currently being evaluated for applications such as the irradiation of deseased kidneys prior to surgical removal, radiation

[1] Faculty of Physics, Babeş-Bolyai University, 3400 Cluj-Napoca, Romania.
[2] Faculty of Pharmacy, University of Medicine and Pharmacy, 3400 Cluj - Napoca, Romania

synovectomy of arthritic joints and irradiation of malignant tumours in the liver [4].

This study aims to investigate two vitreous aluminium-silicate systems containing yttrium and dysprosium as rare earth elements that may be activated by neutron irradiation to become radioactive with possible applications as radiotherapeutic glasses.

EXPERIMENTAL

The investigated glass systems $20M_2O_3$ $20Al_2O_3 \cdot 60SiO_2$ where M = Y or Dy (mol %) were obtained from component oxides of reagent grade purity, mixed in corresponding proportions for the desired compositions. The homogenised mixtures introduced in sintered corundum crucibles were successively heat treated in an electric furnace for 5 hours at 1200^{o}C and at 1300^{o}C. In order to obtain vitreous samples the reground mixtures were melted at 1400^{o}C for 15 minutes and quickly undercooled by pouring on stainless steal plates at the room temperature. The recrystallisation heat treatment was performed in the same electric furnace at 1200^{o}C for 5 hours.

The samples were irradiated for 83 days using an activation equipment with two isotopic sources Am-Be and Pu-Be providing a total flux of $6 \cdot 10^7$ neutrons/sec. The radioisotopes induced by neutron activation in the irradiated samples were identified by means of a high resolution Ge-Li gamma spectrometer. The specific gamma activity measurements were carried out on a 20160- RFT monochanel analyser equipped with a VA-S-968 scintillation detector and 51021-RFT counter. The analyser with Tl doped NaI crystal worked in integral regime at a cut voltage of 1.1 V. The photomultiplier voltage was of 760 V.

The electron paramagnetic resonance (EPR) spectra were recorded on powder samples, at room temperature, by using a JEOL-type spectrometer in the X frequency band, with 100 KHz field modulation.

RESULTS AND DISCUSSION

The gamma spectra evidenced that in the neutron activated samples $20M_2O_3 \cdot 20Al_2O_3 \cdot 60SiO_2$, (M=Y,Dy) were induced as radionuclides only Y-90 and Dy-165 respectively. No other peaks arising from possible, undesired, impurities were put into evidence in the gamma spectra of the investigated samples.

The specific gamma activities are around 20 Bq/g for the glass containing Y_2O_3 and around 50 Bq/g for that containing Dy_2O_3.

Despite the fact that after neutron activation resonance signals arising from defects induced by irradiation were expected, the EPR spectra recorded from these samples do not evidence any lines arising from irradiation defects. The absence of such signals denotes that the irradiation defects even if they are induced, are characterised, at the room temperature, by very short life times. In order to characterise by EPR the structural changes after different heat treatment procedures, a part of dysprosium ions (under 5 %) was substituted by gadolinium. This replacement was decided having in view that in this low concentration it is very probable that the substituent atoms will enter in the sites of substituted atoms. On the other hand the Gd^{3+} ions as resonant center offer by EPR technique useful information about the neighbourhood around the sites occupied by the rare earth elements in the host matrices. The structural stability of the radioisotopes in glass matrices can be correlated with the local symmetry around rare earth ions.

The structural changes in the local order were determined by sample heat treatment at different temperatures, for different times. The EPR data obtained from these samples depend on the applied heat treatments. Figure 1 shows the resonance spectra recorded from samples having the same composition but which were subjected to different heat treatments. After a 5 hours heat treatment at 1200^{o}C (Fig. 1a) the spectrum is typical of gadolinium ions disposed in sites of week crystalline field in polycrystalline systems [5]. By applying a new heat treatment at a higher temperature (1300^{o}C) the Gd^{3+} EPR spectrum

reveals the U type spectrum features, consisting of resonance lines with $g \approx 2.0$, $g \approx 2.8$ and $g \approx 6.0$ specific to the vitreous systems [6, 7]. One remarks that elements characteristic to the polycrystalline materials are further maintained (Fig. 1b).

This suggests that only a fraction of Gd^{3+} ions are disposed in sites with relatively distorted vicinity. The Gd^3 EPR spectrum after melting heat treatment (Fig. 1) is predominated by the U type spectrum accompanied by features specific to the polycrystalline systems and a superposed narrow line at low magnetic fields, with $g \approx 20$. We also remark the appearance of the line with $g \approx 4.8$ assigned to the Gd^{3+} ions with a lower coordination than six, usually four. In the oxide systems, in general, and particularly in the vitreous matrices the number of the gadolinium ions disposed in sites of tetrahedral symmetries is extremely low. On the other hand the gadolinium ions prefer coordinations higher than six and this is in deed the typical behaviour of all rare earth elements [8]. The presence of the line with $g \approx 4.8$ is better evidenced in the EPR spectrum of the partially recrystallised samples (Fig. 1d) showing that by heat treatment the host matrix imposes for a high fraction of gadolinium ions low coordinated environments. This result supports the assumption that a part of the Gd^{3+} ions occupy in the investigated samples the silicon sites specific of the aluminium-silicate systems, because in these systems the silicon atoms are preponderantly tetracoordinated [9]. This low coordinated gadolinium ions are from structural point of view more unstable than the higher coordinated species, so in biological environment they will be easier solved. The radiotherapeutic glasses must be stable so long their activity decreases at a negligible level. It would be also desirable their dissolution and elimination at the end of the therapy.

The above presented EPR data show that the radioisotope coordination and therefore the stability of rare earth aluminium-silicate glasses can be controlled by partial devitrification heat treatment.

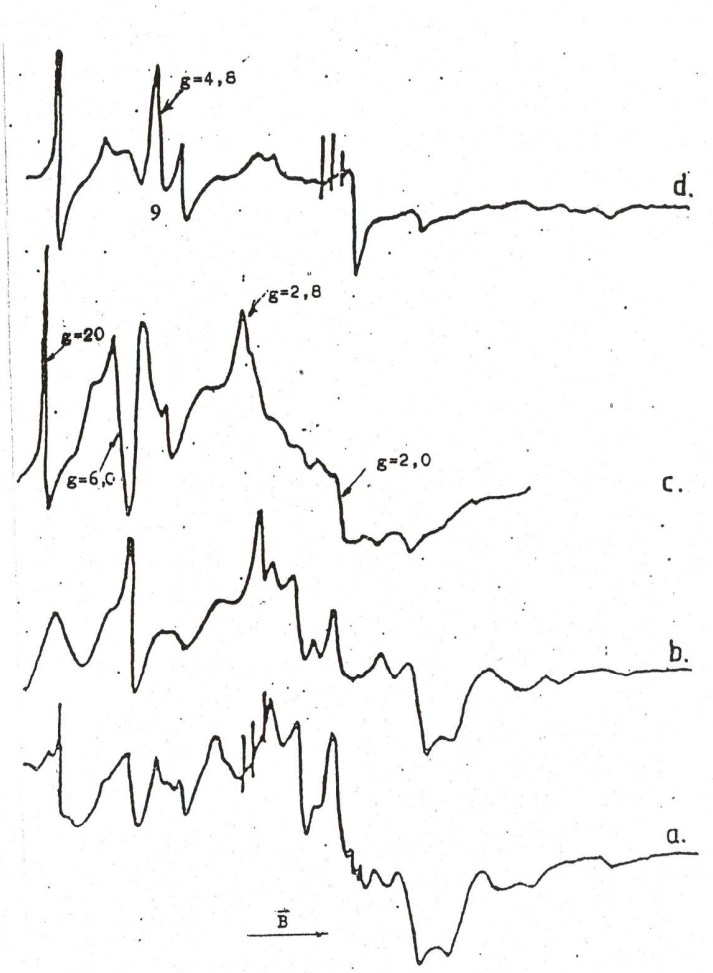

Fig. 1. Gd^{3+} EPR spectra of $20(Dy/Gd)_2O_3 \cdot 20Al_2O_3 \cdot 60SiO_2$ system

a) heat treated at 1200^0C for 5 hours;
b) heat treated at 1300^0C for 5 hours;
c) quenched after melting at 1400^0C for 15 minutes;
d) partially crystallised by heat treatment at 1300^0C for 5 hours after (c) procedure.

CONCLUSIONS

The results of this study indicate that the applied neutron irradiation treatment leads to the activation of the rare earth elements contained in the glass samples and of no other undesired radioisotopes. The gamma activity arising from the sample containing dysprosium is about 2.5 times higher than that arising from the sample containing yttrium. The absence of radiation defects in the neutron activated glasses show a continuous glass network in these samples that is an important aspect for their stability in biological environments. The EPR data indicate that the sites occupied by the rare earth elements in this aluminium-silicate glass matrix are subjected to crystalline fields of strength depending on the heat treatment conditions. The increasing effect of devitrification heat treatment on low coordinated gadolinium ions fraction, more unstable species in biological environments, show the way to assure the stability of these rare earth aluminium-silicate glasses in human body only during the radiotherapy time.

REFERENCES

1. D.E.Day, Th.E.Day, in *An Introduction to Bioceramics*, eds. L. L.Hench & J. Wilson, World Scientific, 1991, p. 305.
2. G.J.Ehrhardt, D.E.Day, *Nucl. Med. Biol*. Int. J. Radiat. Appl. Instr. B, 14, 3, 233 (1987).
3. M.J.Hyatt, D.E.Day, *J. Am. Ceram. Soc*., 70, 10, C-283 (1987).
4. S.Houle, T.K.Yip, F.Shephered, *Radiology*, 172, 2, 857 (1989).
5. K.Koto, H.Mori, Y. Ito, *Solid State Ionics*, 18-19, 700 (1986).
6. D.L.Griscom, J. *Non-Cryst. Solids*, 40, 211 (1980).
7. I.E.Iton, C.M.Brodbeck, S.I.Saib, G.D.Stucky, *J. Chem. Phys*., 79, 185 (1983).
8. I.Ardelean, E.Burzo, D.Mitulescu-Ungur, S.Simon, J. *Non-Cryst. Solids*, 146, 256 (1992).
9. H.Kawazoe, *Annual Reports on NMR Spectroscopy*, 28, 1 (1994).

STUDIA UNIVERSITATIS BABEŞ-BOLYAI, PHYSICA, XLII, 1, 1997

MATRIX EFFECT ON OPTICAL ABSORPTION OF OXIDE GLASSES CONTAINING URANIUM

V. ŞIMON[1], M. TODICA[1], I. ARDELEAN[1], V. MIH[1], S. ŞIMON[1]

ABSTRACT. Four oxide glass systems xUO_3 (100-x) $[2P_2O_5 \cdot Na_2O]$, xUO_3 (100-x) $[2P_2O_5 \cdot PbO]$, xUO_3 (100-x) $[3B_2O_3 \cdot PbO]$ and xUO_3 (100-x) $[3B_2O_3 \cdot SrO]$ were investigated by optical absorption spectroscopy in the UV-VIS range in order to evidence the glass matrix effect on the uranium incorporated in these glasses. The absorption bands centered at 18400 cm^{-1}, 20400 cm^{-1} and 23100 cm^{-1} are observed in both phosphate systems. The absorption bands at 16000 cm^{-1} and 22000 cm^{-1} occur only for uranium ions introduced in the lead-phosphate matrix, while the absorption band centered at 15750 cm^{-1} is recorded only from samples of soda-phosphate matrix. The main absorption bands in the borate systems occur around 15800 cm^{-1} and 23000 cm^{-1}.These results indicate that the phosphate matrices favourise the (3+), (4+) and (6+) valence states of uranium, with the preponderance of U^{4+} ions, while in the borate matrices only (3+) and (6+) states are evidenced and the U^{6+} ions dominates.

INTRODUCTION

In the past decades extensive researches were devoted to glass composition under consideration for use as hosts in the immobilsation of nuclear waste [1-5]. Particular interest is accorded to uranium wastes. The uranium is a multivalent element and its valence state can be influenced by the host material wherein is incorporated. In order to assure a high stability of radionuclides the nuclear waste is disposed in multicomponent glasses [5, 6, 13]. In such systems the phase

[1] Faculty of Physics, Babeş-Bolyai University, 3400 Cluj-Napoca, Romania.

separation is a common phenomenon that implies the appearance of boron poor and rich phases [8]. This is the reason to take into account also borate glasses despite the fact that in the borate glass matrices the most part of uranium ions appear in the (3+) and (6+) valence states. The solubility and stability of the uranium ions in oxide glass matrices also depend on the uranium valence states. On the other hand the presence of particular valence states of multivalent elements in glasses control important physical properties of glasses. Glass properties can be attributed to the occurrence of certain valence states that play a major role due to the applicability of these properties to fields as nuclear waste immobilisation, slag recycling and materials science [9].

Most multivalent elements of the actinide class (U, Pu, Np and other) dissolved in glass posses characteristic absorption spectra in the near-ultraviolet, visible and near-infrared regions. The origin of these electronic spectral bands is the d and f electron energy level splittings of an ion in a particular physical environment. The absorption bands for each ion are characteristic in terms of number, position, shape and intensity. The positions and shapes of the absorptions can be correlated to the ionic state and its local electronic environment (ligand and coordination site), whereas the intensities of the absorptions can be correlated to the concentration of that ion in the glass structure.

In order to establish the influence of the glass matrix on the valence states of the uranium ions and on the relative number of the identified uranium ions in different valence states we carried out an optical absorption study in the UV-VIS range on four glass matrices.

EXPERIMENTAL

The investigated samples are phosphate and borate glasses belonging to the systems $xUO_3(100-x)[2P_2O_5 \cdot M_xO_y]$, where M = Na, Pb and $xUO_3(100-x)[3B_2O_3 \cdot MO]$ where M = Pb, Sr. The samples were prepared from chemical pure compounds UO_3, $(NH_4)_2HPO_4$, $Na_2CO_3 \cdot 10H_2O$, PbO, H_3BO_3 and $SrCO_3$ mixed in suitable amounts according to the desired compositions. Glasses were melted in an electric furnace with superkanthal bars, in sintered corundum crucibles directly introduced into the furnace at 1250^oC and maintained at this temperature for 10 minutes. The melts were vitrified by fast undercooling at room temperature, by pouring onto stainless steel plates. The

composition range of the prepared glasses corresponds to $0 \leq x \leq 20$ mol % UO_3.

Optical absorption spectra were recorded at room temperature on a Specord UV-VIS spectrometer from thin plate samples in the wave number range 13000-30000 cm^{-1}.

RESULTS AND DISCUSSION

The investigated glass matrices $2P_2O_5 \cdot Na_2O$, $2P_2O_5 \cdot PbO$, $3B_2O_3 \cdot PbO$ and $3B_2O_3 \cdot SrO$ evidence no absorption line in the UV-VIS range. By introducing uranium the samples give rise to absorption spectra that consist of band arising from uranium ions in different valence states. All samples containing uranium ions are lightly coloured, the phosphate samples in green and the borate ones in yellow-brown. The green colour is associated to U^{4+} ions, the yellow colour to U^{6+} ions, while red colour is typical for U^{3+} ions. The U^{5+} ions have no absorption in this spectroscopic range [10].

Figure 1 illustrates the absorption spectra recorded from glass samples containing the same amount of uranium in glass matrices with different components. Absorption bands centered at 18000 cm^{-1}, 20400 cm^{-1} and 23100 cm^{-1} occur in both phosphate systems. The 15750 cm^{-1} band appears only in the soda-phosphate glasses while the bands centered around 16000 cm^{-1} and 22000 cm^{-1} are recorded only from lead-phosphate glasses. The optical absorption spectra obtained from borate glasses consist of three absorption bands around 13800 cm^{-1}, 15800 cm^{-1} and 23000 cm^{-1} for the lead containing system and only of two bands around 15800 cm^{-1} and 23000 cm^{-1} for the strontium-borate system.

In oxide glasses the uranium ions generally may appear in valence states between (3+) and (6+). The valence state (4+) is preferred when the immobilisation of radionuclides is the desired application, because this is the best stabilised state in oxide glasses [9]. According to the attribution of the optical absorption bands to different valence states of uranium ions one remarks that the glass matrix influence the uranium valence states in samples prepared in the same conditions.

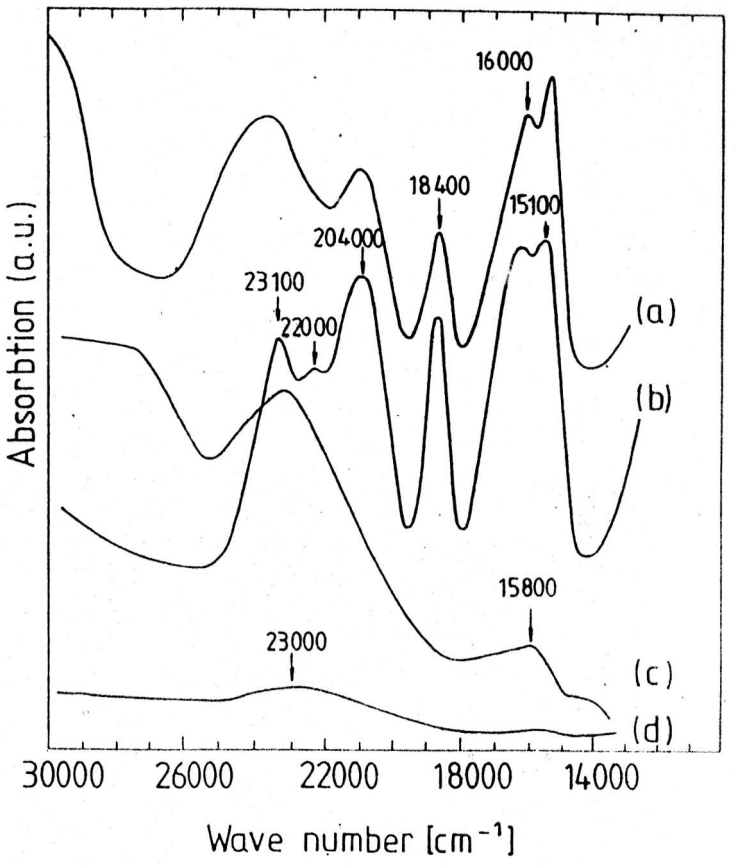

Fig.1. The optical absorption spectra of glass samples containing 10 mol% UO_3 in (a) $2P_2O_5 \cdot Na_2O$, (b) $2P_2O_5 \cdot PbO$, (c) $3B_2O_3 \cdot PbO$ and (d) $3B_2O_3 \cdot SrO$ matrices.

In the phosphate glasses are evidenced uranium ions in (3+), (4+) and (6+) valence states while in the borate glasses only (3+) and (4+) valence states are evidenced. The preponderance of U^{4+} ions in the phosphate matrices and of U^{6+} ions in the borate matrices is also supported by their color [10-12]. Considering the number of the ions in different valence states proportional to the intensity of the corresponding

absorption bands obtained for samples with $5 \leq x \leq 20$ mol % one remarks that the number of U^{4+} ions is about seven times higher than that of U^{3+} ions and nine times higher than that of U^{6+} ions in $xUO_3(100-x)[2P_2O_5 \cdot PbO]$ glasses, whereas in $xUO_3(100-x)[2P_2O_5 \cdot Na_2O]$ glasses both these fractions (U^{4+}/ U^{6+} and U^{4+}/ U^{3+}) are close to 3 [7]. As mentioned, in the borate samples investigated in this study, only U^{3+} and U^{6+} ions are evidenced. The number of U^{6+} ions in comparison with that of U^{3+} ions is approximately four times higher in $xUO_3(100-x)[3B_2O_3 \cdot PbO]$ glasses and two times higher in the in $xUO_3(100-x)[3B_2O_3 \cdot SrO]$ glasses.

CONCLUSIONS

The four glass matrices differently influence the uranium by structural effects, so that the absorption bands are not identical for glass samples containing the same uranium content.

Absorption bands centered at 18400 cm^{-1}, 20400 cm^{-1} and 23100 cm^{-1} are observed in both phosphate systems, absorption bands at 16000 cm^{-1} and 22000 cm^{-1} occur only from lead-phosphate glasses, while the absorption band centered at 15750 cm^{-1} is recorded only from soda-phosphate samples. Two absorption bands at 15800 cm^{-1} and 23000 cm^{-1} are developed both in lead- and in strontium-borate glasses. Only for the strontium-borate system occurs a week absorption band around 13800 cm^{-1}.

The position and intensity of the optical absorption bands in the UV-VIS range indicate the preponderance of U^{4+} ions relative to U^{3+} and U^{6+} ones in the phosphate matrices and of U^{6+} ions relative to U^{3+} ions in the borate matrices. The U^{5+} ions are not excluded from these glasses due to the fact that even if they are present they do not process any absorption bands in the investigated frequency range.

REFERENCES

1. X.Feng, *Mat. Res. Soc. Symp. Proc*., 333, 55 (1994).
2. L.A.Chik, R.O.Lokken, D.M.Strachan, W.M.Bowen, *J. Am. Ceram. Soc.* 69, 114 (1986).
3. P.J.Hayward, F.E.Doern, E.V.Cecchetto, S.L.Mitchell, *Canadian Mineralogist* 21, 611 (1983).
4. H.D.Schreiber, S.J.Kozak, D.G.Wetmore, C.W.Schreiber, J.S.Downey, *Ceramic Trans*. 3, 581 (1988).
5. P.J.Hayward, *Radioactive Waste Forms for the Future*, eds. W Lutze and R.C.Ewing Elserver Science, 1988, p. 427.
6. H.D.Schreiber, G.B.Balazs, T.N.Solberg, *Phys. Chem. Glasses*, 26, 35 (1985).
7. V.Şimon, I.Ardelean, D.Maniu, V.Mih, D.Eniu, S.Şimon, *Studia Univ. Babeş-Bolyai*, Physica, 1, 35 (1996).
8. W.Vogel, J*. Non-Cryst. Solids*, 25, 171 (1977).
9. H.D.Schreiber, *Advances in Materials Characterization*, eds. D. R. Rossington, R. A. Condrate, L. R. Snyder, Plenum, New York, 1983, p.647.
10. H.D.Schreiber and G.B.Balasz, *Phys. Chem. Glasses* 23, 139 (1982).
11. V.Şimon, I.Ardelean, O.Cozar, S.Şimon, J*. Mat. Sci. Lett*. 15, 734 (1996).
12. V.Şimon, I.Ardelean, O.Cozar, S.Şimon, *J.Nucl.Mat*. 230, 306 (1996).
13. W.L.Ebert, J.J.Mazer, *Mater. Res. Soc. Symp. Proc*., vol. 333 (Material Research Society, 1994).

STUDIA UNIVERSITATIS BABEŞ-BOLYAI, PHYSICA, XLII, 1, 1997

THERMAL PROPERTIES OF NiFe2-xAlxO4 SYSTEM

Á. NÉDA[1], ZS. SÁRKÖZI[1]

ABSTRACT. The magnetic phase transition in the NiFe2-xAlxO4 system was studied trough measurements of thermal diffusivity and thermal conductibility in the range of temperature 100 - 600K. It was proved that the temperature dependence of the thermal diffusivity is adequate to point out the phase transition.

INTRODUCTION

The NiFe2-xAlxO4 system was studied earlier in detail from electrical and magnetical point of view [1], but thermal measurements was not performed until now.

The present study of NiFe2-xAlxO4 ferrites discusses the thermal properties (thermal diffusivity, thermal conductivity and specific heat) of the system.

It is shown in reference [2] that the temperature-dependence of the thermal diffusivity and thermal conductivity gives also information about the phase-transition temperature.

The aim of this study is to prouve by thermal measurements the existence of magnetic phase transition and also to make clear the thermal conductivity mechanismus.

EXPERIMENTAL

The samples were sinterized using oxides of p. a. purity. A series of samples was prepared with the concentrations x = 2 (I), x = 1. 4 (IV), x = 1. 2 (V), x = 1. 1 (VI), x = 1. 0 (VII). Thermal diffusivity was determined by the optical impulse method [3], specific heat was measured using the method of adiabatic calorimeter [4].

RESULTS AND DISCUSSION

Fig. 1 shows an 1/T dependence of the thermal diffusivity in case of different samples (VII, VI, V). It results that one can distinguish three different domains for samples with reduced concentration of the Al 3+ ion (VII, VI, V) and only two different domains in case of greater concentration of the above-mentioned ion (Fig. 2 - sample I). These

[1] Babeş-Bolyai University, Faculty of Physics, 3400 Cluj-Napoca, Romania.

domains are characterised by linear variation, while at certain temperature a modification in the slope appears. After Peirels [5], these modifications occur at the Debye temperature, respectively at those temperatures at which the phonon scattering mechanisms modify. According to this theory, thermal diffusivity is described as follows:

$$\lambda = \frac{1}{3}\bar{l}\nu c, \tag{1}$$

where $\bar{l}$ is the mean free path for phonons, ν - the group velocity for phonons, c - the specific heat. The value of $\bar{l}$ is given by different scattering mechanisms, like: the triphononic "u" processes ($\bar{l}_{ff}$), the scattering on defects ($\bar{l}_{fd}$), on electrons ($\bar{l}_{fe}$) and - in case of magnetically ordered materials - on magnons ($\bar{l}_{fm}$). Thus the resulting mean free path is:

$$\frac{1}{\bar{l}} = \frac{1}{\bar{l}_{ff}} + \frac{1}{\bar{l}_{fd}} + \frac{1}{\bar{l}_{fm}} + \frac{1}{\bar{l}_{fe}}. \tag{2}$$

The $\bar{l}_{fd}$ can be considered invariant in the range of high temperatures. Below the high temperature range $\bar{l}_{ff}$ varies like 1/T, while for a low concentration of electrons $\bar{l}_{fe}$ remains constant in a wide temperature range.

It results that the temperature dependence of the mean free path is determined in fact by two phenomena: the triphononic "u" scattering process and phonon - magnon scattering. With regard to the mean free path given by this last mechanism, its variation follows the relation:

$$\bar{l}_{fm} = \bar{l}_0\left(1 - \frac{M(T)}{M(0)}\right)^{-1}, \tag{3}$$

where: M(T) - the magnetisation at temperature T, M(0) - the magnetisation at the perfectly ordered state, $\bar{l}_0$ - the mean free path at the phase transition temperature. One notices that this quantity decreases with increasing temperature until the phase transition. Above this value it remains constant. Returning to Fig. 1., we can assume the following: the first slope modifications (in the low temperature range) for the samples VII, VI, V arises at Debye temperatures.

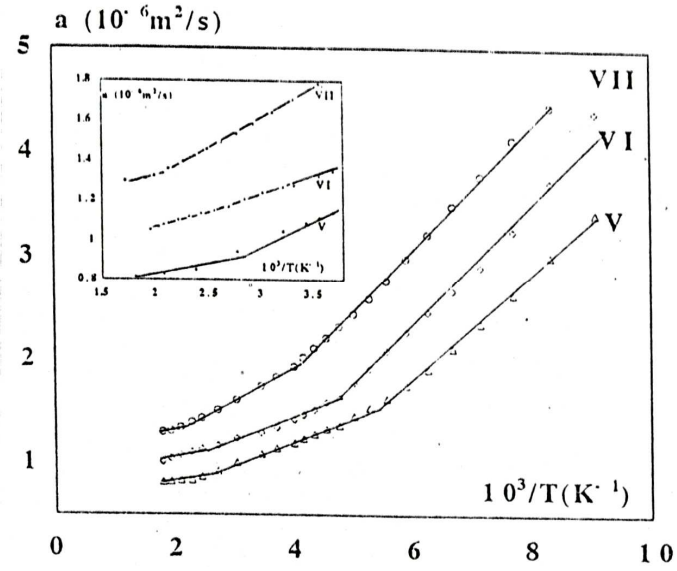

Fig. 1. Thermal diffusivity variation for samples VII, VI, V

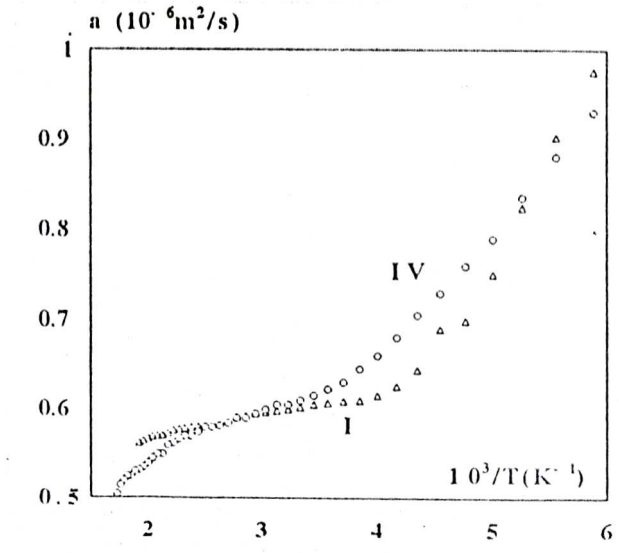

Fig. 2. Thermal diffusivity variation in case of samples I and IV

Their values were confirmed by specific heat measurements. The second slope modification arises at higher temperatures. These values can be determined exactly from the medallion of Fig. 1 Thus, it appears at 464K for the sample VII, at 391K for the sample VI and at 370K in case of sample V. The values determined are in agreement (in terms of the errors of the measurement) with the values determined by L. Kozlowski [2] for the phase-transition. In the case of sample I (Fig. 2), the single slope modification temperature corresponds to the Debye temperature. For the sample IV (Fig. 2), the variation of the diffusivity is no longer linear for the intermediate temperature range. Thus it is not possible to determine the Debye temperature. We consider that this is due to the superposition of the two temperature-regions. The slope-modification for this sample appears at 259K, which corresponds to the phase-transition temperature.

The variation of thermal conductivity is given by:

$$\lambda = a \rho c, \tag{4}$$

where: a - thermal diffusivity, ρ - density, and it is represented in Fig. 3 for samples VII, VI, V and in Fig. 4 for the sample IV. One founds that this variation curve presents a peak at the magnetic phase-transition temperature, peak that can be correlated with an anomaly in the specific heat. With regard to this data, see article [6].

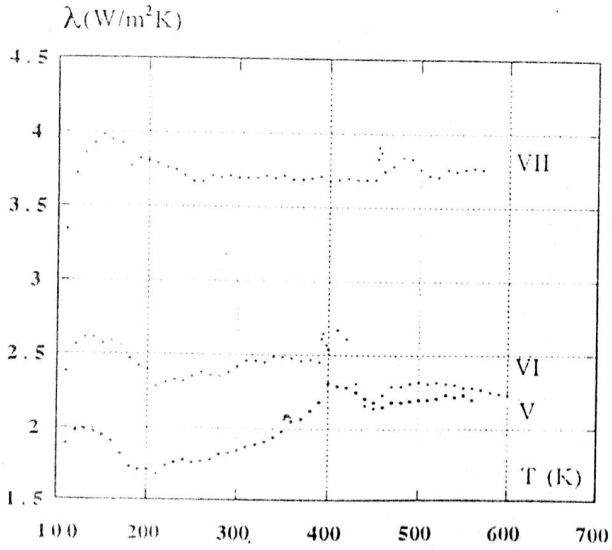

Fig. 3. Thermal conductivity for samples VII, VI, V

As it was shown, the above determined temperatures present coincidence with the data from the paper of Visinevski [1].

From Fig. 3 and Fig. 4 results also that thermal conductivity decreases with increasing Al 3+ concentration. We consider that this decrease arises from the substitution of magnetic Fe3+ ions from the host lattice with Al 3+ ions that have greater scattering section for phonons than Fe3+, as it was shown in [7].

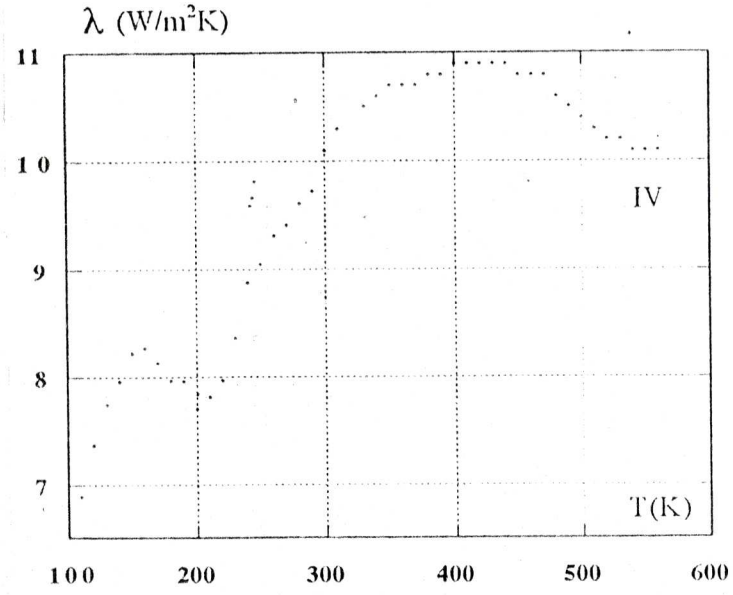

Fig. 4. Thermal conductivity for sample IV

CONCLUSIONS

Magnetic phase transition was put in evidence by thermal data.

It was proved that the thermal diffusivity is an adequate quantity to study the second order phase transition.

It was pointed out that the thermal conductivity varies considerably with the concentration of Al 3+ ions in case of ferrites.

REFERENCES

1. I. I. Visinevski, A. C. Frenkel, V. N. Skripak, *Fiz. Tverd. Tela*, 5, 2691 (1963).
2. L. Kozlowski, W. Zarek, *Act. Phys. Pol*., A42, 6, 663 (1972).
3. F. Kelemen, Á. Néda, F. Bota, *Stud. Cerc. Fiz*., 7, 809 (1964).
4. F. Kelemen, Á. Néda, *Studia Univ. Babe¿-Bolyai*, Ser. Phys. 2, 39 (1970).
5. D. Peirels, *Ann. Phys*. (Leipzig), 3, 1055 (1929).
6. Á. Néda, *Conf. Nat. Fiz*. (Cluj), (1990).
7. Á. Néda, Z. Néda, *Balc. Conf. Phys.* (Izmir), (1995).

STUDIA UNIVERSITATIS BABEŞ-BOLYAI, PHYSICA, XLII, 1, 1997

LES PARAMETRES DE QUALITE DES NOYAUX MAGNETIQUES EN POUDRES, LEURS FACTEURS DETERMINANTS. RESULTATS EXPERIMENTAUX

SABINA PICOŞ[1]

Les plus importants paramètres électriques et magnétiques des noyaux en poudres pressées sont la résistivité, les pertes magnétiques et le facteur de qualité. Les méthodes de déterminer leurs valeurs qui ont été utilisées dans les expériences sont les suivantes:

a) Pour mesurer la résistivité électrique des échantillons on a d'abord déterminé la résistance électrique R en utilisant la relation:

$$\rho = R \frac{S}{L} \tag{1}$$

ou la section S et la longueur L sont les caractéristiques dimensionnelles des échantillons.

Pour mesurer la résistance R des échantillons on a utilisé l'ensemble présente dans la fig. 1, avec les notations suivantes: PW - pont Wheastone - Thomson, G - instrument de zéro, U - source d'alimentation, Rh - rhéostat de réglage et V - voltmètre.

b) Evaluation des pertes magnétiques

Afin de déterminer les pertes magnétiques on a utilisé une méthode en pont qui rend possible la détermination de composantes active et réactive et de l'impédance d'une bobine ayant comme noyaux un tore de poudre ferromagnétique. Le schéma bloc de l'installation est donne par la figure 2; on y utilise les notations suivantes: G - générateur décadique TR-0202; PA - pont d'alimentation SWM-3-2; mV_s - millivoltmètre sélectif TT-1301; VE - voltmètre sélectif TT-1302; T - échantillon et R - résistance calibrée. Du schéma de l'installation (fig. 2) on a séparé le schéma électrique de principe du pont d'admittance (fig.3).

Pour mesurer le champ où se trouve l'échantillon, le bobinage du tore a été lié en série à une résistance calibrée R = 1 Ω d'où on y

[1] Université Technique, IAŞI Roumanie, Email: cattcm@tuiasi.ro

ramasse la chute de tension, mesurée à l'aide du voltmètre électronique VE et ainsi on détermine l'intensité I du courant, qui traverse le bobinage. Au pont PA on compose l'admittance de l' échantillon, en utilisant la relation:

$$y=G-j\cdot B \tag{2}$$

où G est la conductance et B = ωC est la susceptance, toutes les deux étalonnées, R et X = Lω

$$R=\frac{G}{G^2+B^2};\qquad X=\frac{B^2}{G^2+B^2} \tag{3}$$

A la fin on déterminé les pertes totales, données par tgδ.

$$tg\delta=\frac{R-R_0-R'}{(L-L_0)\cdot\omega} \tag{4}$$

où R_0 et L_0 sont la résistance, respectivement l'impédance du bobinage et ω est la pulsation du courant. On a effectué les déterminations pour une fréquence $\nu = 10^3$ Hz.

c) L'évaluation du facteur de qualité Q

On a déterminé les valeurs du facteur de qualité Q pour des fréquences supérieure de la valeur de 10^3 Hz en utilisant quelques Q - mètres Rode-Schwartz BH-36711 et Hewllet-Packard.

RESULTATS EXPERIMENTAUX

La résistivité

Comme facteur déterminant de la qualité des noyaux magnétiques obtenus des poudres de fer électrolytique (ME_1 et ME_2) et du frem (F_1 et F_2) la résistivité varie selon la composition, selon les dimensions et la distribution granulométrique de la poudre (tables 1 et 2 et fig. 4.). Les poudres de fer frem et les poudres électrolytiques sont des poudres de fabrication différente. Les deux sortes de chaque catégorie de poudre ont de dimensions et des distributions granulaires différentes. En étudiant la représentation graphique, on peut constater que:

- la dimension granulaire g des poudres influence la valeur de la résistivité dans le sens qu'elle enregistre un accroissement selon la réduction des dimensions des granules ($q_{EM_1} > q_{EM_2}$ et $q_{F_2} > q_{F_1}$)

puisque le degré de compactage et plus petit dans le cas des granules fins;

- la distribution dimensionnelle des poudres ayant la même composition chimique exerce une certaine influence sur de valeur de la résistivité électrique.

Table 1. La composition chimique des poudres utilisées %

Norme de la poudre	Fe	C	O	Si	SiO_2	Mn	P	S	Cu	N	Ni	Mo
Electrolytique ME_1 et ME_2	99.96	0.00	-	0.006	-	0.01	0.004	0.003	0.008	-	-	-
Frem F_1 et F_2	98	0.03	-	-	0.035	0.04	0.025	0.025	-	-	-	-

Table 2. Répartition granulométrique de la poudre

Poudre	La grandeur des granules (μm)	Répartition %	Forme de la granule
Electrolytique ME_1	sous 0,045	100	feuille polyédrique
Electrolytique ME_2	0,008...0,044	100	feuille polyédrique
Frem F_1 et F_2	sous 0,04	100	polyédrique, irrégulière

Les pertes magnétiques

La relation entre les pertes totales magnétiques (tgδ) et le facteur de qualité Q est donnée par l'expression :

$$Q = \frac{1}{tg\delta} \tag{5}$$

Considérant que le but de l'utilisation de noyaux magnétiques de poudres ferromagnétiques est la réduction de pertes magnétiques engendrées par les courants tourbillonnaires ($tg\delta_f$) on peut écrire:

$$tg\delta_f = \frac{4\pi^2 d^2 \mu L \nu^2}{S\rho} \cdot 10^{-9} \tag{6}$$

$$Q = \frac{S\rho \cdot 10^9}{4\pi^2 d^2 \mu L \nu^2} \tag{7}$$

La relation (6) montre que les pertes magnétiques varient inversement proportionnel avec la résistivité. Conformément a la

dernière relation de calcul le facteur de qualité Q enregistre une variation directe par rapport a la résistivité ρ.

Par la suite, les paramètres physiques des poudres agissent sur le facteur de qualité dans le même sens comme dans le cas de la résistivité électrique.

L'influence de la fréquence du courant d'alimentation sur les pertes magnétiques.

Utilisant les données expérimentales sur la variation des pertes magnétiques de fer électrolytique ME_1 et ME_2 de fer frem F_1 et F_2 on fait les représentations graphiques des figures 5 et 6 qui mettent en évidence les constatations suivantes:

- le domaine de variation de fréquences pour les deux poudres obtenues par le même procédé peut être séparé en deux zones de fréquences ν_i et ν_s ou $\nu_i < \nu_s$;
- pour la zone de fréquences ν_i les noyaux obtenus de granules plus fins ont des pertes magnétiques plus petites et pour celle de fréquences ν_s les pertes magnétiques sont plus réduites que dans le cas des noyaux aux granules plus grands.

La relation (5) montre que la perte magnétique de courants tourbillonnaires enregistre une variation inversement proportionnelle avec la résistivité qui, a son tour a une variation inversement proportionnelle par rapport aux dimensions des granules. Pour la zone de fréquences ν_s, la résistivité augmente pour des granules plus grands dans un rythme qui dépasse celui qui correspond aux granules plus petits.

LE FACTEUR DE QUALITE Q

Le facteur de qualité atteint la valeur maximale pour des granules plus fins, dans le domaine de fréquences ν_i pour des granules plus grands, dans le domaine de fréquences ν_s. On remarque aussi que les valeurs optimales du facteur de qualité se trouvent aussi dans des fréquences élevées pour des noyaux aux granules plus grands (figure 7 et figure 8).

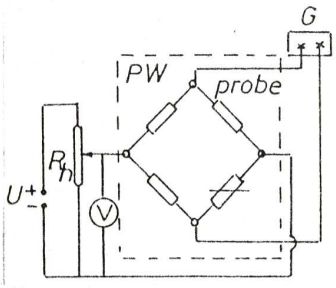

Fig. 1. Détermination de la résistance électrique

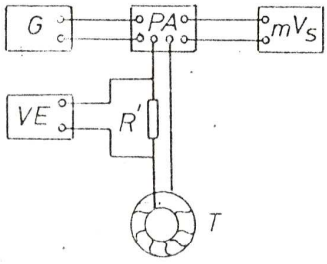

Fig. 2. Schéma pour les pertes magnétiques

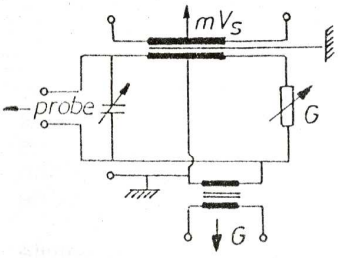

Fig. 3. Schéma du pont d'admittance

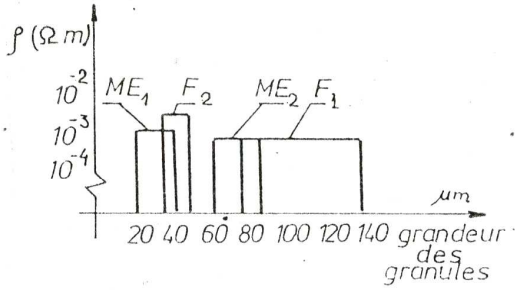

Fig. 4. Variation de la résistivité fonction de paramètres physiques de la poudre

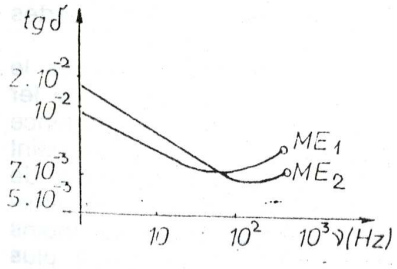

Fig. 5. Les pertes magnétiques fonction fréquence (pour la poudre F_1 et F_2)

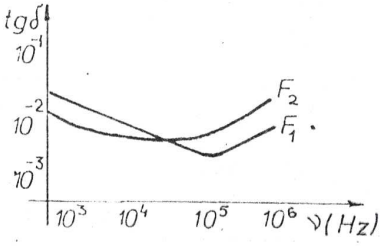

Fig. 6. Les pertes magnétiques fonction de la fréquence (pour la poudre ME_1 et ME_2)

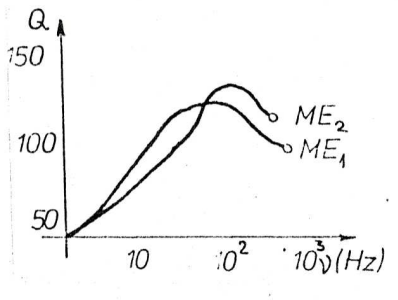

Fig. 7. Le facteur de qualité fonction de la fréquence (pour la poudre ME_1 et ME_2)

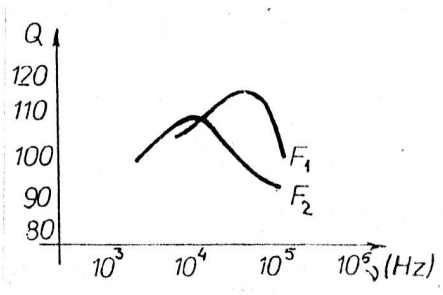

Fig. 8. Le facteur de qualité fonction de la fréquence (pour la poudre F_1 et F_2)

CONCLUSIONS FINALES

La qualité de noyaux magnétiques de poudres de fer électrolytique et de fer frem se trouve dans une relation complexe d'interdépendance avec une série de facteurs physiques (les dimensions et la distribution des granules), chimiques (la composition chimique) et technologique (la méthode d'obtenir de poudres de noyaux).

Le facteur de qualité Q est direct dépendant de la résistivité électrique de noyaux et de la fréquence du courant électrique qui travers la bobine.

Il y a une fréquence optimale dans le cas des noyaux magnétiques pour laquelle le facteur de qualité est maximal et les pertes magnétiques minimales. L'utilisation des fréquences plus élevées ou plus petites que celle optimales, conduit a l'accroissement des pertes magnétiques influençant négativement le facteur de qualité.

Dans le cas de noyaux aux poudres de fer électrolytiques le facteur de qualité est supérieur a celui de noyaux aux poudres de fer frem. Les courbes de variation du facteur de qualité selon la fréquence pour les deux dimensions des granules de la même poudre, ont un point d'intersection qui déterminé la fréquence pour laquelle le facteur de qualité a la même valeur pour les deux dimensions des granules. Ainsi on sépare deux zones conventionnelles: la zone de fréquence moins élevée, favorable aux poudres fines et la zone de fréquence plus élèvée, favorable aux poudres avec des granules plus grandes. Ces zones contiennent sans doute les fréquences optimales correspondantes.

BIBLIOGRAPHIE

1. Scott, G., *Iron Compact for Electromagnetic Applications*, M.Sc.Thesis, Univ.of Warwich, 1971.
2. Goetzel,C., *Treatise on Powder Metallurgy*, vol.1, New-York-London, Interscience Publ.1949.
3. Heister, W., *Untersuchung der frequenzabhangigkeid der stoffewerti feromagnetischer Mischkorper bis zu ser hohen requenzen Archelectrot*,H1, 142, 1973.
4. Picoş, S. *Studiul proprietăților electrice şi magnetice ale pulberilor din materiale feromagnetice în vederea utilizării lor în tehnică*, Editura Institutului Politehnic Iaşi, 1983.

STUDIA UNIVERSITATIS BABES-BOLYAI, PHYSICA, XLII, 1, 1997

EVALUATION OF THE ACTIVATION ENERGY OF LOCAL DYNAMICS IN POLYISOPRENE-TOLUENE-D_8 SOLUTIONS

M. TODICA[1]

ABSTRACT. The temperature dependence of the spin-lattice relaxation time was observed for the polyisoprene toluene D_8 solutions and for the molten polyisoprene, by NMR method. In the extreme narrowing region the correlation time of the local dynamics of the polymeric chain can be directly calculated from this relaxation time. The temperature dependence of the correlation time is analyzed in the concept of the activation energy.

INTRODUCTION

The molecular dynamics in polymeric materials is a complex process which occur in a large spatial and temporary range. Generally the dynamic properties of macromolecules may be analyzed in two different space and time scales:

- long-range fluctuations, which are observed in a large time scale and which are strongly molecular dependent;
- short- range fluctuations, which corresponds to the rapid local motions of the skeletal bonds, and which occur within the dynamically screening length associated with the temporary entanglements. These fluctuations are molecular weight independent.

These two types of fluctuations are responsible of the viscoelastic behavior of the polymeric materials and are related to the terminal and transient zone of the dynamic relaxation modulus, [1]. Rheological measurements of the dynamic relaxation modulus can give rise only indirect information about the molecular dynamics and only about slow motions.

All kinds of molecular fluctuations in polymeric materials are generated by the elementary motions of the C-C and C-H links in the monomeric units, or by the motion of the polymeric segments which

[1] Babes-Bolyai University, Faculty of Physics, 3400 Cluj-Napoca, Romania

include one or many monomers. These rapid motions are not perceived by the rheological measurements, but can affect the dipolar interaction between the nuclear spins and thus the NMR behavior, [2]. As a result the NMR method is an appropriate instrument to observe the local dynamics of the macromolecules. Thermal activation or the presence of the solvent molecules in the vicinity of the monomer units are important factors which can affect this dynamics. The aim of our work is the evaluation of activation energy of the local dynamics of the polymeric links, by NMR method, in polyisoprene-toluene solutions.

EXPERIMENTAL

We studied the molten polyisoprene and the polyisoprene-toluene D_8 solution, with the polymeric concentrations Φ=94%, 78% and 58%. The conformation of the molten polymer is 92% cis and the glass transition temperature is T_g=200±5K. The polymeric sample was supplied by the Manufacture Michelin and the deuterated toluene was purchased from Spectrometrie Spin et Techniques, France. The samples were enclosed in NMR tubes (diameter 4mm) and sealed under a primary vacuum. The concentration of the solution was controlled with an accuracy better than 1%.

All the measurements were performed using a CXP Bruker spectrometer working at 45 MHz, in the temperature range of 254 K to 344K. The spin-lattice relaxation time was measured using the inversion recovery method, [3]. The sample temperature was controlled within 1 K.

RESULTS AND DISCUSSION

The elementary motions which govern the dynamics of the entire chain are the rotations of the C-C and C-H links around the local symmetry axis. Every rotation modify the azimuthal angles of the links and the relative distance between the atoms attached to the polymeric chain and leads to a new local conformation. Every stable conformation is characterized by an minimum of the potential energy. When a macromolecule go from one given conformation to another one, the energy barrier which separate the two states must be overcome. Generally this energy is provided by the thermal activation. The presence of solvent molecules in the vicinity of the polymeric chain can modify the potential energy of each stable conformation of the macromolecule. But every local rotation of the polymeric links

determine a deplacement of the solvent molecules. The dynamics of the solvent molecules depends on its viscosity. In this case the activation energy requested for the modification of the polymeric conformation is an apparent activation energy which contain also the solvent contribution. This parameter is directly connected with the correlation time of the local motions. The correlation time is a microscopic parameter which can be obtained from the spin-lattice relaxation time.

In the polymeric samples the dominant mechanism of the relaxation process is the dipolar interaction between the neighboring protons. Now is well established that the spin-lattice relaxation rate is determined by the Fourier transform of the time-correlation function G(t) of the spin-spin interaction, [4]. Roughly we can write:

$$\frac{1}{T_1} \propto \mathrm{Re} \int_0^{\infty} G(t) e^{i\omega} dt \tag{1}$$

where w is the Larmor frequency. The function G(t) is definite by the equation

$$G(t) = \frac{1}{2}\left\langle 3\left(\bar{e}_x(t)\bar{e}_x(0)\right)^2 - 1\right\rangle \tag{2}$$

In this equation $\bar{e}_x(t)$ is the unit vector in the direction of the polymeric link at the moment t. The brackets indicate an ensemble average. The time request for C-H vector reorientation is determined by how fast G(t) decays to zero. This time may be characterized by <s>, the time integral of G(t).

$$\tau_c = \langle \sigma \rangle = \int_0^{\infty} G(t) dt \tag{3}$$

Often this time is designed as the correlation time of the C-H rotational motion.

The shape of G(t) is related to the specific mechanism of C-H vector reorientation. If C-H vectors undergo isotropic rotational motions, G(t) is a single exponential function with a characteristic correlation time

t. In the most generally case, the reorientation of C-H vectors in polymers is not isotropic and then the function G(t) contains a distribution of time constants t described by the distribution function F(t), so that the correlation function is expressed by the relation:

$$G(t) = \int_0^{\infty} F(t) e^{\frac{-t}{\tau}} dt \tag{4}$$

Many attempts have made to find the explicit form of the correlation function that describe quantitatively the proton relaxation data; single exponential function, nonexponential function, and distribution of correlation times [5,6,7]. Generally this is a difficult task which needs a well knowledge of the microscopic local dynamics of the polymeric links. However, in some particular situations, the correlation time can be calculated directly from the spin-lattice relaxation time.

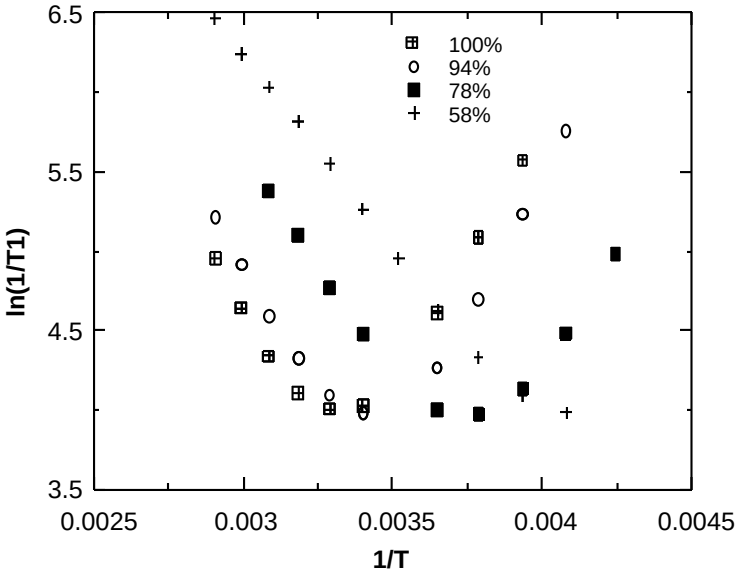

Fig.1. The temperature dependence of the spin-lattice relaxation time of the molten polymer and the polyisoprene-toluene solutions.

When the extreme narrowing condition $\omega\tau<<1$ is fulfilled for all τ that contribute to G(t), then the correlation time τ_c is simply related to the spin-lattice relaxation time by the relation (5), where K is a constant which depends on the microstructure of the polymer.

$$\frac{1}{T_1} = \frac{1}{T_2} = K\tau_c \tag{5}$$

Therefore in the extreme narrowing region the spin-lattice and the spin-spin relaxation times are equal to each other and are independent of the Larmor frequency. Generally this condition is fulfilled in the region where the log(T_1) is a linear function of 1/T.

We utilized this observations to analyze our experimental data. The temperature dependence of the spin-lattice relaxation time for the molten polyisoprene and some polyisoprene toluene solutions are shown in Fig.1. For each sample the minimum value of the relaxation time is observed for a characteristic temperature θ_{min}. We estimated that the extreme narrowing region is situated in the domain of about 50K above the temperatures θ_{min}. We take in this case $\tau_c=K/T_1$. The correlation time which we extract using this procedure is an weighted average of all the time constant that enter in the description of the local polymeric motion. This effective time contains a contribution of the fast local motion of the skeletal bonds, which is described by the correlation function $G_i(t)$, and a contribution of the very slow long-range motions, perhaps and-over-and motions, described by the correlation function $G_0(t)$. Then the total correlation function is $G(t)=a\ G_0(t)+(1-a)G_i(t)$. The parameter "a" is a constant much less that 1, (a<<1), so that we can assume that $G(t)=G_0(t)$ and the integral of $G_i(t)$, the fast part of the correlation function, represent the correlation time of the local motions of the skeletal bonds, [8]. The correlation time can give information about the energy needed to activate the local motion. The first approach to analyze the experimental data of τ_c is based on the Kramers theory, applied to the simplest liquids, [9]. This theory is based on the passage of a particle over a potential energy barrier. The solvent is treated as a random frictional force opposing passage across the barrier. Any spatial

and temporary correlation in the solvent motion is neglected. Helfand has applied Kramers theory to the case of conformational translations of the polymers, [10]. In the high friction limit the rate constant of the isomerization depends on the friction coefficient of the solvent ζ and the energy barrier of the rotational motion, E_a.

$$k \propto \frac{1}{\zeta} \exp\left(-E_a / RT\right) \tag{6}$$

The correlation time measured by NMR experiments is inversely proportional with the rate constant of isomerization. Then the temperature and viscosity dependence of τ_c predicted by Kramers'theory can be expressed as:

$$\tau_c = A\eta \exp\left(E_a / RT\right) \tag{7}$$

The factor A is a constant independent of temperature and viscosity and η is the viscosity of the solvent. This equation must describe the correlation time of the polymeric solutions. In the case of the molten polymer there are not solvent molecules in the system and then the presence of the viscosity factor in the equation (7) is not necessarily. The viscosity in equation (7) can be replaced by a constant. We obtain:

$$\tau_c = A' \exp\left(E_a / RT\right) \tag{8}$$

If we take into account that $\tau_c = K/T_1$, we can calculate the activation energy of the isomerization motion of the molten polymer from the Arrhenius plot of $\ln(1/T_1)$ versus the (1/T) variable, Fig. 2.

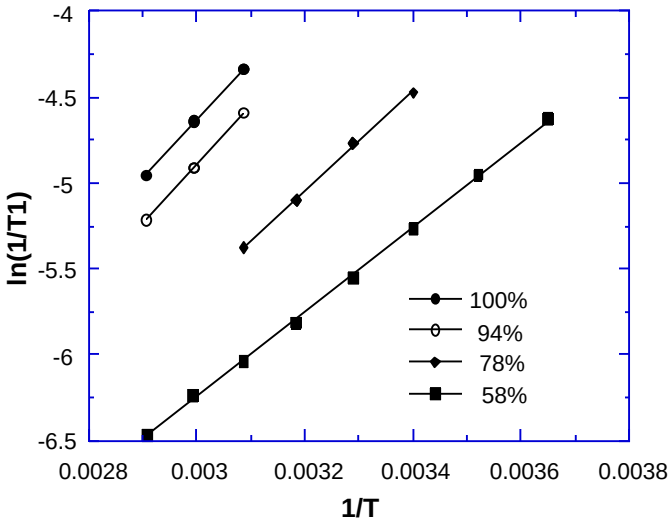

Fig.2. Arrhenius plot of the spin-lattice relaxation time whe the viscosity of the solvent is not take into acount.

We found the value E_a=28 Kj/mol for the molten polymer. It is interesting to see that if we utilize the equation (8) to analyze the data of the solutions, it seems that the Arrhenius behavior is also respected, Fig. 2, and we can calculate an apparent activation energy for each solution. These values are concentration dependents, Fig. 3. It is clear that this apparent activation energy contain also the contribution of the solvent.

To extract the contribution of the polymer to the total apparent activation energy, we must take into account the viscosity factor in equation (7). But it is clear that the contribution of the viscosity in equation (7) depends on the concentration of the solvent. For high solvent concentration the factor h may have an important contribution, but this contribution must decrease when the polymeric concentration increase. This leads to a power law relationship between the correlation time and the viscosity, as it was suggested by Fleming, [11].

$$\tau_c = A\eta^{\alpha} \exp\left(E_a / RT\right) \tag{9}$$

The power exponent is 0<a<1. Ediger found the value a=0.41 for polyisoprene-toluene solutions with 9.7% polymeric concentration, [12].

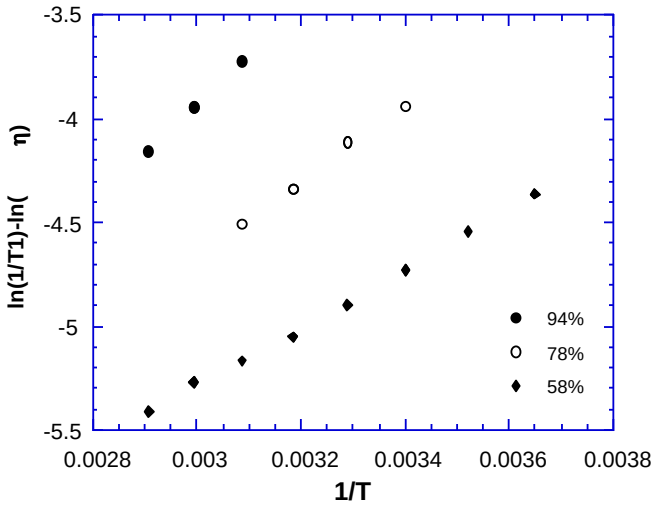

Fig.3. Arrhenius plot of the spin-lattice relaxation time when the viscosity of the solvent is take into acount.

We can assume that a is concentration dependent, so that α=0 for the molten polymer and α=1 for the pure solvent. In this case the activation energy can be calculated only if $\alpha(\Phi)$ and $\eta(\Phi)$ are known for each concentration. When the temperature dependence of $\eta(\Phi)$ and the parameter $\alpha(\Phi)$ are known, then the activation energy of the polymer in solution, can be calculated from the Arrhenius plot of [ln(1/T1)-α ln(η)] versus (1/T) variable. For the toluene the temperature dependence of the viscosity is given by the relation $\eta=A(B+T)^{-C}$ in the temperature range of [273K-380K], with A=1895.4, B= -160.16 and C=1.65, [13]. The values of α can not be calculated from a single solvent. In this case we can not calculate the exact value of activation energy of the polymer. However we can estimate the range domain of values of E_a if we take into account the extreme values α, α=1 and α=0. We assume a linear dependence of [ln(1/T1)-a ln(h)] versus (1/T) variable to calculate the extremes values of E_a. For α=0 the dependence of [ln(1/T1)] versus (1/T) is represented in Fig. 2. and for α=1 the dependence of [ln(1/T1)-α

ln(η)] versus (1/T) is represented in Fig. 3. The apparent activation energy is calculated from the slopes of straight lines of these representations. The values obtained are reported in Fig. 4. The maximal values correspond to α=0 and the minimal values to α=1. We found in this way the domain range of the activation energy of the polymer for each concentration.

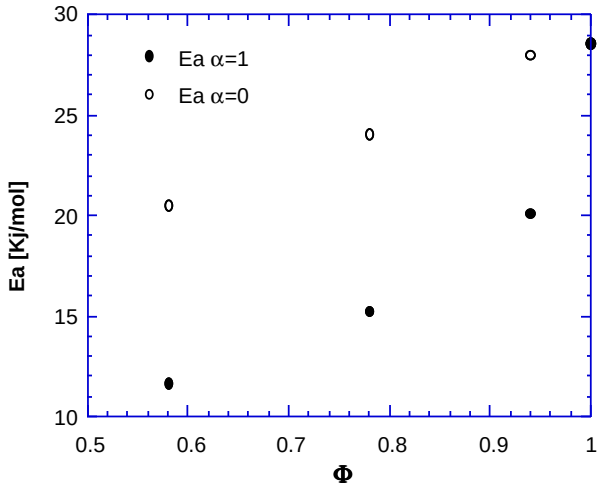

Fig.4. The concentration dependence of the domaine range of the activatin energy of the polymer in solutions.

Extrapolation of ours results to the concentration of 10% show that the value E_a=12Kj/mol found by Ediger at this concentration, with α=0.41, lie in the domain range of ours results. This fact indicate that ours method is a good way to have a roughly estimation of the activation energy. The exact values of E_a can be obtained only if a is known with great accuracy.

CONCLUSION

The local dynamics of the polymeric motion can be investigate by measuring the spin-lattice relaxation time T_1 of the protons attached to the polymeric chain. This macroscopic NMR parameter is directly connected with the correlation time of the local motions, which is a microscopic parameter. The temperature dependence of the correlation time can be expressed by a Cramers-Fleming power law described by

equation (7). The power exponent α of this equation lies in the range of 0 to 1. The extremes values of α may us to estimate the domain range of the values of the activation energy of the local motion for each concentration. The exact value of the activation energy can be calculated only if the temperature dependence of the solvent viscosity and the power exponent a are well known.

REFERENCES

1. J. D. Ferry, *Viscoelasticity of Polymers*, Third edition, New York, John Wiley and Sons, 1980.
2. J. P. Cohen-Addad, *NMR and Fractal Properties of Polymers Liquids and Gels*, Pergamon Press, London, 1992.
3. H. Y. Carr, E. R. Purcell, *Phys. Rev.*, 1954, 94, 630.
4. A. Abragam, *The Principles of Nuclear Magnetism*, Clarendon Press, Oxford, 1961.
5. K. S. Cole, R. H. Cole, *J. Chem. Phys*., 1941, 9, 341.
6. C. K. Hall, E. Helfand, *J. Chem. Phys*., 1982, 77, 3275.
7. R. Dejean de la Batie, F. Laupretre, L. Monnerie, *Macromolecules,* 988, 21, 2045.
8. Y. K. Levine, P. Partington, G. C. K. Roberts, *Mol. Phys*. 1973, 25, 497.
9. H. A. Kramers, *Physica*, 1940, 7, 284.
10. E. Helfand, *J. Chem. Phys*., 1971, 54, 4651.
11. S. H. Courtney, G. R. Fleming, *J. Chem. Phys*., 1985, 83, 215.
12. S. *Glawinkovsk*i, D. J. Gisser, M. D. Ediger, *Macromolecules*, 1990, 23, 3520.
13. International Critical Tables, E. W. Washburn, C. J. West, E. N. Dorsey, M. D. Ring. Mc Graw-Hill, New York, 1930.

STUDIA UNIVERSITATIS BABEŞ-BOLYAI, PHYSICA, XLII, 1, 1997

GAMMA RADIATION EFFECTS ON SOME BIOMOLECULES

V. CHIŞ[1], G. DAMIAN[1], L. DAVID[1], O. COZAR[1], V. ZNAMIROVSCHI[1], L. KAZIMIRSKI[1], D. RISTOIU[1]

ABSTRACT. The yielding of the free radicals as a function of the irradiation dose in some gamma-irradiated anti-inflammatory drugs (Aspirin, Indomethacin and Piroxicam) and aminoacids (Glycine, L-Glutamic Acid, DL-Serine and DL-Asparagine) is analyzed using ESR spectroscopy. The constants of destroying the free radicals by the radiation are obtained by fitting the dose dependence of the ESR signal intensity assuming a first order kinetics of the free radicals formation. The values of the saturation doses are one order of magnitude greater for the irradiated drugs than those corresponding to the irradiated aminoacids.

INTRODUCTION

Free radicals produced in gamma-irradiated crystalline biomolecules are relatively stable intermediate products of a sequence of events, which, as in tissue, is started by the initial absorption of radiation energy. Therefore, quantitative and qualitative analysis of the free radicals may provide a more biologically relevant dosimetry, particularly since the free radicals are key intermediates in the processes leading to biological damage of cellular components.

This work is aimed to study the formation kinetics in four gamma-irradiated aminoacids (Glycine, L-Glutamic Acid, DL-Serine, and DL-Asparagine) and three gamma-irradiated anti-inflammatory drugs (Aspirin, Indomethacin and Piroxicam) and to compare the yielding of free radicals in these samples with the case of alanine. This kind of studies could provide very useful information about the possibility to use this type of biological samples for radiation control purposes.

[1] Babeş-Bolyai University, Faculty of Physics, RO-3400 Cluj-Napoca, Romania

The structure of the free radicals obtained in the above mentioned gamma-irradiated aminoacids at room temperature was discussed in another paper [1]. The identity of the radio-induced free radicals in these samples was established by analyzing the hyperfine structure of their ESR spectra and by using the microwave power saturation method. It was shown that the room temperature stable free radicals in these samples are produced by deamination or hydrogen abstraction mechanism.

We have made also a study of the gamma-irradiated Aspirin, being able to identify three different free radicals produced by gamma rays at room temperature [2]. It was shown that the ESR spectrum of gamma irradiated Aspirin has changed by increasing the radiation dose suggesting that different radicals are formed at different levels of adsorbed dose. For high values of doses, the total spectrum represents a sum of the spectra corresponding to the three different free radicals simultaneously present in the sample: the radical ROO formed by hydrogen abstraction from the carboxyl group, the second one of the form $R\text{-}CH_2$ formed by hydrogen abstraction from the methyl group and the last one formed by hydrogen addition at one of the carbon atoms of the ring.

EXPERIMENTAL

The powdered samples investigated were irradiated in air at room temperature using the "Gamma Chamber 900" unit which give a compact and uniform density of radiations in the $1000cm^3$ volume. The dose rate of the source was determined using a Fricke ferrous sulfate dosimeter. The irradiation doses were in the range 2. 4 - 160 KGy for drugs and 1. 5-16. 5 KGy for aminoacids. The samples were irradiated at the lowest dose, observed and re-irradiated to each of the successive cumulative doses. ESR spectra were recorded at room temperature with an ESP 300 BRUKER X-band spectrometer with a field modulation frequency of 100 KHz. . The ESR signal intensity, which is proportional to the relative yield of radicals, represents the area under the absortpion curve and it was determined by double integration of the corresponding ESR spectrum. The

samples investigated were purchased from Sigma Chemical Co. and used without further purification.

RESULTS AND DISCUSSION

The absorbed dose was measured using a Fricke dosimeter which give a precision of 1-2% in the range of 20-400 KGy of the absorbed dose. The principle of the Fricke dosimetry consist in the radiolitical oxidation of the Fe^{2+} ions to obtain Fe^{3+} ions [3]. The absorbed dose in the solution is calculated using the equation [4]:

$$D(Gy) = 9.64 \cdot 10^6 \frac{\Delta D}{\left[\varepsilon(Fe^{3+}) - \varepsilon(Fe^{2+})\right] G \rho l} \quad (1)$$

where ΔD is the optical density of the probe solution, ε the extinction coefficient, ρ the probe density, l the thickness of the probe solution in the spectrophotometer and G is the radiochemical efficiency, defined as the number of molecules of a specific radiation product formed per 100 eV of energy deposited in the sample. Molar extinction coefficient $\varepsilon(Fe^{2+})$ can be neglected due to the fact that $\varepsilon(Fe^{2+})/\varepsilon(Fe^{3+})$ ratio is $5 \cdot 10^{-4}$ for λ=303nm [5]. We have used a standard Fricke solution: 10^{-3} M $FeSO_4$ and 10^{-3} M NaCl in a high purity 0. 4 M H_2SO_4 solution. In these conditions, the radiochemical efficiency is G=15. 6 [6]. The solutions were saturated with oxygen before irradiations. For different irradiation times, the optical density ΔD and the extinction coefficient ε were measured using a SPECORD UV-VIS spectrophotometer working in the range 54000-12500 cm^{-1}. The measured absorbed dose as a function of irradiation time is shown in Fig. 1. An average debit dose of D=35. 27Gy/hour is obtained from our measurements.

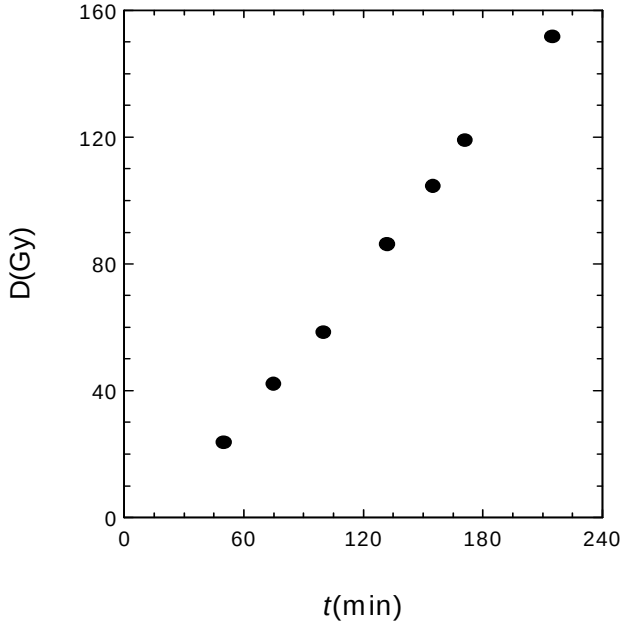

Fig. 1. Dose dependence vs. the irradiation time.

ESR spectra of gamma-irradiated Indomethacin and Piroxicam do not show significant qualitative changes by increasing the radiation dose in the range 2. 4-160KGy. These spectra show only a single central line centered at g≈2. 004, having a width of ≈15G for Indomethacin and ≈12G for Piroxicam. Due to the fact that no hyperfine structure can be detected, the assignment of these spectra to a certain free radical is very difficult. However, g factor and line-widths parameters are characteristic to the radical ROO or RO [7] formed by hydrogen or hydroxyl abstraction from the COOH group of the neutral molecules. Because there is no evidence of the signal from OH radical which should be very anisotrop [7, 8] we attributed the spectra of Indomethacin and Piroxicam to a radical of the form ROO formed by hydrogen abstraction in which the unpaired electron is probably delocalized over the entire carboxyl group [9].

The formation kinetics of the free radicals is described by an equation of the form:

$$R = R_{lim}\left[1 - \exp(-\kappa D)\right] \quad (2)$$

where R_{lim} represents the steady state concentration of the radicals, D represents the irradiation dose and κ is the constant of destroying the free radicals by the radiation [10].

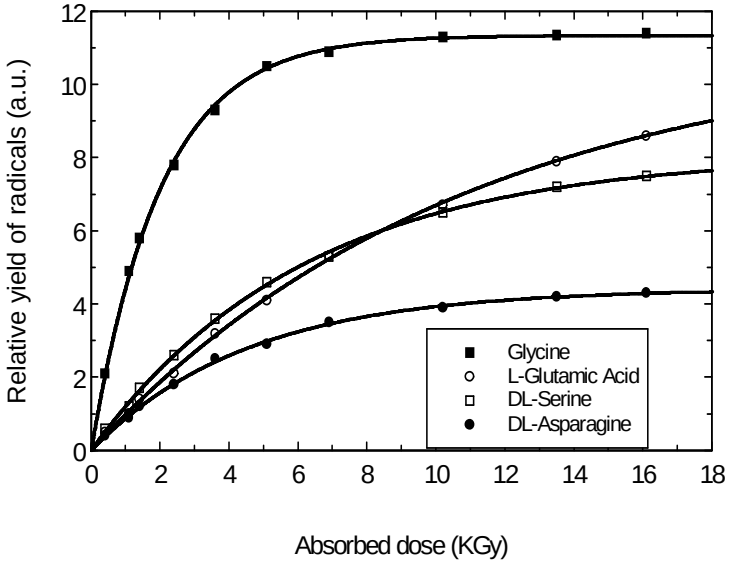

Fig. 2. The relative yield of radicals in four γ-irradiated aminoacids as a function of dose. The continuous lines represent the best fit calculated values.

The shape of the ESR spectra corresponding to the four investigated aminoacids doesn't change by increasing the irradiation dose and it implies that even if in the irradiated sample are more radicals simultaneously present they are not forming in steps but appear at the same value of dose and the detected radicals do not result one from another. The dose response of the investigated gamma-irradiated aminoacids from 1. 5 to 16. 5 KGy recorded immediately after irradiation is shown in Fig. 2. As it can be seen, for all the investigated sample and for low values of doses, the number of the generated free radicals increases

rapidly and almost linear in the dose range up to 4KGy. The curves for DL-Serine and L-Glutamic Acid remain almost linear in the whole range of the irradiation dose while for Glycine and DL-Asparagine they present a saturation over about 8 KGy. These last curves can be explained taking into account that the distance between radicals decreases by increasing of their concentration and the radical-radical reactions compete with radical yielding, so that the radicals are being destroyed at a rate approaching that at which they are being created [11].

Experimental data were fitted by a first order kinetics (eq. 2). The fit procedure is based on a least square method and the corresponding best fit parameters κ are given in Table 1. These values are in very good agreement with those generally found for polipeptideds [12]. Using the fit parameters and the ratio R/R_{lim}=0. 98 one obtains the following saturation doses: ≈10KGy for Glycine, ≈20KGy for DL-Asparagine, ≈25KGy for DL-Serine and ≈45KGy for L-Glutamic Acid, values which are of the same order with the value corresponding to a radiosterilized drug [13].

Table 1. Best fit parameters of the yielding of free radicals in four gamma irradiated aminoacids.

	$\kappa(KGy^{-1})$
Glycine	0. 498
L-Glutamic Acid	0. 092
DL-Serine	0. 161
DL-Asparagine	0. 221

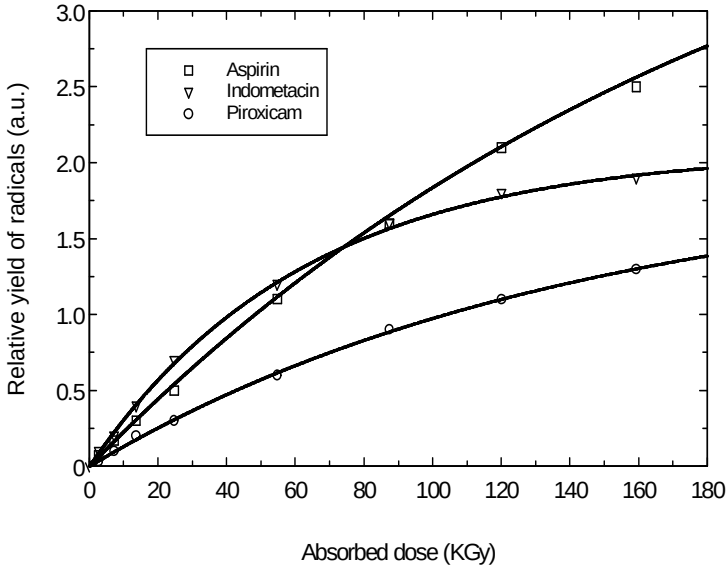

Fig. 3. The relative yield of radicals in three γ-irradiated drugs as a function of dose. The continuous lines represent the best fit calculated values.

The dose response of the investigated gamma-irradiated drugs from 2. 4 to 160 KGy recorded immediately after irradiation is shown in Fig. 3. Experimental data were fitted also with the first order kinetics and the best fit parameters corresponding to the three drugs are given in Table 2. As shown in Fig. 3 the number of the generated free radicals increases almost linear for low values of dose for all the samples.

Table 2. Best fit parameters of the yielding of free radicals in three gamma irradiated anti-inflammatory drugs.

	$\kappa(KGy^{-1})$
Aspirin	0. 006
Indomethacin	0. 017
Piroxicam	0. 014

This information implies that the free radicals must result from a reaction which follows very rapidly from the primary step of radiolysis. At higher values of the irradiation dose, the intensity of the ESR signal tends slowly to saturate. This dependence implies that the process of destroying the radicals by the radiation became comparable with the rate of their formation process. The values of the κ parameter are very close to those corresponding to other aromatic compounds [14]. Using the fit parameters κ and the ratio R/R_{lim}=0. 98 the following values of the saturation doses are obtained: ≈650 KGy for Aspirin, ≈230 KGy for Indomethacin and ≈280 KGy for Piroxicam. These values are much over the dose of 25 KGy corresponding to a radiosterilized drug [13]. The dose dependence of the relative yield of the radicals is comparable with the case of alanine [15], suggesting the possibility to use these anti-inflammatory drugs as gamma dosimeters. The tissue-equivalent drugs samples also appear to be appropriate for radiation therapy level dosimetry.

CONCLUSIONS

ESR spectroscopy is a very useful tool for the investigation of gamma-radiation effects in crystalline biomolecules which have no zero dose signal and the radiation induced free radicals are stable. The shape of the ESR spectra of gamma-irradiated Indomethacin and Piroxicam doesn't change by increasing the irradiation dose suggesting that only one radical is produced by gamma rays in these samples at room temperature.

The relative yield of free radicals in the investigated samples is described by a first order kinetics. The constants of destroying the free radicals by the radiation corresponding to the four aminoacids and to the three anti-inflammatory drugs are in very good agreement with the values obtained for polipeptides and aromatic compounds, respectively.

The relative yield of radicals in gamma-irradiated aminoacids is linear dependent with the irradiation dose only for low values of doses and it is rapidly approaching a limiting value over about 8 KGy, especially for Glycine and DL-Asparagine. The saturation doses for the aminoacids investigated are comparable with the dose corresponding to a radiosterilized drug. The relative yield of radicals in gamma-irradiated drugs is almost linear dependent with the irradiation dose under 100 KGy and the saturation doses are one order of magnitude greater than that corresponding to a radiosterilized drug.

REFERENCES

1. V. Chiż, O. Cozar, G. Damian, L. David, C. Cosma, R. Semeniuc, T. Drăgoiu, *Studia UBB Physica*, XXXIX (1), 17(1994).
2. O. Cozar, V. Chiş, L. David, G. Damian, I. Barbur, *J. Radioanal. Nucl. Chem.,* 220, 241(1997).
3. G. Lemaire, J*. Chim. Phys*., 91, 1192 (1994).
4. K. Sehested, E. Bjergbakke, N. W. Holm, H. Fricke, in: *Dosimetry in Agriculture, Industry, Biology and Medicine*, IAEA STI/PUB/311, Viena, p. 379, 1973.
5. K. van Laere, *Phd. Thesis*, University of Gent, 1992.
6. C. Ferradini, J. Pucheault, *Biologie et l'action des rayonnements ionisants*, Ed. Masson, Paris, 1983.
7. D. A. Svistunenko, G. T. Rikhireva, M. K. Pulatova, N. M. Emanuel, U. Eichhoff, *Bruker Report*, ISSN 0724-0185 (1992).
8. S. Yamanchi, N. Hirota, *J. Am. Chem. Soc*., 107, 5021 (1985).
9. D. H. Giamolva, D. F. Church, W. A. Pryor, *J. Am. Chem. Soc*., 108, 6646 (1986).
10. P. Riesz, T. C. Smitherman, C. D. Scher, *Int. J. Radiat. Biol*., 17, 389 (1970).
11. Y. Lion, G. Denis, M. M. Mossoba, P. Riesz, *Int. J. Radiat. Biol.*, 43, 71 (1983).
12. A. F. Usatii, I. C. Lazurkin, *Elementarnie procesi himii visokih energii*, p. 209, Nauka, Moskva, 1965.
13. F. Zeegers, B. Tilquin in "ESR Applications in Organic and Bioorganic Materials", B. Catoire (Ed.), Springer-Verlag, Berlin, 1992, p. 291.
14. L. A. Trofimov, A. A. Martinova, *Himia visokih energii*, 3, 279(1969).
15. D. Regulla, U. Deffner, *Int. J. Appl. Radiat. Isot.*, 33, 1101(1982).

STUDIA UNIVERSITATIS BABEŞ-BOLYAI, PHYSICA, XLII, 1, 1997

SPECTROSCOPIC AND MAGNETIC PROPERTIES OF THE DIMERIC $[CU(SO_4)\cdot(1,4\text{-DIHYDRAZINOPHTALAZINE})\cdot H_2O]_2$ COMPLEX

L. DAVID[1], O. COZAR[1], V. CHIŞ[1], D. RISTOIU[1], C. BĂLAN[1]

ABSTRACT. Copper (II) sulphate complex with 1,4-Dihydrazinophtalazine (DHP) was prepared and investigated by UV/VIS, IR and ESR spectroscopies and magnetic susceptibility measurements. The complex appears to have a square-pyramidal arrangement of C_{4v} symmetry with four nitrogen atoms in the basal (xOy) plane and an apical oxygen atom from a coordinated water molecule. Powder ESR spectrum and magnetic susceptibility measurements show the existence of dimeric species characterised by a fairly strong antiferromagnetic exchange coupling ($2J = -92\ cm^{-1}$).

INTRODUCTION

1,4-Dihydrazinophtalazine (DHP) is a drug with diminution effects of the blood pressure, being also used for the preparation of other kinds of drugs [1]. The structural formula of DHP (Fig. 1) suggests that it can function as multifunctional ligand because it contains six nitrogen atoms.

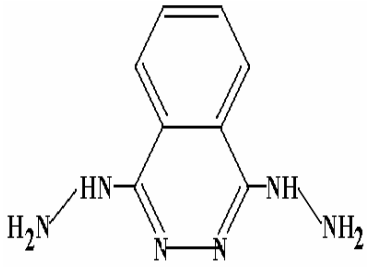

Fig. 1. Molecular structure of 1,4-Dihydrazinophtalazine (DHP).

[1] Babeş-Bolyai University, Faculty of Physics, 3400, Cluj-Napoca, Romania

The therapeutical effects often depend on the presence or absence of the metallic ions; thus any information concerning the interaction between metallic ions and DHP molecules are usefully and welcome .

For obtaining further information on the local structure of the metal ion the $[CuSO_4 \cdot DHP \cdot H_2O]_2$ compound was prepared and investigated by electronic, IR and ESR spectroscopies and by magnetic susceptibility measurements.

EXPERIMENTAL

The $[CuSO_4 \cdot DHP \cdot H_2O]_2$ was prepared as previously reported [3]. The electronic spectra were recorded using a SPECORD UV-VIS and diffuse reflectance spectra with a VSU-2G Carl-Zeiss Jena Spectrophotometer, in MgO pellets. Infrared spectra were recorded in the range 400-4000 cm^{-1} with a UR-20 Carl-Zeiss Jena Spectrophotometer, in KBr pellets. ESR measurements were performed at 9. 4 GHz (X-band) using a Varian E9 Spectrometer. Low temperature spectra were recorded by using an Oxford Instruments ESR 9 liquid-helium continuous-flow cryostat. The magnetic susceptibility of the powder sample was measured in temperature range 2. 4-300 K in a field of 2 T using a Metronique Ingenierie MSO3 SQUID magnetometer. Diamagnetic corrections were estimated from Pascal's constants.

RESULTS AND DISCUSSION

The diffuse reflectance spectrum of the title compound exhibits a band at 17500 cm^{-1} with a shoulder at 16500 cm^{-1} assigned to the $t_{2g} \rightarrow b_{1g}$ (d-d) transition. This can be correlated with a D_{4h} distorted symmetry particularly with a pentacoordinated species of C_{4v} symmetry [3-5]. It was found that dimeric species also exhibit a band in this range [6,7].

The values of the most important absorption IR bands are given in Table 1. The bands from 3500-2800 cm^{-1} region are characteristic for N-H and O-H stretching vibrations and those from 1700-1600 cm^{-1} region for the deformations of hydrazine group and water molecules [8,9]. Only one broad band at 1615 cm^{-1} is observed in the spectrum of Cu(II) complex, but there are two bands (δNH_2, δH_2O) in the IR spectrum of $DHP \cdot H_2SO_4 \cdot 2H_2O$.

The sulphate derivates exhibit the absorption bands at 1200-900 cm^{-1} (symmetric and antisymmetric stretching of the sulphate ion) and at 650-400 cm^{-1} (deformations of the same ion) [10]. The presence of ionic sulphate groups is suggested by $\Delta\nu_3(A_2)$ splitting (Table 1) which has different values for different symmetries [$\Delta\nu_3(C_{2v})$=120 cm^{-1}; $\Delta\nu_3(C_{3v})$=90 cm^{-1}; $\Delta\nu_3$ (uncoordinated, ionic) = 35-60 cm^{-1}]. Thus we can assume as a

result from Table 1 that the sulphate groups are present as non-coordinated counter ions.

Table 1. *IR absorption bands (cm^{-1})*

	$DHP{\cdot}H_2SO_4{\cdot}2H_2O$	$[Cu(SO_4){\cdot}DHP{\cdot}H_2O]_2$
νNH_2: $\nu_{as}(E)$+	3500	3460
$\nu_s(A_1)$	3330	3400
νOH_2: $\nu_{as}(B_1)$+	3100	3220
$\nu_s(A_1)$	2850	2860
$\delta NH_2(E)$	1632	1615
$\delta OH_2(A_1)$	1665	
$\delta M\text{-}OH_2$		755
$\nu_3(SO_4)$ (A_2)	1120	122; 1075; 1060
$\nu_1(SO_4)$ (A_1)	990	980
$\nu_4(SO_4)$ (F_2)	615	610
$\nu_2(SO_4)$ (E)	470	472

According to literature data [11] the 755 cm^{-1} band was assigned to $M\text{-}OH_2$ deformation vibrations.

Thus we may consider that the molecule of prepared compound contains basically two CuN_4O cromophores, the four nitrogen atoms being provided by two DHP molecules and the oxygen by a water molecule. A similar coordination mode has been recently reported by Ferraro et al. [12] in the case of copper(II)-bilirubinate (BR) complex where the Cu^{2+} is bonded to four nitrogen atoms coming from two molecules of BR. The water of hydration upon crystallisation is also coordinated at Cu^{2+} ion.

The powder ESR spectrum of the compound exhibits at room temperature an absorption typical for randomly oriented triplet state (S=1) of dimeric species having an axial symmetry with a small rhombic distortion [13]. The parallel (z) and the perpendicular (xy) allowed)Ms="1 fine structure transitions resulting from the zero-field splitting are shown in Fig. 2.

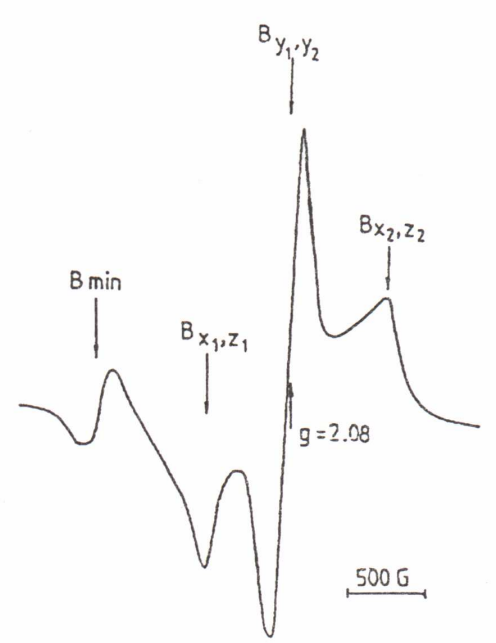

Fig. 2. Powder ESR spectrum of $Cu_2(SO_4)_2 \cdot 2DHP \cdot 2H_2O$ complex at room temperature

The strong central signal (≈3200 G) may be attributed to the contribution of dimeric $B_{y1,y2}$ absorption and also to the mononuclear impurities of spin S=1/2. The half field absorption (≈1590 G) is due to the forbidden $M_s=\pm 2$ transitions characteristic to dimeric species in which the Cu-Cu distance is longer than in the copper acetate-like dimers [14].

The spectrum of dimeric species can be described by the following spin Hamiltonian [15]:

$$\mathbf{H}=\beta\,\mathbf{g}\mathbf{S}\mathbf{B}+\mathrm{D}\left(\mathrm{S}_z^2-\frac{2}{3}\right)+\mathrm{E}\left(\mathrm{S}_x^2-\mathrm{S}_y^2\right)1$$

where $ is the Bohr magneton, **B** is the external magnetic field, **g** is the anisotropic Landé splitting tensor, **S** is the total spin vector, D and E are the zero field splitting parameters.

The magnetic field resonance absorption values allowed us to calculate $g_{\|}$, $g_{\perp}$, D, E and J parameters, following the procedure described by Chasteen [16]. We have obtained the values: 2J=-92 cm^{-1}, $g_{\|}$=2. 214, $g_{\pm}$=2. 089, D_{exp}=0. 080 cm^{-1}, D_{dd}= -0. 159 cm^{-1}, D_{ex}=0. 239 cm^{-1}, E=-0. 026 cm^{-1}.

The monomeric species absorptions (≈3200 G) increase with the

decrease of temperature (Fig. 3). The central part of the 4. 2 K spectrum is typical for isolated Cu^{2+} in a square-planar environment in the xOy plane. Characteristic values of the ESR parameters ($g_{||}$= 2. 207, $g_{\perp}$=2. 056, $A_{||}$=190 G) suggest the presence of CuN_4 chromophore [17]. The intensity of "half-field" transition decreases with the decrease of temperature and it can be shown even at 4. 2 K.

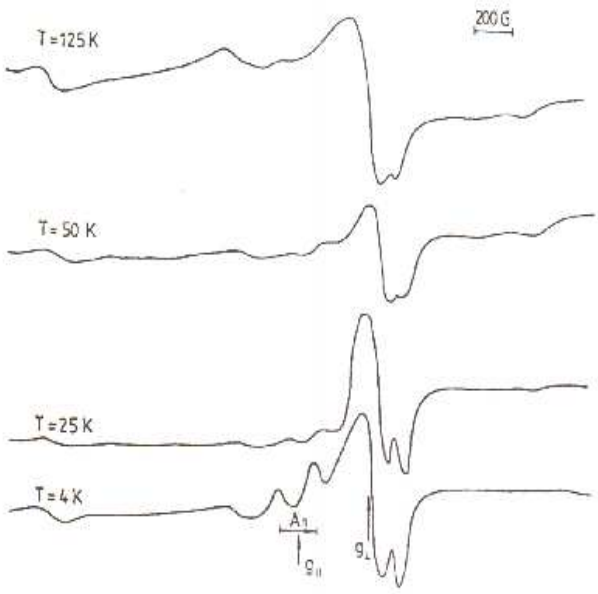

Fig. 3. Powder ESR spectra of $Cu_2(SO_4)_2 \cdot 2DHP \cdot 2H_2O$ complex in the 4÷125 K temperature range.

The magnetic susceptibility data show also the presence of dimeric species characterised by an antiferomagnetic coupling (Fig. 4). The separation between singlet and triplet state (2J) obtained by the fitting of experimental data with a $H=-2JS_1S_2$ Hamiltonian [18] are in agreement with those obtained from ESR spectra. The fitting values for the magnetic susceptibility data are: 2J= -92 cm^{-1}; g=2. 014; R=0. 032 [19].

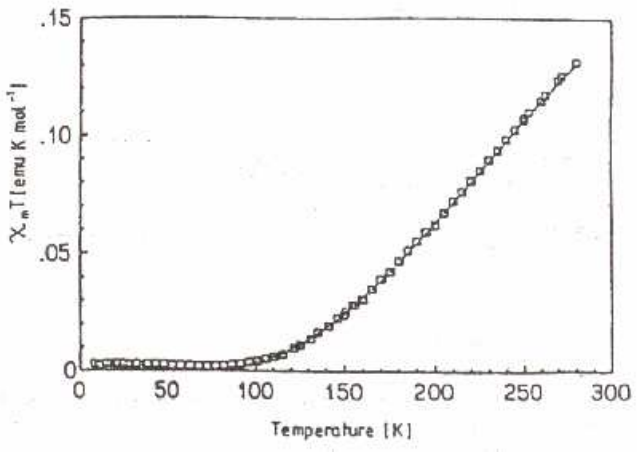

Fig. 4. Temperature dependence of $\chi_m T$ for $[CuSO_4 \cdot DHP \cdot H_2O]_2$ complex. The solid line represent the best fit calculated values.

CONCLUSIONS

IR spectra of the ligand and metal complex show that only one water molecule is coordinated at Cu ion and the others crystallised water molecules and SO_4^{2-} ion are ionic bonded. The diffuse reflectance spectrum suggests the existence of the C_{4v} local symmetry for the metal ions and the presence of dimeric species. ESR spectra at room temperature confirm the presence of dimeric species characterised by a fairly strong antiferromagnetic exchange coupling. The monomeric species of CuN_4 chromophore in the xOy plane prevail at 4. 2 K. The magnetic susceptibility data showed also the presence of dimeric species characterised by an antiferomagnetic coupling with a singlet-triplet separation of 92 cm^{-1}.

REFERENCES

1. R. Meier, J. Tripod, *Arch. Expl. Pathol. Phatmahol*. , 223, 338(1957).
2. R. Micu-Semeniuc, O. Cozar, L. David, R. Semeniuc, *Rev. Roum. Chem*. , 42(7), 627(1997).
3. B. J. Hathaway, A. A. Tomlinson, *Coord. Chem. Rev*. , 5, 1(1970).
4. B. J. Hathaway, D. E. Billing, *Coord. Chem. Rev.* , 5, 143(1970).
5. W. K. Musker, M. S. Hussain, *Inorg. Nucl. Chem. Lett. ,* 3, 271(1961).
6. L. Dubicki, *Austr. J. Chem. ,* 25, 1141(1972).
7. B. J. Edmondson, A. B. Lever, *Inorg. Chem*. , 4, 1608(1965).
8. D. Scargill, *J. Chem. Soc*. , 4444(1961).
9. H. Clark, C. S. Williams, *J. Chem. Soc.* , A, 1425(1966).
10. Iu. Ia. Haritonov, E. N. Deiciman, Zhur. *Neorg. Khim*. , 10, 853(1965).
11. G. Sartori, C. Furlani, A. Damiani, J. Inorg. *Nucl. Chem*. , 8, 119(1958).
12. J. R. Ferrero, J. G. Wu, R. D. Soloway, W. H. Li, Y. Z. Xu, G. R. Shen, *Appl. Spec. ,* 50, 7, 923(1996).
13. C. J. Gomez-Garica, E. Coronado, P. Gomez-Romero, N. Casan-Pastor, *Inorg. Chem*. , 32, 89(1993).
14. A. Bencini, D. Gatteschi, "EPR of Exchange Coupling Systems", Springer-Verlag, Berlin, 1990.
15. P. Sharrock, C. H. Thibandeau, A. Caille, *Inorg. Chem*. , 2, 510(1979).
16. N. D. Chasteen, *Inorg. Chem.* , 10, 2339(1971).
17. R. K. Ray, G. B. Kauffman, *Inorg. Chim. Acta*, 173, 207(1990).
18. R. L. Carlin, "Magnetochemistry", Springer-Verlag, Berlin, 1986.

STUDIA UNIVERSITATIS BABEŞ-BOLYAI, PHYSICA, XLII, 1, 1997

THEORETICAL CALCULATION FOR THE IONIZATION-EXCITATION OF THE HELIUM

L. NAGY[1], ZS. FÜLÖP[1]

ABSTRACT. The ionization-excitation cross-sections of the helium for proton and antiproton (electron) impact have been evaluated. We have performed theoretical calculations taking into account electron-correlation and time-ordering. We have used a perturbation expansion in the projectile-electron interaction, and have included in our calculations the first-order and the time-ordered second-order (TS2) terms. Electron correlation have been taken into account in the ground state by the use of configuration-interaction (CI) wavefunctions. Our results are in reasonable agreement with the experimental data.

INTRODUCTION

The many-electron processes in atomic and molecular collisions, like double ionization, ionization-excitation, double excitation, double capture, transfer excitation, have attracted much interest in the last decade.

The single electron transitions are relatively well understood. The electron correlation may be neglected in the description of these processes, and the independent electron approximation (IEA) is valid.

In the last years it has become clear, that in the interpretation of the two-electron transitions in atoms induced by charged particles and photons one must go beyond the independent-electron approximation. The study of these transitions is of fundamental importance in the understanding of few-body dynamics and the investigation of electron correlation effects. Theoretical [1-13] and experimental [14-19] studies have shown that at moderately fast velocities cross sections for negative projectiles are higher than those obtained with positive projectiles. The two-electron transitions may be described in terms of a coherent sum of first- and second-order amplitudes of a Born expansion in the interaction strength Z (projectile charge). The square of such a first- plus second-order amplitude yields to a

[1] Faculty of Physics, Babeş-Bolyai University, 3400 Cluj-Napoca, Romania

Z^3 contribution to physical observables such as transition probabilities and cross-sections. These Z^3 effects are reproduced by theoretical calculations only, if electron correlation is taken into account. In the IEA the first- and second-order amplitudes are 90^0 out of phase, and do not interfere.

The most studied target concerning the two-electron transitions was the helium atom. There have been published several experimental data and theoretical results for the different two-electron processes in the helium by charged particle impact. Calculations have been made for the double ionization [3-5], double excitation [6-10] and for the ionization-excitation [11,12] of the helium. Reading and Ford [4] have made the first elaborate calculations for a two-electron transition, the double ionization of helium, using the forced impulse method. They have shown that, for the double ionization, even for relatively high energies, there are significant non-dipole contributions, and the Z^3 terms are important. They have reproduced the difference in the cross sections for positively and negatively charged projectiles. In a recent, more complete work [4] they have reported very good quantitative agreement with experimental data for the double-ionization cross-section of helium by charged particles.

Theoretically the double excitation have been investigated by several authors using the coupled channel method [7,8]. One of us have performed a perturbation-expansion calculation for this process [10], and have obtained good quantitative agreement with the experimental data.

Less studied process is the simultaneous excitation and ionization. Cross-sections for the ionization-excitation of helium following electron and H^+, H_2^+ and H_3^+ ion impact have been measured [14,19]. The most recent measurements [14] have been performed for the velocity range from 3. 8-8. 5 a. u. for electrons, 1. 4-7. 5 a. u. for protons and 1. 4-4. 0 a. u. for H_2^+ and H_3^+ ions. The cross-section ratio of ionization-excitation to excitation have been also examined. The experimental data for the helium by proton and electron impact show that cross sections obtained with negative projectiles are higher than those for positive projectiles for the velocities above 3 a. u. (similarly to the double ionization).

There are only a few theoretical calculations for this two-electron transition. Rudge [11] have performed first-Born calculations. The first-order approximation for a two-electron transition is valid only for very high projectile velocities. This is the reason why at moderately high velocities the results of Rudge fail to reproduce the experimental data.

One of us have made second-order perturbation-expansion calculations for the ionization-excitation [12]. In those calculations electron-electron interactions have been taken into account by a mean-field

potential. In spite of this approximation, our method have gone beyond the IEA, because the change in the mean-field potential during the collision and the time-ordering effects have been taken into account. By this method the first-order amplitude is totally due to the shake mechanism (the relaxation of the second electron orbital after the transition of the first caused by a projectile-electron interaction). Electron correlation in the initial and the final states have been neglected. This is the reason why we have obtained our cross sections below the experimental data, and the difference between the data obtained positive and negative projectiles was too small.

In the present paper we present the improvement of the previous calculations taking into account the electron correlation in the ground state.

THEORETCAL FRAMEWORK

We have adopted the semiclassical approximation, meaning that the projectile is treated classically, and moves on a straight line trajectory. Further, as described in more detail in Ref. 2 and 3, we perform a perturbation expansion in terms of the projectile-electron interaction, and stop at the second-order term. The perturbation potential is the sum of the two projectile-electron interactions

$$V(t)=V_1(t)+V_2(t). \tag{1}$$

The first- and second-order transition amplitudes can be written [2]

$$a^{(1)} = -i\int_{-\infty}^{\infty} dt e^{i(E_f-E_i)t}\left\langle f\left|[V_1(t)+V_2(t)]\right|i\right\rangle \tag{2}$$

$$a^{(2)} = -\sum_k \int_{-\infty}^{\infty} dt e^{i(E_f-E_k)t}\left\langle f\left|[V_1(t)+V_2(t)]\right|k\right\rangle \times$$

$$\times\int_{-\infty}^{t} dt' e^{i(E_k-E_i)t'}\left\langle k\left|[V_1(t)+V_2(t)]\right|i\right\rangle. \tag{3}$$

In these formulae |*i*> stands for the initial state, |*k*> for the intermediate and |*f*> for the final state of the two-electron system. The cross section is obtained by squaring the modulus of the sum of the two amplitudes and integrating over the impact parameter

$$\sigma = \int |a^{(1)} + a^{(2)}|^2 \, d^2b \tag{4}$$

The two-electron wavefunctions $|i\rangle, |f\rangle$ and $|k\rangle$ cannot be calculated exactly. A good approximation can be reached by the use of configuration-interaction (CI) wavefunctions, which are written as a sum of products of one-electron orbitals:

$$|i\rangle = \sum_l c_l |i_1^l\rangle |i_2^l\rangle \tag{5}$$

$$|f\rangle = \sum_j d_j |f_1^j\rangle |f_2^j\rangle \tag{6}$$

$$|k\rangle = \sum_s b_s |k_1^s\rangle |k_2^s\rangle \tag{7}$$

Introducing the initial and final-state correlated wavefunctions in the first-order amplitude, one gets a sum of products of overlap integrals and one-electron transition amplitudes

$$a^{(1)} = -i \sum_l \sum_j c_l d_j^* \langle f_2^j | i_2^l \rangle \int_{-\infty}^{\infty} dt e^{i(E_f - E_i)t} \langle f_1^j | V_1(t) | i_1^l \rangle -$$

$$-i \sum_l \sum_j c_l d_j^* \langle f_1^j | i_1^l \rangle \int_{-\infty}^{\infty} dt e^{i(E_f - E_i)t} \langle f_2^j | V_2(t) | i_2^l \rangle \tag{8}$$

These terms can be interpreted as follows. The term containing the basic configurations both from the initial and the final states (l=1 and j=1, c_1 and d_1 being the largest coefficients), can be regarded as the shake term. If the one-electron orbitals from the initial and the final basic configurations have the same symmetry, the overlap integral $\langle f_i^1 | i_i^1 \rangle$ (for i equals 1 or 2) may be non-zero, and the shake process contributes to the transition of the second electron.

The terms with j=1 and l¹1 are responsible for the initial state correlation, while those with j¹1 and l=1 express the final-state correlation.

The terms with $j \neq 1$ and $l \neq 1$ contain both initial- and final-state correlation, but usually are less important, because both coefficients c_l and d_j are small.

In case of the ionization-excitation the final-state correlation is less important, because one electron leaves the atom, and the other remains bound. This is the reason why the final-state wavefunction is approximated by a simple product of two one-electron wavefunctions, where the continuum electron is screened by the excited one. In these conditions the first-order amplitude becomes

$$a^{(1)} = -i\sum_l c_l \left\langle f_2^{ex} \middle| i_2^l \right\rangle \int_{-\infty}^{\infty} dt e^{i\Delta E t} \left\langle f_1^{c} \middle| V_1(t) \middle| i_1^l \right\rangle -$$

$$-i\sum_l c_l \left\langle f_1^{c} \middle| i_1^l \right\rangle \int_{-\infty}^{\infty} dt e^{i\Delta E t} \left\langle f_2^{ex} \middle| V_2(t) \middle| i_2^l \right\rangle. \qquad (9)$$

Here DE is the energy transfer to electron system, V_1 and V_2 are the interaction potentials of the projectile with electron 1 and 2 respectively. The first term can be interpreted as the transition of one electron due to the interaction with the projectile to the continuum followed by a relaxation of the other electron to the final excited state (shake-up), while in the second term the projectile-electron interaction causes directly the excitation of one electron followed by a relaxation of the other electron to the continuum (shake-off). The initial-state correlation is very important, because neglecting it, the shake-up to the final *p* state would not be possible because the overlap integral of the initial *s* and the final *p* state would be zero. Taking into account the correlation, we have important contribution to the initial state from configurations of type *npn'p*.

In the second-order term the transition is caused by two consecutive projectile-electron interactions, meaning that the second-order process is possible without electron correlation. Assuming that the electron correlation would lead only to a small correction to the second-order amplitude, we have neglected the ground-state correlation in this term, taking into account for the initial state only the basic configuration.

With this approximation, the second order amplitude can be written:

$$a^{(2)} = -\int_{-\infty}^{+\infty} dt e^{i(\Delta E_0 - \Delta E^{ion})t} \left\langle f_2^{ex} \left| V_2(t) \right| i_2 \right\rangle \int_{-\infty}^{t} dt' e^{i(\Delta E^{ion} + \varepsilon_{f_1}^c)t'} \left\langle f_1^c \left| V_1(t') \right| i_1 \right\rangle -$$
$$- \int_{-\infty}^{+\infty} dt e^{i(\Delta E_0 - \Delta E^{ex} + \varepsilon_{f_1}^c)t} \left\langle f_1^c \left| V_1(t) \right| i_1 \right\rangle \int_{-\infty}^{t} dt' e^{i\Delta E^{ex} t'} \left\langle f_2^{ex} \left| V_2(t') \right| i_2 \right\rangle \quad (10)$$

In this term we keep track of the time ordering: the energy transfer to the individual electron depends on the order of the interactions. If the excitation occurs first, followed by an ionization, the energy transfer to the excited electron is ΔE^{ex}, and the ionization potential is $\Delta E_0 - \Delta E^{ex}$. If the ionization is first, then the ionization potential is ΔE^{ion}, and the excitation energy is $\Delta E_0 - \Delta E^{ion}$. Here $\Delta E_0 = \varepsilon_{f_2}^{ex} - E_0$ is the total energy transfer without the continuum state energy, and ΔE^{ex} and ΔE^{ion} are the experimental single ionization and excitation energies.

In the present calculation the final-state continuum one-electron wavefunctions have been calculated numerically. For the initial CI wavefunction we have used the wavefunctions computed by Nesbet and Watson [20]. The most important 7 configurations are products of 1s,2s,3s,2p and 3p one-electron orbitals

$$\Psi_1 = \Psi(s_1;0)\Psi(s_1;0);$$
$$\Psi_2 = \Psi(s_2;0)\Psi(s_2;0);$$
$$\Psi_3 = \frac{1}{\sqrt{2}}[\Psi(s_2;0)\Psi(s_3;0) + \Psi(s_3;0)\Psi(s_2;0)];$$
$$\Psi_4 = \Psi(s_3;0)\Psi(s_3;0);$$
$$\Psi_5 = \frac{1}{\sqrt{3}}[\Psi(p_1;1)\Psi(p_1;-1) - \Psi(p_1;0)\Psi(p_1;0) + \Psi(p_1;-1)\Psi(p_1;1)];$$
$$\Psi_6 = \frac{1}{\sqrt{6}}[\Psi(p_1;1)\Psi(p_2;-1) - \Psi(p_1;0)\Psi(p_2;0) + \Psi(p_1;-1)\Psi(p_2;1) +$$
$$+\Psi(p_2;1)\Psi(p_1;-1) - \Psi(p_2;0)\Psi(p_1;0) + \Psi(p_2;-1)\Psi(p_1;1)]; \quad (11)$$
$$\Psi_7 = \frac{1}{\sqrt{3}}[\Psi(p_2;1)\Psi(p_2;-1) - \Psi(p_2;0)\Psi(p_2;0) + \Psi(p_2;-1)\Psi(p_2;1)].$$

Here the numbers in brackets represent magnetic quantum numbers. The wavefunctions are normalized.

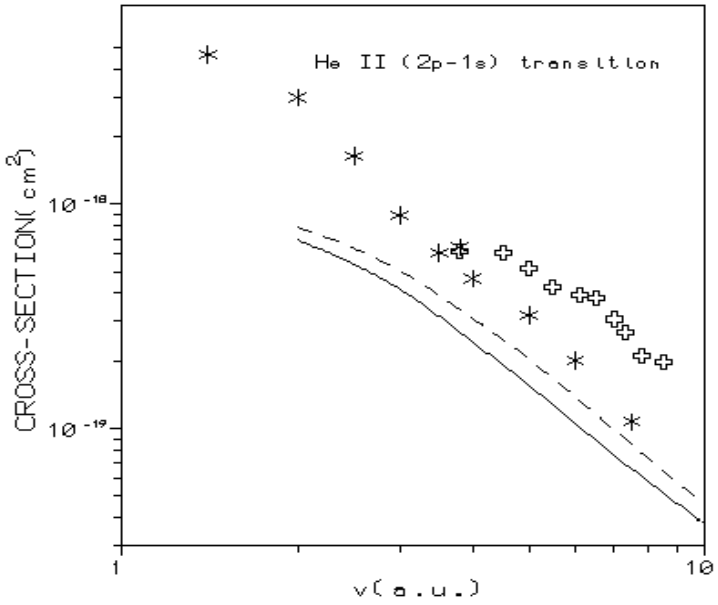

Fig. 1. Ionization-excitation cross-section of the helium by charged particle impact as a function of the projectile velocity. The dashed line represents our results for antiprotons and the solid line is for protons. ∗ stands for the experimental data obtained with protons and ✣ for equivelocity electrons [14].

RESULTS AND DISCUSSION

We have performed calculations for the simultaneous ionization and excitation of the helium to the 2*p* state by proton and antiproton (electron) impact for projectile velocities above 3 a. u. The initial state is described by correlated wavefunctions and the final state by a product of two one-electron wavefunctions. In the calculation of the amplitude and cross-sections, integrals over angles have been performed analytically, while the radial integrals in the matrix-element, the integrals over time, ejected electron energy, and the impact parameter have been calculated numerically.

Figure 1 shows our calculated cross sections as a function of the projectile velocity compared with the experimental data of Bailey et al [14]. Relative to our previous results [12] the calculated cross sections are much closer to the experimental data. Furthermore, the electron correlation in the initial state contributes substantially to the interference of the first- and second-order amplitudes leading to a larger difference in cross sections obtained for negatively and positively charged projectiles.

However, our results does not fit perfectly the experimental data. Electron correlation in the intermediate state (scattering correlation) may be important, too, and should be taken into account in further calculations.

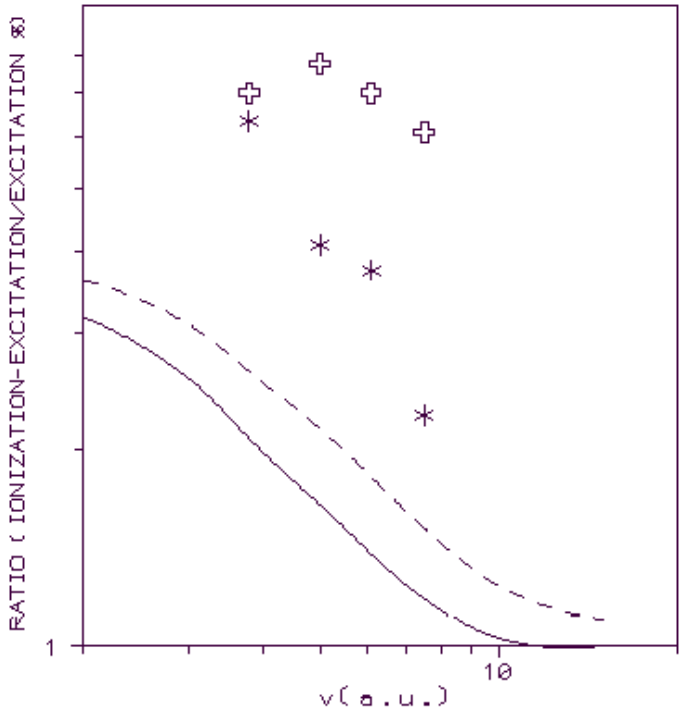

Fig. 2. The ratio of the ionization-excitation cross section to excitation of the 2p state as a function of the projectile velocity. Dashed line stands for antiproton results, solid line for protons, while stars represent experimental ratio for protons and crosses for electrons [14].

On figure 2 is represented the cross-section ratio of ionization-excitation to excitation. The figure shows a good qualitative agreement with the experimental data, but the experimental data are approximately two times higher than our calculated values. The high-velocity limit of this ratio tend to about 1%.

CONCLUSIONS

We can conclude that the inclusion of the CI wavefunctions in the description of the initial state of the target have improved substantially our previous calculations for the ionization-excitation of the helium by charged particle impact [12]. Our calculated cross-sections are in satisfactory agreement with the experimental data, and at the moment are the only one to reproduce the dependence of the ionization-excitation cross section on the sign of the projectile charge.

Further improvement may be reached by taking into account the electron correlation during the collision (scattering correlation).

REFERENCES

1. J. H. McGuire, *Adv. At. Mol. Opt. Phys*. 29, 217 (1991).
2. L. Nagy, *Nucl. Instr. Meth*. B 124, 271 (1997).
3. L. Nagy et al, *J. Phys.* B 30, 1939 (1997).
4. J. F. Reading, A. L. Ford, *J. Phys*. B 20, 3747 (1987).
5. A. L. Ford, J. F. Reading, *J. Phys*. B 27, 4215 (1994).
6. J. H. McGuire, J. C. Straton, *Phys. Rev*. A 43, 5184 (1991).
7. W. Fritsch, C. D. Lin, *Phys. Rev*. A 41, 4776 (1990).
8. F. Martin, A. Salin, *J. Phys*. B 28, 639 (1995).
9. A. L. Gudunov, V. A. Schipakov, *J. Phys*. B 26, L811 (1993).
10. L. Nagy, D. Bodea, *Nucl. Instr. Meth*. B 124, 401 (1997).
11. M. R. H. Rudge, *J. Phys*. B 21, 1887 (1988).
12. L. Nagy et al, *Phys. Rev.* A 52, R902 (1995).
13. L. Nagy, L. Vegh, *Phys. Rev*. A 50, 3984 (1994).

14. M. Bailey, R. Bruch, E. Rauscher, S. Bliman, *J. Phys*. B 28, 2655 (1995).
15. L. H. Andersen, P. Hvelplund, H. Knudsen, S. P. Moller, A. H. Sorensen, K. Elsner, K. G. Rensfeld, E. Uggerhoj, *Phys. Rev*. A 36, 3612 (1987).
16. J. P. Giese, M. Schulz, J. K. Swensen, H. Schoene, M. Benhennu, S. L. Varghese, C. R. Vane, P. F. Dittner, S. M. Shafroth, S. Datz, *Phys. Rev.* A 42, 1231 (1990).
17. A. Bordenave-Montesquieu et al, *J. Phys*. B 28, 653 (1995).
18. O. Pedersen, F. Folkmann, J. Phys. B 23, 441 (1990).
19. S. Fulling, R. Bruch, E. A. Rauscher, P. A. Neil, E. Trabert, P. H. Heckmann, J. H. McGuire, *Phys. Rev*. Lett. 68, 3152 (1992).
20. R. K. Nesbet, E. Watson, *Phys. Rev.* 110, 1073 (1958).

STUDIA UNIVERSITATIS BABEŞ-BOLYAI, PHYSICA, XLII, 1, 1997

QUANTUM CHAOS IN MULTI--MATRIX MODELS

E. VINTELER[1]

ABSTRACT. We propose a possible resolution for the problem of why the semicircular law is not observed, whilst the random matrix hypothesis describes well the fluctuation of energy spectra. We show in the random 2-matrix model that the interactions between the quantum subsystems alter the semicircular law of level density. We consider also other types of interactions in the chain- and star-multimatrix models. The connection with the Calogero-Sutherland models is briefly discussed.

1. INTRODUCTION

In heavy nuclei, the complicated many-body interactions lead to statistical theories which explain only the average properties. One of these theories is the random matrix hypothesis [1][2] (see also the more recent book [3]). It supposes that the nuclear hamiltonian in a arbitrary basis of functions is a N×N matrix with N large and elements distributed at random. The joint probability function of the eigenvalues $\lambda_1 \ldots \lambda_N$ of this matrix model is given by:

$$P(\lambda_1 \ldots \lambda_N)=\exp(-\Sigma_{i=1}^{N} \lambda_i^2) \, \Pi_{i<j}(\lambda_i-\lambda_j)^{\beta} \qquad (1.\ 1)$$

where β=1, 2, 4 for orthogonal, hermitean and, respectively unitary ensembles.

This probability distribution gives the familiar phenomenon of level repulsion: the likelihood of having neighboring energy levels separated by an energy spacing $\Delta\lambda_{ij}=\lambda_i-\lambda_j$ becomes vanishingly small as $\Delta\lambda_{ij}\to 0$. For two levels λ_1, λ_2, the plot of the probability $P(\Delta\lambda)$ in terms of energy spacing $\Delta\lambda=\lambda_1-\lambda_2$ shows a rise from zero for $\Delta\lambda=0$, reaches a peak (known as Wigner's surmise) and then decreases rapidly. This behaviour is completely different from the classical one, given by the Poisson distribution $P(\Delta\lambda)=\exp(-\Delta\lambda)$.

[1] Institute of Molecular and Isotopical Technology str. Donath 65-103, Cluj-Napoca 3400, Romania

Integrating over eigenvalues $\lambda_{k+1}\ldots\lambda_N$ we get the joint distribution function for few levels:

$$P(\lambda_1\ldots\lambda_k) = \int d\lambda_{k+1}\ldots d\lambda_N\, P(\lambda_1\ldots\lambda_N) \qquad (1.\ 2)$$

All these joint distribution functions can be expressed in terms of the Dyson correlation function $K(\lambda_1, \lambda_2)$:

$$P(\lambda_1\ldots\lambda_k) = \Sigma_\sigma(-1)^\sigma K(\lambda_1, \lambda_{\sigma 1})\ \ldots K(\lambda_k, \lambda_{\sigma k}):$$

where (is the permutation of k levels.

In the special case k=1 the Dyson correlation function coincides with level density $K(\lambda, \lambda)=P(\lambda)$.

The density of levels for the 1-matrix model satisfies the semicircular law:

$$P(\lambda)= (\beta N/2- \lambda^2)^{1/2}$$

and the Dyson correlation function behaves for $\sigma<<$(as:

$$K(\lambda-\sigma/2, \lambda+\sigma/2)\approx\sin(\pi\sigma P(\lambda)/ (\pi\sigma(\beta N/2))$$

Many experimental data of level distribution in nuclei confirm the statistical properties of the random matrix theory. There exists a universality of level fluctuation laws, as described by the Dyson correlation function. The fluctuation properties are shared by broad classes of models: several chaotic models [4], mesoscopic systems [5], etc. The random matrix hypothesis is in some respects a disappointing theory: although it predicts beautifully the observed level fluctuations, it fails to describe adequately the density of levels. The semicircular law was never observed in the experiments.

A possible resolution of problem is to consider instead one random matrix few random matrices in interaction. As we will see, even a small interaction gives a calitatively new behaviour for the level density.

An interesting generalization of the random matrix hypothesis is to consider q matrices describing q nuclear systems in interaction. The total action of such system is:

$$S_1=\Sigma_{\alpha=1}^{q}\Sigma_{i=1}^{N}(t_\alpha(\lambda_i^{(\alpha)})^2 + u_\alpha\lambda_l^{(\alpha)}) + \Sigma_{\alpha=1}^{q}\Sigma_{i=1}^{N} c_\alpha\lambda_i^{(\alpha)}\lambda_i^{(\alpha+1)} \qquad (1.\ 3)$$

This system describes a chain of matrices with neighbour interaction. We can add a term describing the two-body interaction of constituent nuclear subsystems:

$$\Sigma|_{\alpha-\beta| \neq 1}\Sigma_{i=1}^{N} c_{\alpha,\beta}\lambda_i^{(\alpha)}\lambda_i^{(\beta)}$$

We have different sets of energy levels $\lambda_1^{(\alpha)} \ldots\lambda_N^{(\alpha)}$, $\alpha=1\ldots q$ with distribution probability:

$$P(\lambda_1^{(1)}, \ldots \lambda_N^{(1)} \ldots \lambda_1^{(q)}, \ldots\lambda_N^{(q)})= \exp(S)\Pi_{i<j} (\lambda_i^{(1)} -\lambda_j^{(1)}) (\lambda_i^{(q)} -\lambda_j^{(q)}) \qquad (1.\ 4)$$

We have level repulsion only for the first and last energy level set. Hence for this model the intermediate energy level sets are "classical" and interact with "quantum" first and last energy level sets. Integrating over all intermediate matrices we remain with a two-matrix model.

Kharchev and others have considered the so-called conformal matrix models that contain additional repulsion terms also for intermediate matrices [6].

Another special random matrix model is the star-matrix model having the action:

$$S_2=\Sigma_{i=1}^{N} (t_0 (\lambda_i^{(0)})^2 + u_0\lambda_i^{(0)})+\Sigma_{\alpha=1}^{q}\Sigma_{i=1}^{N} (t_\alpha(\lambda_i^{(\alpha)})^2 + u_\alpha\lambda_i^{(\alpha)}) + \quad (1.\ 5)$$
$$+\Sigma_{\alpha=1}^{q}\Sigma_{i=1}^{N} c_\alpha\lambda_i^{(\alpha)}\lambda_i^{(0)}$$

The joint distribution of this model reduces again to that of 2-matrix model.

2. QUANTUM CHAOS IN TWO-MATRIX MODEL

In the more wide context of quantum chaos, the one-matrix model describes the statistical properties of the non-integrable model with hamiltonian [7]:

$$H=H_0+u\varphi$$

the hamiltonian H_0 is deterministic and (is an external random perturbation.

For example, the one-matrix model could describe hydrogen in a random magnetic field.

The two-matrix model describes the correlation between the energy spectra of two systems with the hamiltonians:

$$H_\alpha=H_{\alpha 0}+u_\alpha\varphi,\ \alpha=1,\ 2$$

For example, it could describe an electron moving in a ring threaded by a magnetic flux (described by the hamiltonians $H_{\alpha 0}$) and with the electron scattering on impurities in the ring (described by the random interaction φ). This example is important in the study of mesoscopic systems [8], [9].

In this section we show that the 2-matrix pure probability distributions $P(\lambda, \lambda')$, $P(\mu, \mu')$ do not behave qualitatively different from those of 1-matrix model. The spectra are only shifted and rescaled due to the interaction φ.

Instead, the mixed probability distribution $P(\lambda, \mu)$ is specific only to the 2-matrix model. When the two spectra of H_1 and H_2 are rescaled identicaly (the rescalings are equal $a_1=b_1$ in rel. (2. 5) or $\varepsilon=0$ in rel. (2. 17)), the hamiltonians $H_1=H_2$ and reduces to that of the 1-matrix model. In this case $P(\lambda, \mu)$ reduces to the usual semicircular law.

When we have a small asymmetry in the spectra ($\varepsilon \neq 0$ in rel. (2. 17) we get a qualitatively new picture: $P(\lambda, \mu(\lambda)$ presents peaks and valeys as we increase the asymmetry ε. The observed behaviour is the quantum analog for chaotical behaviour of two interacting classical oscilators.

For equal frequencies, the two oscilators are resonant and behave as a single oscilator. From the quantum point of view, the spectra are equally spaced and there is no energy transfer between the oscilators. When the frequencies are slightly different the probability $P(\lambda, \mu)$ describes the quantum analog of beating.

We apply the orthogonal polynomial method [2] to our two-matrix model. Other useful approaches (not used here) to study these models are the saddle-point method [10] and the supersymmetric method [11].

We introduce the distribution probability:

$$P(\lambda_1 \ldots \lambda_N, \mu_1 \ldots \mu_N) = \exp \Sigma_{i=1}^{N} (V_1(\lambda_i) + V_2(\mu_i) + c_i \lambda_i \mu_i) \Pi_{i<j} (\lambda_i - \lambda_j)(\mu_i - \mu_j) \quad (2.\ 1)$$

with $V_\alpha = t_\alpha \tau^2 + u_\alpha \tau$, $\alpha = 1, 2$ and the joint distribution function:

$$P(\lambda_1 \ldots \lambda_i, \mu_1 \ldots \mu_j) = \int d\lambda_{i+1} \ldots d\lambda_N \, d\mu_{j+1} \ldots d\mu_N \, P(\lambda_1 \ldots \lambda_N, \mu_1 \ldots \mu_N) \qquad (2.\ 2)$$

We study the particular case of the probability distributions for the correlation between only 2 energy levels.

2. 1. *The pure probability distributions $P(\lambda, \lambda')$, $P(\mu, \mu')$*

We demonstrate that the level densities $P(\lambda)$, $P(\mu)$ and the joint probability distributions $P(\lambda_1, \lambda_2)$, $P(\mu_1, \mu_2)$ coincide with those of the hermitean 1-matrix model with distribution probability (1. 1.):

$$P(\lambda)=P_{Herm}(\lambda'),\ P(\mu)=P_{Herm}(\mu') \qquad (2.\ 3)$$
$$P(\lambda_1, \lambda_2) =P_{herm}(\lambda_1', \lambda_2'),\ P(\mu_1, \mu_2) =P_{Herm}(\mu_1', \mu_2')$$

The new joint probability distributions $P(\lambda, \mu)$ behave in a different way because we have not energy repulsion between levels of different sets.

If we set from the beginning the coupling c=0 we get two independent orthogonal 1-matrix models and we have:

$$P(\lambda, \mu) =P_{Orth}(\lambda')P_{Orth}(\mu')$$

For $c \neq 0$, $P(\lambda, \mu)$ behaves like the 1-matrix Dyson correlation function:

$$P(\lambda, \mu) \approx K(\lambda, \mu)$$

When c (0, $P(\lambda, \mu)$ does not split into two orthogonal 1-matrix models.
Here λ', μ' are related with the coefficients of the potentials V_i in relation (2. 1):

$$\lambda'=(\lambda-a_0)/ (2a_1)^{1/2},\ \mu'=(\mu-b_0)/ (2b_1)^{1/2} \qquad (2.\ 4)$$

through the relations:

$$a_0 = \frac{c_1u_2 - 2\,t_2u_1}{4t_1t_2 - c_{11}^2}, b_0 = \frac{c_1u_1 - 2\,t_1u_2}{4t_1t_2 - c_{11}^2},$$
$$a_1 = -\frac{2\,t_{2_1}}{4t_1t_2 - c_{11}^2}, a_0 = -\frac{2\,t_{1_1}}{4t_1t_2 - c_{11}^2} \qquad (2.\ 5)$$

In the rest of this section we demonstrate the above relations.

Orthogonal polynomials (and η:

$$\xi_n(\lambda) = \lambda^n+\ldots,\ \eta_n(\mu) = \mu^n+\ldots$$

satisfy the orthogonality condition:

$$\int d\alpha d\mu \xi_n(\lambda)\, \eta_m(\mu) \exp(V_1+V_2+c\lambda\mu) = h_n\, \delta_{nm} \qquad (2.\ 6)$$

where $h_n=h_0\, R^n$ and $R=c/(4t_1t_2-c^2)$.

For quadratic potentials as those in (2. 1) we have the following recursion relations of the orthogonal polynomials:

$$\lambda\xi_n(\lambda) = \xi_{n+1}(\lambda) + a_0\xi_n(\lambda) + a_1\xi_{n-1}(\lambda) \qquad (2.\ 7)$$

$$\mu\eta_n(\mu) = \eta_{n+1}(\mu) + b_0\eta_n(\mu) + b_1\eta_{n-1}(\mu)$$

Solving these recursion relations it follows that ξ, (are Hermite functions:

$$\xi_n(\lambda) = \alpha_n H_n(\lambda'),\ \eta_m(\mu) = \beta_m H_m(\mu')$$

To get the proportionality coefficients α_n, β_m we use the orthogonality relation and the Gauss transform:

$$(2\pi u)^{-1/2}\int dy \exp[-(x-y)^2/2u]\, H_n(y) = (1-2u)^{n/2} H_n((1-2u)^{-1/2} x) \qquad (2.\ 8)$$

Writing the action as:

$$S=V_1(\lambda)+V_2(\mu)+c\lambda\mu=t_1\lambda^2 + u_1\lambda+ t_2\mu^2 + u_2\mu+c\lambda\mu=$$

$$=S_0+t_2[\mu+(u_2+c\lambda)/2t_2]^2-[(\lambda-a_0)/(2a_1)^{1/2}]^2$$

with:

$$S_0= -(t_1u_2^2 + t_2u_1^2-c\,u_1u_2)/(4t_1t_2-c^2)$$

we have:

$$\int d\lambda d\mu \xi_n(\lambda)\,\eta_m(\mu)\exp(V_1+V_2+c\lambda\mu) =$$

$$=\alpha_n\beta_m\delta_{nm}\exp(S_0)\,2\pi(2c)^n\, n!/(4t_1t_2-c^2)^{(n+1)/2} = \qquad (2.\ 9)$$

$$= h_0\delta_{nm}[c/(4t_1t_2-c^2)]^n$$

In conclusion

$$\xi_n(\lambda) = (2(n!)^{-1/2}\, 2^{-n/2}\,(2a_1)^{n/2} H_n(\lambda') \qquad (2.\ 10)$$

$$\eta_m(\mu) = (2(n!)^{-1/2}\, 2^{-n/2}\,(2b_1)^{n/2} H_n(\mu')$$

and

$$h_0 = (4t_1t_2-c^2)^{-1/2}\exp(S_0)$$

We can now calculate the joint probability distribution $P(\lambda, \mu)$. Since we can write the two Vandermonde determinants in terms of orthogonal polynomials ξ_n, η_m

$$\Delta(\lambda)\Delta(\mu)= \Sigma_n\xi_n(\lambda_1)\,\Xi_n(\lambda_2\ldots\lambda_N)\Sigma_m\eta_m(\mu_1)\,\Theta_m(\mu_2\ldots\mu_N)$$

and the algebraic complements satisfy:

$$\int \Pi_{i=2}^{Nd}(d\lambda_i\, d\mu_i)\,\Xi_n(\lambda_2\ldots\lambda_N)\,\Theta_m(\mu_2\ldots\mu_N) = (N-1)!\,\delta_{nm}$$

we get for the joint probability distribution the following relation:

$$P(\lambda, \mu)= (1/N) \exp(S) \Sigma_{n=0}^{N-1} h_n^{-1} \xi_n (\lambda)\eta_n (\mu)$$

It is easy to derive the expression for symmetric joint distribution of pairs of eigenvalues in terms of $P(\lambda, \mu)$:

$$P(\lambda_1 \ldots \lambda_k, \mu_1 \ldots \mu_k) = \Sigma_\sigma (-1)^\sigma P(\lambda_1, \mu_{\sigma 1}) \ldots P(\lambda_k, \mu_{\sigma k})$$

Integrating in $\lambda_{j+1} \ldots \lambda_k$ we obtain the asymmetric joint distribution of eigenvalues:

$$P(\lambda_1 \ldots \lambda_j, \mu_1 \ldots \mu_k) = \Sigma_\sigma (-1)^\sigma P(\lambda_1, \mu_{\sigma 1}) \ldots P(\lambda_j, \mu_{\sigma j}) P(\mu_{\sigma j+1}) P(\mu_{\sigma k})$$

In the limit of large N we have the usual behaviour of semi-circular law:

$$P(\lambda)= (2N- \lambda'^2)^{1/2}, P(\mu)= (2N-\mu'^2)^{1/2\lambda}$$

2. 2. *The mixed probability distribution $P(\lambda, \mu)$*

To calculate the joint distribution of two eigenvalues $P(\lambda, \mu)$ in the large N limit we associate it with the quantum mechanical system :

$$[1/2 p_\lambda^2+p_\mu^2)/2+V_1(\lambda)+V_2(\mu)+c\lambda\mu]\varphi_n(\lambda)\psi_m(\mu)=E_{nm}\, \varphi_n(\lambda)\psi_m(\mu)$$

where $p_\lambda=i\delta/\delta\lambda$, $p_\mu=i\delta/\delta$(are the usual momenta operators and

$$\varphi_n(\lambda) = \exp(-\lambda'^2/2)\eta_n(\lambda) \qquad (2.\ 12)$$
$$\psi_m(\mu) = \exp(-\mu'^2/2)\xi_m(\mu)$$

For c=0 we get two decoupled quantum systems:

$$(p_\lambda^2+\lambda'^2)\varphi_n(\lambda)=2E_{1,\,n}\varphi_n(\lambda) \qquad (2.\ 13)$$
$$(p_\mu^2+\mu'^2)\psi_m(\mu)=2E_{2,\,m}\psi_m(\mu)$$

where $E_{nm}=E_{1,\,n}+E_{2,\,m}$.

In the large N limit E_{nm} behaves like $\approx N$ and since we are searching for symmetric solutions we have $E_{1,\,n}=E_{2,\,m} \approx N/2$. The joint distribution of two eigenvalues $P(\lambda, \mu)$ will be:

$$P(\lambda, \mu)= (2E_{1,\,n}-\lambda'^2)^{1/2} (2E_{2,\,n}-\mu'^2)^{1/2} \qquad (2.\ 14)$$

or

$$P(\lambda, \mu)= (N-\lambda'^2)^{1/2} (N-\mu'^2)^{1/2}$$

We can see that for c=0, $P(\lambda, \mu)$ is the product of density energy levels for orthogonal ensembles. If we integrate the last matrix, we get the 1-matrix model. In our case this is equivalent with the condition $2E_{2,\,m}=p_\mu^2+V_2(\mu)=0$ in (2. 13) or in other words the second system has no

contribution in the joint distribution of two eigenvalues. The equation (2. 14) is replaced by:

$$P(\lambda)= (N-\lambda'^2)^{1/2}$$

For c(0, after summing relation (2. 11) and using the asymptotic formula (n large) for the Hermite polynomial (near the origin):

$$H_n=\exp(x^2)[\Gamma(n+1)/\Gamma(n/2+1)] \cos [(2n+1)^{1/2}-n\pi/2]+O(n^{-1/2})$$

we obtain (up the exponent $S+(\lambda'^2+\mu'^2)/2$):

$$P(\lambda, \mu)\approx\sin [(2N)^{1/2}(\lambda'-\mu')]/ [\pi N(\lambda'-\mu')], \lambda, \text{(near 0)} \quad (2.\ 15)$$

We also get for arbitrary λ, (with $|\lambda-\mu|<< \lambda, \mu$:

$$P(\lambda, \mu)\approx[\sin (2N-(\alpha l)^2)^{1/2} (\alpha\lambda)\varepsilon]/[\pi N \varepsilon(\alpha\lambda)] \quad (2.\ 16)$$

where:

$$\varepsilon= 1/ (2a_1)^{1/2} - 1/ (2b_1)^{1/2}$$
$$\alpha= (1/ (2a_1)^{1/2} - 1/ (2b_1)^{1/2})/2 \quad (2.\ 17)$$

This result was also obtained independently by [12] (see also the paper [13]) in the more general case when λ, (are arbitrary with no other restrictions. (I would like to thank D'Anna for pointing me out his paper with Brezin and Zee [12])

For the asymmetric potential $t_1=1/(a+\tau)^2$, $t_2=1/(a-\tau)^2$, ($\tau<< a$) and a small interaction $c\approx0$, we have $\varepsilon\approx\tau/a^2$, $\alpha\approx1/(2a)$ and $\varepsilon<< \alpha$. When $\tau\rightarrow0$ (symmetric potential) $P(\lambda,\mu\approx\lambda)$ tends to the level density of hermitean 1-matrix model $P_{Herm}(\lambda)$. The interaction (even a small one) of asymmetric energy levels changes dramatically the level density $P(\lambda, \lambda)$ of the system.

If for $\tau\rightarrow0$ we get the usual semicircular law, a small asymmetry creates some peaks in the level density $P(\lambda, \lambda)$ (see figure 1).

In figure 1 we represent the level density P(x, x) in terms of the energy $x=\alpha\lambda$ and the asymmetry $y=N\varepsilon$. For y=0 we have the semicircular law $P(x, x)=(2N-x^2)^{1/2}$ and for small y \neq 0 we get the oscilations of level density. (see formula 2. 16).

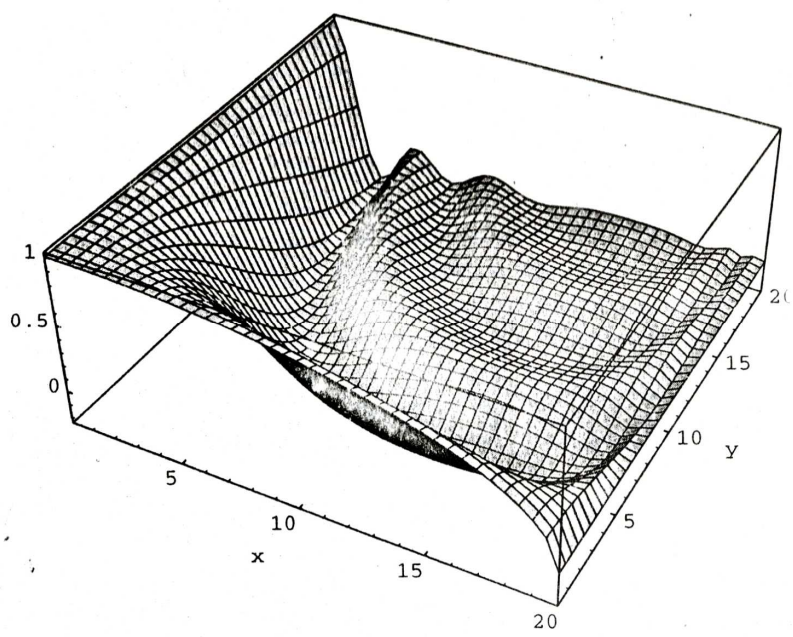

Figure 1 represents the level density P(x, x) in terms of the energy x=α(and the asymmetry y=Nε. For y =0 we have the semicircular law P(x, x)= $(2N-x^2)^{1/2}$ and for small y (0 we get the oscilations of level density.

3. q-MATRIX MODEL

As a random q-multimatrix model we choose the model with partition function:

$$Z=\int \quad \Pi_{\alpha=1}^{q} l_{(}\Delta(l_1)\ \Delta(l_q)\ \exp(\Sigma_{\alpha=1}^{q} t_{(}\lambda_\alpha{}^2 + \Sigma_{\alpha=1}^{q-1} c_{(}\lambda_{(}\lambda_{\alpha+1} \quad (3.\ 1)$$

We show that the joint probability is :

$$P(\lambda_\alpha,\ \lambda_\beta)=P_{herm}\,(\lambda_\alpha',\ \lambda_\beta'),\ 1((\leq((q \qquad (3.\ 2)$$

where:

$$\lambda_\alpha'=\lambda_\alpha/\ (2a_\alpha)^{1/2}$$

The parameters $a_{(}$are the coefficients of the Q-matrices.

To calculate the joint probability $P(\lambda_\alpha, \lambda_\beta)$ we integrate over all other eigenvalues $d\lambda_l^{(\gamma)}$, $\gamma(\alpha, \beta$. In this way we obtain the joint probability of two-matrix model for which we already know the result.

However, the physics of the multi-matrix model is richer than that of the 2-matrix model. But this could be observed only in the joint probabilities with at least 3 energy levels. Another issue is that we can study the interaction between the intermediate " classical" (or Poisson) sets of energy levels (those with $2(\alpha(q-1$ and linear potentials $V_\alpha = s_(\lambda_\alpha)$ and the "quantum" sets (with $\alpha=1, q$). We can interpret the q-matrix like an one-dimensional chain of atoms with localized states. Disorder is introduced through the boundary "quantum" atoms. The interesting problem is to compute the necessary conditions to have extended, conducting states. A concrete application of this model is the chain of polyacetilene.

The $Q(\alpha)$ have only three non—vanishing diagonal lines, the main diagonal and the two adjacent lines.

$$Q(\alpha) = b_(I_+ + a_(\varepsilon_- \qquad (3.\ 3)$$

where in the particular cases we know that $b_1 = 1$ and $a_q = R$. We can write the parameters in terms of the determinants of two matrices (weuse the results of the paper [14]):

$$\begin{aligned} b_(&= (-1)^(c_1c_2\ldots c_{\alpha-1})^{-1} \det X_{\alpha-1} \\ R &= (-1)^(c_1c_2\ldots c_{\alpha-1} \det X_q \\ a_(&= (-1)^(c_1c_2\ldots c_{\alpha-1} \det X_{\alpha+1} / \det X_q \end{aligned} \qquad (3.\ 4)$$

The matrices $X_($and Y_α, are given by relations:

$$X_\alpha \equiv. \left(\begin{array}{cccccc} 2t_1 & c_1 & 0 & ... & 0 & 0 \\ c_1 & 2t_2 & c_2 & ... & 0 & 0 \\ 0 & c_2 & 2t_3 & ... & 0 & 0 \\ ... & ... & ... & ... & ... & ... \\ 0 & 0 & 0 & ... & 2t_{\alpha-1} & c_{\alpha-1} \\ 0 & 0 & 0 & ... & c_{\alpha-1} & 2t_\alpha \end{array}\right) \qquad (3.\ 5\text{-}3.\ 6)$$

and

$$Y_\alpha \equiv. \left(\begin{array}{cccccc} 2t_\alpha & c_\alpha & 0 & ... & 0 & 0 \\ c_\alpha & 2t_{\alpha+1} & c_{\alpha+1} & ... & 0 & 0 \\ 0 & c_{\alpha+1} & 2t_{\alpha+2} & ... & 0 & 0 \\ ... & ... & ... & ... & ... & ... \\ 0 & 0 & 0 & ... & 2t_{q-1} & c_{q-1} \\ 0 & 0 & 0 & ... & c_{q-1} & 2t_q \end{array}\right)$$

Of course $Y_1=X_q$.

Besides the usual orthogonal polynomials (which could be introduced as in 2-matrix models case), we introduce also the basic intermediate functions (this was made previously for multi-matrix models in [15]):

$$\xi_n^{(\alpha)}(l_\alpha) = \int \Pi_{\beta=1}^{\alpha-1} dl\_\{\beta\}\xi_n(\lambda_1)\exp(S_\alpha) \qquad (3.\ 7)$$

$$\eta_n^{(\alpha)}(l_\alpha) \int \Pi\_\{\beta=\alpha+1\}\^\{q\} dl_\beta \exp(S_\alpha') \qquad (3.\ 8)$$

where we denote

$$S_\alpha=\Sigma_{\beta=1}^{\alpha-1} t_(\lambda_\beta^2 +\Sigma_{\beta=1}^{\alpha-1} c_(\lambda_(\lambda_{\beta+1}$$

$$S_\alpha'=\Sigma_{\beta=\alpha+1}^{q-1} t_(\lambda_\beta^2 +\Sigma_{\beta=\alpha}^{q-1} c_(\lambda_(\lambda_{\beta+1}$$

Obviously we have:

$$\xi_n^{(1)}(l_1)=\xi_n(\lambda_1), \qquad \eta_n^{(q)}((_q)=\eta_m(\lambda_q).$$

In the general case for arbitrary potentials one sees immediately that $\xi^{(\alpha)}$ and $\eta^{(\alpha)}$ are not polynomials anymore. In the case of gaussian potentials these intermediate functions are again Hermite functions, but with different arguments. In the general case, they still satisfy an orthogonality relation

$$\int \Pi_{\gamma=\alpha}{}^{(}d\lambda_{(}\xi_n{}^{(\alpha)}(\lambda_\alpha)\ \exp(S\text{-}S_\alpha\text{-}S_\alpha')(\lambda_\alpha)\eta_m{}^{(\beta)}(\lambda_\beta) = \delta_{nm}h_n,\ c \qquad (3.\ 9)$$

The equations satisfied by basic intermediate functions are:

$$\lambda_\alpha\xi^{(\alpha)}=Q_\alpha\xi^{(\alpha)},\ 1((\leq q \qquad (3.\ 10)$$
$$\lambda_\alpha\eta^{(\alpha)}=Q_\alpha\eta^{(\alpha)},\ 1((\leq q$$

These equations together with the explicit form of Q-matrices permits to find the basic intermediate functions $\xi_n{}^{(\alpha)}$, $\eta_m{}^{(\alpha)}$:

$$\lambda_{(}\xi_n{}^{(\alpha)}\ (\lambda_\alpha) = b_\alpha\xi_{n+1}(\lambda_\alpha) + a_\alpha\xi_{n-1}(\lambda_\alpha) \qquad (3.\ 11)$$
$$\lambda_{(}\eta_n{}^{(\alpha)}\ (\lambda_\alpha) = (a_{(}/R)\ \eta_{n+1}(\lambda_\alpha) + b_\alpha R\ \xi_{n-1}(\lambda_\alpha)$$

Solving these recursion relations it follows that $\xi^{(\alpha)}$, $\eta^{(\alpha)}$ are Hermite functions for gaussian potentials:

$$\xi_n{}^{(\alpha)}\ (\lambda_\alpha) = (2(n!)^{-1}\ 2^{-n/2}\ (2a_1)^{n/2}\ H_n(\lambda_\alpha'),$$
$$\eta_n{}^{(\alpha)}\ (\lambda_\alpha) = (2(n!)^{-1}\ 2^{-n/2}\ (R^2/2a_1)^{n/2}\ H_n(\mu_\alpha')$$

Using intermediate basic functions we get for joint probability:

$$P(\lambda_\alpha, \lambda_\beta)= \int\ (\Pi_{i=2}{}^{N}\ d\lambda_i{}^{(\alpha)}d(_i{}^{(\beta)})\ (\Pi_{i=1}{}^{N}\Pi_{\gamma=\alpha+1}{}^{\beta\text{-}1}\ d\lambda_i{}^{(\gamma)}$$
$$\det_{ij}[\xi_i{}^{(\alpha)}\ ((_j{}^{(\alpha)})]\det_{ij}[\eta_i{}^{(\alpha)}\ (_j{}^{(\alpha)})]\exp(S\text{-}S_\alpha\text{-}S_\beta') \qquad (3.\ 12)$$

Integrating over eigenvalues $d\lambda_i{}^{(\gamma)}$, $\gamma=\alpha+1$, \… β-1 we obtain the joint probability of two-matrix model for which we already know the result. Hence we get the result (3. 2).

All the derivation above is valid also for more general potentials, polynomial-like $V_\alpha(\tau)=\Sigma_{k=1}{}^{p(}t_k\tau^k$ or not.

The sufficient ingredients are the coefficients of the Q-matrices.

4. STAR-MATRIX MODEL

This model is interesting because it is supposed to describe the q-Potts model on a random lattice [16]. It was also used to describe the cristal growth. The limiting cases q(0 and q(1 describe the tree-polymers, and the percolation respectively.

We study the star-matrix model with partition function:

$$Z=\left(\Pi_{i=1}^{N}\left(dl_i^{(0)}\Pi_{\alpha=1}^{q}dl_i^{(\alpha)}\right)\Pi_{i<j}\left[\left(\lambda_i^{(0)}-\lambda_j^{(0)}\right)\Pi_{\alpha=1}^{q}\left(\lambda_i^{(\alpha)}-\lambda_j^{(\alpha)}\right)\right]\right.$$

$$\exp\{\Sigma_{i=1}^{N}[V_0(\lambda_i^{(0)})+\Sigma_{\alpha=1}^{q}V_\alpha(\lambda_i^{(\alpha)})+\Sigma_{\alpha=1}^{q}c_(\lambda_i^{(\alpha)}\lambda_i^{(0)}]\} \qquad (4.\ 1)$$

We define the orthogonal polynomial basis as ξ_n and (instead of one conjugate polynomial η_m q+1 polynomials $\eta_m^{(\alpha)}$:

$$\int d\lambda^{(0)}\Pi_{\alpha=1}^{q}d\lambda^{(\alpha)}\xi_n^{(\alpha)q}(\lambda^{(0)})\exp[V_0(\lambda_i^{(0)})+\Sigma_{\alpha=1}^{q}(V_\alpha(\lambda_i^{(\alpha)})+c_(\lambda_i^{(\alpha)}\lambda_i^{(0)})]\times\Pi_{\alpha=1}^{q}$$

$$\eta_{m\alpha}^{(\alpha)}(\lambda^{(\alpha)})=h_n\delta_{nm},\ m=m_\alpha,\ \alpha=1,\ \ldots\ q \qquad (4.\ 2)$$

This basis is unusual but it works quite well at least for gaussian potentials:

$$V_\alpha(\tau)=t_\alpha\tau^2+u_(\tau,\ \alpha=0,\ 1,\ \ldots\ q.$$

We introduce Q-matrices as:

$$\int d\lambda^{(0)}\Pi_{\alpha=1}^{q}d\lambda^{(\alpha)}\xi_n^{(\alpha)q}(\lambda^{(0)})\lambda^{(\alpha)}\exp[V_0+\Sigma_{\alpha=1}^{q}(V_(+c_(\lambda^{(\alpha)}\lambda^{(0)})]\times\Pi_{\alpha=1}^{q}$$

$$\eta_{m\alpha}^{(\alpha)}(\lambda^{(\alpha)})=h_n Q_{\alpha,\,nm},\ m=m_\alpha,\ \alpha=1,\ \ldots\ q \qquad (4.\ 3)$$

The coupling conditions are:

$$q\,P_0+2t_0Q_0+u_0+\Sigma_{\alpha=1}^{q}c_(Q_(=0$$

$$P_\alpha+2t_(Q_\alpha+u_\alpha+c_(Q_0=0,\ \alpha=1,\ \ldots\ q. \qquad (4.\ 4)$$

With the following parametrization of Q-matrices:

$$Q_0=I_++a_0I_0+a_1\varepsilon_- \qquad (4.\ 5)$$

$$Q_(=b_\alpha/R_(I_++d_(I_0+R_\alpha\varepsilon\_-,\ \alpha=1,\ \ldots\ q$$

we arrive at the equations:

$$
\begin{aligned}
&2\, t_{(}R_{\alpha}+c_{(}a_1=0\\
&2\, t_{(}b_{\alpha}+n+c_{(}R_{\alpha}=0\\
&2\, t_{(}d_{\alpha}+u_{\alpha}+c_{(}a_0=0\\
&2\, t_0+\Sigma(c_{(}b_{\alpha}/\, R_{\alpha})=0\\
&2\, t_0\, a_0+u_0+(c_{(}d_{\alpha}=0\\
&2\, t_0\, a_1+qn+(c_{(}R_{\alpha}=0
\end{aligned}
\qquad (4.\ 6)
$$

By solving the coupling conditions we get :

$$
\begin{aligned}
&a_1 = -\,(2q/\, A), \qquad a_0=(1/\, A)[\Sigma(c_{(}u_{\alpha}/\, t_{\alpha})-2u_0]\\
&b_{\alpha}= -\,(1/\, 2t_{\alpha}^{2})[\{c_{\alpha}^{2}\, q/\, A)+t_{\alpha}], \quad R_{\alpha}=(c_{(}q/\, t_{(}A)\\
&d_{\alpha}= (1/\, At_{\alpha})[c_{(}u_0-\, 2t_0\, u_{\alpha}+u_{(}\Sigma(c_{\alpha}^{2}\, /\, 2t_{\alpha})\, -\, c_{(}((c_{(}u_{\alpha}/2t_{\alpha})]
\end{aligned}
$$

where $A= 4t_0-(c_{\alpha}^{2}\, /\, t_{\alpha}$.

We can obtain the basic functions for star matrix model, in the same way we get them for q-matrix model:

$$
\begin{aligned}
&\xi_n(\lambda^{(0))}= H_n\,(\lambda^{(0)\,\prime}),\\
&\eta_m^{(\alpha)}(\lambda^{(\alpha))}=R_{\alpha}^{\,n}\, H_n(l^{(\alpha)\,\prime}), \qquad \alpha=0,\, 1\ldots q
\end{aligned}
$$

with:

$$
\lambda^{(0)'} = (\lambda^{(0)}\, -\, a_0)/(2a_1)^{1/2}, \qquad \lambda^{(\alpha)'} = (\lambda^{(\alpha)}\, -\, d_{\alpha})/(2b_{\alpha})^{1/} \qquad (4.\ 8)
$$

Since these basic functions satisfy the relation:

$$
\eta_n(l^{(0))}= \int \quad \exp[V_0+\Sigma_{\alpha=1}^{\,q}\, (V_{(}+\, c_{(}\lambda^{(\alpha)}\lambda^{(0)})]\, \eta_n(l^{(\alpha))} \qquad (4.\ 9)
$$

we can integrate over Vandermonde determinants:

$$
\det_{ij}[\eta_i^{(0)}(\lambda_j^{(0))}]= \int \quad \exp[V_0+\Sigma_{\alpha=1}^{\,q}\, (V_{(}+\, c_{(}\lambda^{(\alpha)}\lambda^{(0)})]\, \det_{ij}\, [\eta_i^{(\alpha)}(l_j^{(\alpha))}] \qquad (4.\ 10)
$$

Then we have for the joint probability of two eigenvalues the simple expression:

$$
P(\lambda^{(\alpha)},\, \lambda^{(\beta)})(P_{herm}(\lambda'^{(\alpha)},\, \lambda'^{(\beta)}), \qquad \alpha,\, \beta=0,\, 1\ldots\, q \qquad (4.\ 11)
$$

with λ', μ' given by equation (4. 8).

5. GENERALIZED CALOGERO-SUTHERLAND MODEL

The connection with Calogero model permits the calculation of the joint distribution functions for random multimatrix models for other ensembles, different from the hermitean one. This relation is interesting due to the fact that such matrix models might be directly related with conformal field theories with the central charge $c=1-6(\sqrt{\beta}-1/\sqrt{\beta})^2$, as was stated in [17] (where $\beta=1, 2, 4$ for orthogonal, hermitean and unitary matrices respectively).

We obtain the Calogero model related to the 2-matrix model. The eigenvalue problem for Calogero model follows from the heat equation satisfied by the Itzykson- Zuber integral.

We introduce the kernel:

$$K(X, Y| t)= <X|\exp\{-t D\}|Y>= \quad (5.\ 1)$$

$$=(2(t)^{-N2/2} \int dU \exp[-(1/ 2t)Tr (XUYU^{+})]$$

which is related with the Itzykson-Zuber integral $K(X, Y| t=1)=\exp(- (1/ 2t) Tr(X^2+Y^2))I(X, Y)$:

$$I(X, Y)= \int dU \exp[Tr (XUYU^{+})]= \quad (5.\ 2)$$

$$=(\det_{ij} (\exp \{x_i y_j\}) / (\Delta(X)\Delta(Y))^{\beta/2}$$

where $\beta=1, 2,$ or 4 depending on how are the matrices X, Y: orthogonal, hermitean or unitary respectively.

The kernel (5. 1) satisfies the heat equation [18][19]:

$$(d /d t+D_X) KK(X, Y|t)=\delta(X, Y) \quad (5.\ 3)$$

where $KK(X, Y|t)=(\Delta(X)\Delta(Y))^{\beta/2} K(X, Y| t)$ and the laplacian is:

$$D_X= - (1/ 2) \Sigma_i d^2 /d x_i^2 +(\beta/ 2)((\beta/2)-1)\Sigma_{i<j} [1/ (x_i-x_j)^2] \quad (5.\ 4)$$

Solving equation (5. 3) gives:

$$KK(X, Y|t)=(2(t)^{-N2/2} \Sigma_{(}\eta_{(}\exp[- (1/ 2t) \Sigma_i (x_{\sigma(i)}-y_i)^2] \quad (5.\ 5)$$

from which follows the expression for the Itzykson-Zuber integral ((is the permutation).

We introduce the function:

$$\varphi(X|t)= \int KK(X, Y|t)\varphi(Y)\, dY \quad (5.\ 6)$$

that fulfills the heat equation with initial condition $\varphi(X|t=0)=\varphi(X)$.

We can search for stationary solutions in the form $\varphi(X|t)=\Sigma_n\varphi_n(X)\exp\{-E_n\ t\}$ where $\varphi_n(X)$ satisfies the Calogero equation (without potential term):

$$[-\ (1/\ 2)\ \Sigma_i\ d^2\ /d\ x_i^2\ +(\beta/\ 2)((\beta/2)-1)\Sigma_{i<j}\ [1/\ (x_i-x_j)^2]\ \varphi_n(X)\ =E_n\ \varphi_n(X) \qquad (5.\ 7)$$

The eigenvalues of matrix X are chosen such that $y_1<y_2\ldots\ <y_n$. These eigenvalues $y_{1\ldots}\ y_n$ are mapped by the kernel KK(X, Y|t) into $x_{\sigma(1)}\ \ldots\ x_{\sigma(N)}$.

For t(0, the kernel KK(X, Y|t) tends to $\Sigma_(\eta_(\delta^N(x_{\sigma(i)}-y_i)$. Hence if we consider $\psi(X)$ as a particular solution of Calogero model with $x_1<x_2\ldots\ <x_n$, the function $\varphi(X|t=0)$ is the general solution for eigenvalues x_i in arbitrary order, being the linear combination of functions $\psi((X)$:

$$\varphi(X|t=0)=\Sigma_(\psi((X),\ \psi((X)=\eta_(\psi(X)$$

where (is the permutation of eigenvalues x_i ; $\eta_(=-1$ for free fermions ($\beta=2$ for hermitean matrices) and $\eta_(=+1$ for free bosons (((0 for harmonic oscillator). We see that for generic value of (the system describes particles with fractional statistics (anyons).

For t going to infinity the dominant contribution is given by the vacuum configuration $\varphi_0(X)$. The kernel KK(X, Y|t) plays the role of instanton propagator connecting the initial vacuum configuration $\psi_0(Y)=(\Delta(Y))^{\beta/2}$ to final vacuum configuration $\varphi_0(X)=(\Delta(X))^{\beta/2}$.

For 2-matrix model we can define the generalized Calogero system:

$$\{(\beta/\ 2)((\beta/2)-1)\Sigma_{i<j}\ [\ (\lambda_i-\lambda_j)^{-2}\ +\ (\mu_i-\mu_j)^{-2}]\ -\ (1/\ 2)\ (\Sigma_i\ d^2\ /d\ \lambda_i^{2\ +}\Sigma_i\ d^2\ /d\ \mu_i^2)$$
$$\times\varphi_n(\lambda)\ \psi_m(\mu)\ =\ E_{nm}\ \varphi_n(\lambda)\psi_m(\mu) \qquad (5.\ 8)$$

This system describes 2 interacting systems of anyons. Hence all results valid in the 2-matrix model with $\beta=1$can be extended to arbitrary (and given a meaning in terms of the generalized Calogero's anyons.

When c=0 the generalized system splits into two Calogero systems:

$$[-\ (1/\ 2)\ \Sigma_i\ d^2\ /d\ \lambda_i^2\ +(\beta/\ 2)((\beta/2)-1)\Sigma_{i<j}\ [1/\ (\lambda_i-\lambda_j)^2+\ \Sigma\lambda'^2]\ \varphi_n(\lambda)\ =E_{1,\ n}\ \varphi_n(\lambda)$$

$$[-\ (1/\ 2)\ \Sigma_i\ d^2\ /d\ \mu_i^2\ +(\beta/\ 2)((\beta/2)-1)\Sigma_{i<j}\ [1/\ (\mu_i-\mu_j)^2+\ \Sigma\mu'^2]\ \varphi_n(\mu)\ =E_{2,\ n}\ \varphi_n(\mu) \qquad (5.\ 9)$$

The ground states can be written in terms of the eigenfunctions (2. 11):

$$\varphi_0(\lambda)=(\det_{ij} \xi_i(\lambda_j))^{\beta/2}\exp(-\Sigma_i \lambda_i'^2/2) \qquad (5.\ 10)$$
$$\psi_0(m)=(\det_{ij}\eta_i(m_j))^{\beta/2}\exp(-\Sigma_i m_i'^2/2)$$

We can see that the probability of amplitudes (5. 10) is the partition function of the 2-matrix model:

$$Z=\int d\lambda_1 \ldots d\lambda_n |\varphi_0(\lambda)|^2=\int dm_1 \ldots dm_n |\psi_0(m)|^2$$

The system (5. 10) permits us to calculate the joint probability P(l, m) for general ensemble. It coincides with formula (2. 14) (for c=0) where we replace N by (N/2:

$$P(\lambda, \mu)=\{(N/2-\lambda'^2\}^{1/2}\{(N/2-\lambda'^2\}^{1/2} \qquad (5.\ 11)$$

6. CONCLUSIONS

These models present interest in the study of quantum chaos for q systems interacting in various ways. The density of levels depends on the total energy which behaves like N, for large N. The interaction of q subsystems redistribute the energy between the subsystems and change in non-trivial way the joint distribution functions. Different kinds of interaction (chain or star- type) give different probabilities for energy levels.

REFERENCES

1. C. E. Porter, *Statistical Theories of Spectra: Fluctuations, a collection of reprints*, (Academic Press, New York and London, 1965).
2. M. L. Mehta, *Random Matrices*, (Academic Press, New York and London, 1967).
3. Nakamura, *Quantum chaos* (Cambridge University Press, England, 1993)/
4. M.-J. Giannoni, A. Voros, Z. Zinn-Justin (eds.), *Chaos and Quantum Physics* (North-Holland, Amsterdam, 1991).
5. B. Kramer (ed.), *Quantum coherence in mesoscopic systems*, NATO ASI Ser. B, Phys. 254 (Plenum, New York, 1991).
6. S. Kharchev et al., Nucl. Phys. B 380, 181 (1992).

7. B. D. Simons, P. A. Lee, B. L. Altshuler, Phys. Rev. Lett. 72, 64(1993).
8. B. D. Simons, B. L. Altshuler, Phys. Rev. Lett. 70, 4063 (1993).
9. D. Simons, P. A. Lee, B. L. Altshuler, Phys. Rev. Lett. 70, 4122 (1993).
10. Brezin, Nucl. Phys. B424, 435 (1994), Nucl. Phys. B441, 409 (1995).
11. Kazakov, Nucl. Phys. B354, 614(1991).
12. E. Brezin, in *Applications of field theory to statistical mechanics*, Springer Lecture Notes in Physics, vol. 216, p. 215 (Springer, Berlin, 1984).
13. B. Efetov, Adv. Phys. 32, 53 (1983).
14. J. D'Anna, E. Brezin, A. Zee, Nucl. Phys. B443, 433 (1995).
15. Brezin, A. Zee, Nucl. Phys. {\bf B402}, 613 (1993).
16. L. Bonora, F. Nesti, E. Vinteler, Int. J. Mod. Phys. A11 (1996) 1797.
17. Bonora, C. S. Xiong, Nucl. Phys. (1991).
18. S. Kharchev et al. , Nucl. Phys. B 380, 181 (1992).
19. Awata, Y. Matsuo, S. Odake, J. Shiraishi, Nucl. Phys. B449 (1995) 347.
20. M. L. Mehta, Comm. Math. Phys. 79, 327(1981).
21. C. Itzykson, J. B. Zuber, J. Math. Phys. 21, 411 (1980).

STUDIA UNIVERSITATIS BABEŞ-BOLYAI, PHYSICA, XLII, 1, 1997

CUMULATIVE EFFECTS OF CRYSTALLIZATION FROM SOLUTION

E. VINTELER[1]

ABSTRACT. The experimental data of crystallization from solution show that the samples behave differently when the crystal samples grow in near null magnetic field or in geomagnetic field. In near null magnetic field are produced more nuclei, which grow slower. The experimental data can be explained by assuming that geomagnetic field modifies the mobility of the ions on the growing surface. To explain the macroscopic changes on the nucleation and crystal growth rate, we suppose that the geomagnetic effect cumulates due to the correlation in time. This cumulative effect is due to the special properties which appear at the crystal-solution interface.

INTRODUCTION

In work [1] was shown that the crystallization of different substances (NaCl, $MnCl_2$, $FeCl_2$, $Fe(NH_4)_2(SO_4)_2$) from solution behaves differently when the crystal samples grow in near null magnetic field or in geomagnetic field. The experimental results are in agreement with other related to crystallization and precipitation of different inorganic systems. The results can be stated as follows:

- the near null magnetic field did not change the total time required to get a complete crystallization;
- the near null magnetic field significantly decreased the NaCl nucleation and crystal growth rate;
- the symmetry axes of the grown crystals in the presence of the geomagnetic field are independent on its direction. A comparison of the X-ray spectra for samples in geomagnetic and in near null magnetic field at the end of crystallization process shows that the near null magnetic field had no effect on the crystalline lattice.

[1] Institute of Isotopic and Molecular Technology, str. Donath. 100, Cluj-Napoca 3400, Romania

The experimental data can be explained only by assuming that geomagnetic field modifies the mobility of the ions on the growing surface (there are no structural changes of the crystalline lattice). The geomagnetic energy interaction is much smaller than the thermal noise energy. This implies that in usual conditions, the geomagnetic effect is "forgotten" after a short (relaxation) time. To explain the macroscopic changes on the nucleation and crystal growth rate, we suppose that the geomagnetic effect cumulates due to the correlation in time. The system has "memory" and its further evolution depends on the present state. This cumulative effect is due to the special properties which appear at the crystal-solution interface.

Our theory can be applied also to other systems where the energy of external perturbation is much smaller than the thermal noise energy. The cumulative effects can appear only in systems where the studied process (crystallization, precipitation etc.) consists of a chain of elementary reactions with back-reaction, in other words when the last reactions of the chain catalyze the first reactions.

THE MACROSCOPIC THEORY

The nucleation rate depends on the excess free (nucleation) energy at criticality:

$$I_N = \nu \exp(- g_c / kT) \qquad (1)$$

(where N_0 is the number of lattices sites per unit area and ν - the number of molecules arriving per unit time towards the critical nucleus).

The nucleus, an incomplete monomolecular layer of a critical size, is created on the heterogeneous surface (glass) by thermal fluctuations. Assuming a circular layer of radius *r*, the excess free energy of the total system has the formula:

$$g(r) = - kT \ln s (\pi^2 / a^2)+ \gamma (2 \pi/a) \qquad (2)$$

The supersaturating ratio $s=[Cl]^-/[Cl]^-_{sat}$ is expressed in terms of the concentration of Cl anions, and $[Cl]^-_{sat}$ the concentration of the same anions at the saturation point. The other parameters are: γ- the edge free energy per molecule and *a*- the lattice pace.

The thermodynamic probability of eq. (2) has a minimum equal to:

$$\exp (- g_c / kT) = \exp (- \pi (\gamma / kT)^2 / \ln s) \qquad (3)$$

From the experimental results, it can be deduced that the rate of nucleation in near null magnetic field is greater than the rate value obtained under the geomagnetic field B=0. 047 mT. This means that:

$$(g_c)_{B=0\ mT} < (g_c)_{B=0.\ 047\ mT} \quad (4)$$

According to eq. (3) the required decrease in the value of the excess free energy could be due to: i) the edge free energy per molecule $\gamma<\gamma_B$ in the near null magnetic field is decreased. The magnetic interaction can be introduced by a linear term μ_γ B, where μ_γ is the effective magnetic momentum of charged ions. The edge free energy in geomagnetic field γ_B is related to the value in near null magnetic field by the formula:

$$\gamma_B = \gamma+\mu_\gamma B \quad (5)$$

The edge free energy is compared to thermal energy *kT* and a brief comparation shows that $\mu B/kT<< 1$, hence the geomagnetic effect is negligible when compared to thermal noise. The magnetic interaction cannot explain alone the decrease of the excess free energy. ii) the supersaturating ratio *s* is increased in the near null magnetic field. The saturation concentration $[Cl]^-_{sat}$ cannot be modified, as the crystallographic lattice of the NaCl crystal does not change. The increase of *s* might be explained by supposing that the near null magnetic field increase locally the probability of an encounter between Na^+ and Cl^- by acting on the Brownian motion of the charged ions. The supersaturating ratio s_B in geomagnetic field is related to the value in near null magnetic field by the formula:

$$s_B=s \exp(\mu_s B/ kT) \quad (6)$$

where μ_s is of the same order of magnitude as the effective magnetic momentum μ_γ of ions. The variation of the applied magnetic field seems too low to induce alone such a mechanism (in the critical free energy formula (3) *s* stands under a logarithm, hence for change of *n* orders of magnitude of the value *s* we get a *n* times change in g_c). Because this, in the following considerations we will consider only the effect of geomagnetic field on the edge free energy γ.

The conclusion of macroscopic theory is that neither explanation i) and ii) is a solution of our puzzle. Because this, we pass to microscopic theories, first in near null magnetic field and after to our original contribution - the microscopic theory in magnetic field.

THE MICROSCOPIC THEORY IN NEAR NULL MAGNETIC FIELD

To understand better the process of nucleation we consider the microscopic theory developed by Becker-Doring [2] and Frank [3] (see also [4], [5], [6]). They took a sequence of processes passing through a sequence of stages with first-order rate constants:

$$[0] \underset{b_1}{\overset{f_1}{\rightleftarrows}} [1] \underset{b_2}{\overset{f_2}{\rightleftarrows}} [2] \ldots \underset{b_n}{\overset{f_n}{\rightleftarrows}} [n] \underset{b_{n+1}}{\overset{f_{n+1}}{\rightleftarrows}} \ldots$$

where f_n and b_n are the forward and backward transition rate constants to and from stage *n*:

$$f_n/b_n = \exp [-(g_n - g_{n-1})/ kT] \tag{7}$$

The free energy for stage *n* is given by:

$$g_n = - (kT / \ln s)\, n + 2 \gamma n^{1/2} \tag{8}$$

which reduces to eq. (2) for a circular cluster of radius *r.*
The kinetic of the system is governed by the system of equations:

$$\begin{aligned} J_n &= f_n Q_{n-1} - b_n Q_n \\ dQ_n / dt &= J_n - J_{n+1} \end{aligned} \tag{9}$$

where Q_n is the occupation number of stage *n* and J_n is the net transition rate from stage *n-1* to stage *n*.

The equations (9) can be rewritten in the following form:

$$J_n = (V_{n-1} - V_n) / R_n \tag{10}$$

characterized by the coefficients:

$$\begin{aligned} V_n &= Q_n / C_n \\ R_n &= 1 / (b_n C_n) \\ C_n &= \prod_{i=1}^{n} (f\_i/b\_i) \end{aligned} \tag{11}$$

When a steady state of occupation is realized, the common rate of transition *J* is given by:

$$J = V_0 / \sum_{n=1}^{\infty} R_n \tag{12}$$

In this case, the coefficients C_n, R_n are equilibrium constants and are expressible in terms of the free energy g_n (using eq. (7)):

$$C_n = \exp (- g_n / kT) , (C_0 = 1)$$
$$R_n = (b_n)^{-1} \exp (g\_n / kT)$$

The maximum energy is:

$$g_n^* = \gamma (n^*)^{1/2}$$
$$\text{at} \qquad n^* = (\gamma / kT \ln s)^2 \qquad (13)$$

Using these expressions, the steady rate nucleation *J* of eq. (12) is dominantly determined by the terms R_n in the summation ΣR_n within Δn of n* for which g_n is within about *kT* of its quasi-parabolic maximum g_n^* ($g_n^* - g_n \cong kT$). By use of Taylor expansion of eq. (8) about n* we have:

$$\Delta n = (|(d^2 g_n / d^2 n)_{n^*}| / \pi kT)^{1/2}$$

he nucleation rate is given by:

$$I_N = J/S = (b_{n^*} / \Delta n) (V_0 / S) \exp (-g_n^* / kT) \qquad (14)$$

which is similar to eq. (1) up to correction Δn (by making the identifications $\nu = b_n^* = f_n^*$ and $V_0 / S = N_0$).

THE MICROSCOPIC THEORY IN MAGNETIC FIELD

In this subsection we consider the microscopic theory of nucleation taking in consideration the cooperative effects.

The rate constants in the presence of magnetic field *B* have the form:

$$f_i^B / b_i^B = (f_i / b_i) \exp (\mu_i B / kT) \qquad (15)$$

We introduce the new coefficient μ_i which represents the effective magnetic momentum at i-th stage. If we consider that the geomagnetic field influences only the edge free energy γ, then using relations (5) and (7) we have for great *i*:

$$\mu_i = - \mu_\gamma \sqrt{i}$$

If instead the geomagnetic field influences only the supersaturating ratio *s*, then using relations (6) and (7) we have:

$$\mu_i = \mu_s$$

Hence, using μ_i we can study the influence of geomagnetic field on both parameters of theory, the free energy γ and supersaturating ratio *s*.

The new coefficients are (see eqs. (11)):

$$C_n^B = C_n \exp\left(-\frac{1}{kT}\sum_{i=1}^{n} \mu_i B\right) \qquad (16)$$

$$R_n^B = Rn \exp\left(+\frac{1}{kT}\sum_{i=1}^{n} \mu_i B\right)$$

The coefficients R_n^B can be rewritten in the form:

$$R_n^B = (b_n)^{-1} \exp(g_n^B / kT)$$

where the free energy in the presence of magnetic field *B* is:

$$g_n^B = g_n + B \sum_{i=1}^{n} \mu_i$$

The minimum of free energy:

$$\frac{dg_n^B}{dn} = \frac{dg_n}{dn} + \mu_n B = 0$$

fixes the critical number of steps n_B^* in magnetic field:

$$n_B^* = [\gamma / (kT \ln s - \mu B)]^2 \qquad (17)$$

which can be approximated in terms of $n^* = (\gamma / kT \ln s)^2$ (n^* is the critical number of steps without magnetic field (13):

$$n_B^* \cong n^* + 2n^* \mu_n^* B / (kT \ln s)$$

The critical free energy has the form:

$$(g_n^{B*} / kT) \cong (g_n^* / kT) + 2n^* \mu_n^* B / (kT) + \frac{1}{kT}\sum_{i=1}^{n^*} \mu_i B$$

Introducing the last expression in the formula of nucleation rate (14) we get:

$$I_N^B = I_N \exp\left[- \frac{B}{kT} \left(2n^* \mu_n^* + \sum_{i=1}^{n^*} \mu_i \right) \right] \qquad (18)$$

We make a rough estimate considering that $\gamma / kT \cong 1$ is a typical value in a solution. Then, for a super-saturation of 10% or s=1. 1 we have in near null magnetic field $g_n^* / kT \cong 10$ and the critical number of steps is $n^* \cong 100$.

We make the following estimates for the relative variations of the edge free energy $(\gamma_B - \gamma) / \gamma \cong 10^{-3}$ and of the super-saturation ratio energy $(s_B - s) / s \cong 10^{-3}$ (this means that the interaction energy is much smaller than the thermal energy kT, of the order 10^{-3}). Using these estimates, we calculate the nucleation rates in external magnetic field in 2 cases, when variation of nucleation rate is due entirely to:
1. variation of edge free energy and
2. variation of super-saturation ratio.

1. For the special case of constant magnetic momentum $\mu_i = \mu_s$ the nucleation rate in external magnetic field simplifies to:

$$I_N^B = I_N \exp (-3n^* \mu_s B / kT)$$

2. For the case $\mu_i = - \mu_\gamma \sqrt{i}$, we apply relation (18) and we have:

$$I_N^B = I_N \exp \left[- (2n^* + \sqrt{n^*}) (\mu_s B / kT) \right]$$

Using these relations and the estimates of free energy and super-saturation ratio we have the following estimate for the variation of nucleation rate:

$$(I_N - I_N^B) / I_N \cong 0.5$$

The conclusion is that small relative variations of the edge free energy and of the super-saturation ratio of the order 10^{-3} can produce observable changes in the nucleation rate I_N in the presence of geomagnetic field.

A small interaction energy is required to produce such changes. The obtained results are useful in explaining other experimental data concerning different systems (for ex. precipitation, adsorption etc.) where the weak effect cumulates.

REFERENCES

1. L. Copaescu, E. Vinteler, V. V. Morariu, *Effect of near null magnetic field on NaCl crystallization from solution*, submitted to Biophysical Journal.
2. R. Becker, W. Doring, Ann. Phys. , 24, (1937), 719.
3. F. C. Frank, J. Cryst. Gr. , 13/14, (1972) 154.
4. M. Volmer, *Kinetik der Phasenbildung*, Dresden, 1939.
5. N. Cabrera, R. V. Coleman, in *The Art and Science of Growing Crystals*, Ed. J. J. Gilman, John Wiley, New York, 1963.
6. W. K. Burton, N. Cabrera, F. C. Frank, Phil. Trans, A243, (1951), 299.

STUDIA UNIVERSITATIS BABEŞ-BOLYAI, PHYSICA, XLII, 1, 1997

BRST COHOMOLOGY FOR THE INDUCED W3-GRAVITY

C. BUIA[1], L. TĂTARU[2]

ABSTRACT. A new method for finding out the BRST cohomology for the induced W3-gravity, based on the existence of an operator δ which allows us to decompose the space-time derivative d as a BRST comutator is presented. The BRST differential algebra is obtained by imposing the zero curvature conditions for the underlying Lie algebra SL(3) decomposed with respect to an SL(2) subalgebra.

W-algebras have turned out to interwines internal symetries with space-time ones in two dimensions and, due to this fact, to be of central interest in two dimensional physics. Originally introduced [1] as an extension of the conformal algebra by the spin-3 primary field, it soon became clear that W-algebras are related to other structures of the theoretical physics such as gauged WZNW-models [2],[3],[4] and Toda field theories [5]. In the reduction of WZNW theories to Toda field theory [3],[4] an important ingredient is the identification of a SL(2) subalgebra of the underlying Lie algebra and the arrangement of the remaining generators in irreducibile representations with respect to the SL(2) subalgebra. The W-currents correspond to the highest weight genetators in the SL(2) decomposition and they are conformally covariant tensors with one exception, the SL(2) current, which behaves as a projective connection.

The dynamical realization of W-algebra arises in W-gravity [6],[7] where W-currents couple to some W-gauge fields which are generalizations of the Beltrami differentials. In some models of W-gravity [7],[8] the W-currents are no longer holomorphic and the Ward identities for W-symetry are anomalous. These anomalies must satisfy the Wess-Zumino consistency conditions [9] and these conditions allow us to define anomalies as nontrivial solutions of a BRST equation of the form:

[1] University of Genova, Physics Department, via Dodecaneso 33, Italy
[2] Babeş-Bolyai University, Physics Departament, M. Kogălniceanu 1, 3400 Cluj-Napoca, Romania

$$s\Delta = 0 \qquad (1.1.)$$

where Δ is the integral of a local polynomial in the fields and their derivatives and s is the BRST differential.
Writting $\Delta \int A$, where A is a two form, eq.(1) translates into the local conditions:

$$\begin{aligned} sA + dQ &= 0 \\ sQ + dQ^1 &= 0 \\ sQ^1 &= 0 \end{aligned} \qquad (1.2)$$

where Q and Q^1 are local polynomials in the fields. The equations occur due to the vanishing cohomology of the external differential d. They are called descent equations.

In this paper we have adopted a purely algebraic point of view introduced by Garajeu, Lazzarini, and Grimm [10] (see also [11]) and we have considered the W-algebra in terms of differential BRST algebra generated by W-currents, W-gauge fields and W-ghosts and by the BRST differential s. The structure of W-algebra as well as its BRST transformations can be obtained from the zero curvature conditions and the Russian formula.Within this algebraic formalism one can look for nontrivial solutions of the consistency equation (1).

STRUCTURE OF W3 -GRAVITY

We shall work in two space-time dimensions with the complex coordinates (z, z).

The W-currents, W-gauge fields and W-ghost fields can be constructed by starting with a simple Lie algebra G which can be arranged in reprezentations with respect to the principal SL(2) subalgebra. Introducing the Lie valued gauge potentials:

$$A = dz\, A_z(z, \bar{z}) + d\bar{z}\, A_z(z, \bar{z}) \qquad (2.1)$$

and the Lie valued ghost fields (and writting down their BRST transformations for A and (in the form of Russian formula:

$$F=dA-AA=F=dA-AA \qquad (2.2)$$

where:

$$d=d+s$$
$$A=A+\omega$$

In addition we shall perform :

* a convenient field dependent redefinition called the conformal parametrization, of A and ω
* the highest weight parametrization
* the zero curvature conditions
* the projective parametrization.

All these transformations and conditions do not change the form of the Russian formula, which can be used all the time. Thus we will obtain the general form of the solutions of the descent equations and afterwards we will impose these conditions to the find answers.However in the calculation we will take into consideration the field redefinitions and the zero curvature conditions.

In order to solve the descent equations we define the conformal parametrization:

$$\begin{aligned} \Gamma &= g_o A = g_o A g_o^{-1} + g_o d g_o^{-1} \\ c &= g_o \omega g_o^{-1} + g_o s g_o^{-1} \end{aligned} \tag{2.3}$$

with $g_0=\exp[\alpha^0 L_0]$, L_0, L_-, L_+ being the generators of the subgroup SL(2).

Next we impose the zero curvature condition:

$$g_o F = d\Gamma - \Gamma^2 = 0$$

Furthermore we shall use two methods to solve the descent equation. The first is based on the Sullivan theorem regarding the decomposing of a Lie algebra in a minimal subalgebra and a contractive one that we shall apply to the BRST algebra. The cohomology group of the contractive part is trivial so the cohomology group of the minimal subalgebra coincides with that of the given Lie algebra. Because of this we can limit ourself to solve the descent equation in the minimal subalgebra fact that simplifies our work. This method is a little more complicated but permits us to calculate solutions of different ghost number as well as solutions containing matter fields.

In the second method we shall follow Sorella [14],[15]. First we introduce a even differential of degree zero δ:

$$\begin{aligned} \delta\Gamma &= 0 \\ \delta c &= +\Gamma \\ \delta\xi &= +\Gamma^2 \end{aligned} \tag{2.5.}$$

with $\xi = dc$. Due to the zero curvature conditions F = 0 the differentials d,s and δ obey the following algebraic relations:

$$[s,\delta]=-d \tag{2.6}$$
$$[d,\delta]=0 \tag{2.7}$$

In particular (2.6) shows that the operator δ decomposes the exterior derivative d as a BRST commutator.Eq. (2.7) is a direct consequence of the zero curvature conditions.

Eq. (2.6),(2.7) define an algebraic setup which gives a simple procedure for solving the tower of descent equations.In order to accomplish this task we shall use the following identity:

$$e^{\delta} s e^{-\delta} = s + d \tag{2.8}$$

which is a direct consequence of (2.6),(2.7).Eq. (2.8) can be written in a more useful way:

$$e^{\delta} s = (s+d) e^{\delta} \tag{2.9}$$

The simplest nontrivial solution of the equation: $s\omega=0$ is the ghost monomial:

$$\omega_o = \frac{1}{(2n+1)!}\,\mathrm{tr}(c^{2n+1}) \tag{2.10}$$

with: $c=c^{\alpha}T_{\alpha}$

This fact is a direct consequence of the BRST transformations for the ghost c^{α}. Besides, it can be proved that in our case (n=1) it is the unique solution with the ghost number three.

By application of identity (2.9) to (2.10) one gets:

$$(s+d)[e^{\delta}\omega_0(c)]=(s+d)\omega_0(c-\Gamma)=0 \tag{2.11}$$

By projecting out from (2.11) the terms with a given ghost number, one obtain the descent equations.

The most general solution of eq.(2.11) has the form:

$$\omega=\omega_0(c-\Gamma)+(s+d)\eta \tag{2.12}$$

where $\eta(c\Gamma)$ is an arbitrary form. The anomaly can be calculated from $\omega_0(c-\Gamma)$ by projecting out the term with the ghost number 1. In fact we eventually find:

$$A=k\,\mathrm{tr}(c\Gamma^{2n}) \tag{2.13}$$

with k-numerical constant.

From eq.(2.13) we can obtain the anomalies for W_{2n+1}-gravity. However if one wants to obtain the concrete expansion of A then we have to take into account the aditional conditions imposed on Γ and c. These conditions can be solved in the general case but we shall limit ourself to the W_3-gravity.

BRST STRUCTURE OF W3-GRAVITY

Now, in order to fix the notations, let us consider a decomposition of a given Lie algebra SL(3) with respect to some SL(2) subalgebra.There are two possible decompositions, corresponding to two different W_3-algebras of Zamolodchikov [1] and Polyakov and Bershadsky [12],[13]. We shall consider in the sequel only the decomposition $W_3^{(1)}$ in which the eight generators of SL(3) are split into three $\{L_{\pm1}, L_0\}$ and five $\{T_{\pm2}, T_{\pm1}, T_0\}$ (i.e. SL(2) spin two). The comutation relations for this generators are:

$$\begin{aligned}
&[L_k, L_l]=(k-l)L_{k+l}\\
&[L_k, T_m]=(2k-m)T_{k+m}\\
&[T_m, T_n]=-1/3(m-n)(2m^2+2n^2-mn-8)L_{m+n}\\
&(k,l=-1,0,+1;\quad m,n=-2,-1,0,+1,+2)
\end{aligned} \tag{3.1.}$$

From a concret three-dimensional representation of these generators (given in [10])it is easy to calculate the matrix $g_{ab}=g_{ba}=Tr(T_a, T_b)$, necesary in the sequel:

$$g^1{}_{-+}=-4,\ g^1{}_{00}=2$$

for$\{L_0, L_\pm\}$ and

$$g^t{}_{-2,+2}=16,\ g^t{}_{-2,+1}=-4,\ g^t{}_{00}=8/3$$

for $\{T_{\pm2}, T_{\pm1}, T_0\}$ the rest of the elements being zero. W-currents and W-ghost fields can be obtained from the 1-form Lie algebra valued potential:

$$A=A^kL_k+A_1{}^mT_m=dz\ A_z+d\bar{z}\ A_{\bar{z}} \tag{3.2}$$

the Lie algebra valued Fadeev-Popov ghosts:

$$\omega=\omega^kL_k+\omega_1{}^mT_m \tag{3.3}$$

and the covariant matter fields:

$$\Sigma = \begin{pmatrix} \Sigma_+ \\ \Sigma_0 \\ \Sigma_- \end{pmatrix} \tag{3.4}$$

by the method described in §2. In adition we have to introduce the matter field $\Sigma(z, \bar{z})$ transforming under the group G as:

$$^{g}\Sigma = U(g)\Sigma \tag{3.5}$$

in some reprezentation U(g) of the group. Second, the BRST transformation of A and ω can be obtained from the "Russian formula" or the Maurer-Cartan horizontality conditions:

$$F = F, D\Sigma = D\Sigma \tag{3.6}$$

where the field strenght F and the covariant derivative $D\Sigma$ are defined by:

$$\begin{aligned} F &= dA - AA \\ D\Sigma &= d\Sigma + A\Sigma \end{aligned} \tag{3.7}$$

The W-gauge structure given by the fields A and Σ is a special gauge called the conformal parametrization. This gauge consists in a redefinition of the A and Σ which has theb form of a gauge transformation of the form:

$$g_0 = e^{\alpha^0 L_0} \tag{3.9}$$

such that the part of the gauge potential A_z^- corresponding to L_- and dz is 1, i.e.:

$$^{go} A_z^- = 1 \tag{3.10}$$

Since the action of g_0 on A is given by (2.3) and g0 has the form (3.9), eq.(3.2) yields:

$$\begin{aligned} ^{go} A_a^{\rho k} &= A_a^{\rho k} e^{-ka^0} \\ ^{go} A^{\pm} &= A^{\pm} e^{+\alpha^0} \end{aligned} \tag{3.11}$$

and the condition (3.10) gives:

$$\alpha^0 = -\ln A_x^- \tag{3.12}$$

The gauge potential in conformal parametrization is defined by:

$$\Gamma =^{go} A = \Gamma^{k} L_{k} + \Gamma_{a}^{pk} T_{pk}^{a} = dz\Gamma_{z} + d\bar{z}\Gamma_{\bar{z}} \qquad (3.13)$$

The ghost field in the conformal parametrization is defined by:

$$c = g_0 \omega\ g_0^{-1} + g_0 s g_0^{-1} \qquad (3.14)$$

and the matter field by:

$$\Psi = ^{g0}\Sigma \qquad (3.15)$$

with the covariant derivative:

$$D(\Gamma)\Psi = d\Psi + \Gamma\Psi = ^{g_0} D(A)\Sigma \qquad (3.16)$$

It is important to observe that the gauge potentials A_z and A_z are conformally covariant of weight (1,0) and (0,1) respectively and the new gauge potential (3.13) has definite conformal weight. Thus

$$\Gamma_{a}^{\rho k} = A_{a}^{\rho k} (A_{z}^{-})^{k}$$

has the conformal weight (k,0),

$$\Gamma^{-} = dz + d\bar{z}\frac{A_{\bar{z}}^{-}}{A_{z}^{-}} = dz + d\bar{z}\upsilon_{\bar{z}}^{z} = \upsilon^{z} \qquad (3.18)$$

has the conformal weight (-1,0),

$$\begin{aligned} &\Gamma^{0} = A^{0} - d\alpha_{0} = dz\left(A_{z}^{0} + \partial \ln A_{z}^{-}\right) + d\bar{z}\left(A_{\bar{z}}^{0} + \bar{\partial} \ln A_{z}^{-}\right) = \\ &= dz\chi_{z} + d\bar{z}\chi_{\bar{z}} = \chi \end{aligned} \qquad (3.19)$$

has the conformal weight (0,0) and

$$\begin{aligned} &\Gamma^{+} = dzA_{z}^{+}A_{z}^{-} + d\bar{z}A_{\bar{z}}^{+}A_{z}^{-} = \\ &= dz\lambda_{zz} + d\bar{z}\lambda_{\bar{z}z} = \lambda_{z} \end{aligned} \qquad (3.20)$$

has the conformal weight (1,0).

In the sequence we impose the highest weight gauge condition:

$$\Gamma_{z}^{k} = 0 \qquad (3.21)$$

where $k = -2, -1, 0, +1$, and using the zero curvarure conditions we project the horizontality conditions for the gauge potentials:

$$F(\Gamma) = F(\Gamma) = 0 \tag{3.22}$$

for different ghost numbers.From (3.22) we obtain the following relations between gauge potentials and also between ghost fields (grouped for the SL(2) substructure and respectively SL(3) structure):

$$\begin{aligned}
&\chi_{\bar{z}} = \partial \upsilon^{x}_{\bar{z}} + \upsilon^{x}_{\bar{z}} \chi_{z} \\
&\bar{\partial} \chi_{z} = \partial \chi_{\bar{z}} - 2\lambda_{\bar{z}z} + 2\upsilon^{z}_{\bar{z}} \lambda_{zz} - 16\Gamma^{+2}_{z} \Gamma^{-2}_{\bar{z}} \\
&\bar{\partial} \lambda_{zz} = \partial \lambda_{\bar{z}z} + \lambda_{zz} \chi_{\bar{z}} - \lambda_{\bar{z}z} \chi_{z} - 4\Gamma^{+2}_{z} \Gamma^{-1}_{\bar{z}} \\
&c = \partial c^{z} + c^{z} \chi_{z}
\end{aligned} \tag{3.23}$$

$$\begin{aligned}
&\Gamma^{-1}_{\bar{z}} = \partial \Gamma^{-2}_{\bar{z}} + 2\chi_{z} \Gamma^{-2}_{\bar{z}} \\
&2\Gamma^{-0}_{\bar{z}} = \partial \Gamma^{-1}_{\bar{z}} + \chi_{z} \Gamma^{-1}_{\bar{z}} + 4\lambda_{zz} \Gamma^{-2}_{\bar{z}} \\
&3\Gamma^{+1}_{\bar{z}} = \partial \Gamma^{0}_{\bar{z}} + 3\lambda_{zz} \Gamma^{-1}_{\bar{z}} \\
&4\Gamma^{+2}_{\bar{z}} = \partial \Gamma^{+1}_{\bar{z}} - \chi_{z} \Gamma^{+1}_{\bar{z}} + 4\upsilon^{z}_{\bar{z}} \Gamma^{+2}_{z} + 2\lambda_{zz} \Gamma^{0}_{\bar{z}} \\
&\bar{\partial} \Gamma^{+2}_{z} = \Gamma^{+2}_{\bar{z}} - 2\chi_{z} \Gamma^{+2}_{\bar{z}} + 2\chi_{\bar{z}} \Gamma^{+2}_{z} + \lambda_{zz} \Gamma^{+1}_{\bar{z}} \\
&c^{-1} = \partial c^{-2} + 2\chi_{z} c^{-2} \\
&2c^{0} = \partial c^{-1} + \chi_{z} c^{-1} + 4\lambda_{zz} c^{-2} \\
&3c^{+1} = \partial c^{0} + 3\lambda_{zz} c^{-1} \\
&4c^{+2} = \partial c^{+1} - \chi_{z} c^{+1} + 4c^{z} \Gamma^{+2}_{z} + 2\lambda_{zz} c^{0}
\end{aligned} \tag{3.24}$$

as well as the BRST transformations for gauge and ghost fields:

$$\begin{aligned}
&s\upsilon^{z}_{\bar{z}} = \bar{\partial} c^{z} - \upsilon^{z}_{\bar{z}} c + c^{z} \chi_{\bar{z}} - 4\Gamma^{+1}_{\bar{z}} c^{-2} + c^{+1} \Gamma^{-2}_{\bar{z}} + 2\Gamma^{0}_{\bar{z}} c^{-1} - 2c^{0} \Gamma^{-1}_{\bar{z}} \\
&s\chi_{z} = \partial c - 2c_{z} + 2c^{z} \lambda_{zz} - 16\Gamma^{+2}_{z} c^{-2} \\
&s\chi_{\bar{z}} = \bar{\partial} c - 2\upsilon^{z}_{\bar{z}} c_{z} + 2c^{z} \lambda_{\bar{z}z} - 16\Gamma^{+2}_{\bar{z}} c^{-2} + 16c^{+2} \Gamma^{-2}_{\bar{z}} + 2\Gamma^{+1}_{\bar{z}} c^{-1} - 2c^{+1} \Gamma^{-1}_{\bar{z}} \\
&s\lambda_{zz} = \partial c_{z} + \lambda_{zz} c - c_{z} \chi_{z} - 4\Gamma^{+2}_{z} c^{-1} \\
&s\lambda_{z} = \bar{\partial} c_{z} + \lambda_{zz} c - c_{z} \chi_{\bar{z}} - 4\Gamma^{+2}_{\bar{z}} c^{-1} + 4c^{+2} \Gamma^{-1}_{\bar{z}} + 2\Gamma^{+1}_{\bar{z}} c^{0} - 2c^{+1} \Gamma^{0}_{\bar{z}}
\end{aligned} \tag{3.25}$$

$$\begin{aligned}
&s\Gamma^{-2}_{\bar{z}} = \bar{\partial} c^{-2} + 2\chi_{\bar{z}} c^{-2} - 2c\Gamma^{-2}_{\bar{z}} - \upsilon^{z}_{\bar{z}} c^{-1} + c^{z} \Gamma^{1}_{\bar{z}} \\
&s\Gamma^{-1}_{\bar{z}} = \bar{\partial} c^{-1} + \chi_{\bar{z}} c^{-1} - c\Gamma^{-1}_{\bar{z}} - 2\upsilon^{z}_{\bar{z}} c^{0} + 2c^{z} \Gamma^{0}_{\bar{z}} + 4\lambda_{\bar{z}z} c^{-2} - 4c_{z} \Gamma^{-2}_{\bar{z}} \\
&s\Gamma^{0}_{\bar{z}} = \bar{\partial} c^{0} - 3\upsilon^{z}_{\bar{z}} c^{+1} + 3c^{z} \Gamma^{+1}_{\bar{z}} + 3\lambda_{\bar{z}z} c^{-1} - 3c_{z} \Gamma^{-1}_{\bar{z}} \\
&s\Gamma^{+1}_{\bar{z}} = \bar{\partial} c^{+1} + \chi_{\bar{z}} c^{+1} - c\Gamma^{+1}_{\bar{z}} - 4\upsilon^{z}_{\bar{z}} c^{+2} + 4c^{z} \Gamma^{+2}_{\bar{z}} + 2\lambda_{\bar{z}z} c^{0} - 2c_{z} \Gamma^{0}_{\bar{z}} \\
&s\Gamma^{+2}_{\bar{z}} = \bar{\partial} c^{+2} + 2\chi_{\bar{z}} c^{+2} + 2c\Gamma^{+2}_{\bar{z}} + \lambda_{\bar{z}z} c^{+1} - c_{z} \Gamma^{+1}_{\bar{z}} \\
&s\Gamma^{+2}_{z} = \bar{\partial} c^{+2} + 2\chi_{z} c^{+2} + 2c\Gamma^{+2}_{z} + \lambda_{zz} c^{+1}
\end{aligned} \tag{3.26}$$

$$
\begin{aligned}
&sc^{z} = cc^{z} + 4c^{-2}c^{+1} - 2c^{-1}c^{0} \\
&sc = 2c_{z}c^{z} + 16c^{-2}c^{+2} - 2c^{-1}c^{+1} \\
&sc_{z} = c_{z}c \ + 4c^{-1}c^{+2} - 2c^{0}c^{+1}
\end{aligned}
\tag{3.27}
$$

$$
\begin{aligned}
&sc^{-2} = -c^{z}c^{-1} + 2cc^{-2} \\
&sc^{-1} = -2c^{z}c^{0} + cc^{-1} + 4c_{z}c^{-2} \\
&sc^{0} = -3c^{z}c^{+1} + 3c_{z}c^{-1} \\
&sc^{+1} = -4c^{z}c^{+2} - cc^{+1} + 2c_{z}c^{0} \\
&sc^{+1} = -2cc^{+2} + c_{z}c^{+1}
\end{aligned}
\tag{3.28}
$$

In an analogue way from (3.6) we obtain for the matter fields the relations:

$$
\begin{aligned}
&\partial\psi_{z} = \chi_{z}\psi_{z} - \sqrt{2}\lambda_{\bar{z}z}\psi + 4\Gamma_{\bar{z}}^{+2}\psi^{z} \\
&\bar{\partial}\psi_{z} = \chi_{z}\psi_{z} - \sqrt{2}\lambda_{\bar{z}z}\psi - \sqrt{2}\Gamma_{\bar{z}}^{+1}\psi + 4\Gamma_{\bar{z}}^{+2}\psi^{z} \\
&\partial\psi = \sqrt{2}\psi_{z} - \sqrt{2}\lambda_{zz}\psi^{z} \\
&\bar{\partial}\psi = \sqrt{2}\upsilon_{\bar{z}}^{z}\psi_{z} - \frac{4}{3}\Gamma_{\bar{z}}^{+1}\psi + \sqrt{2}\Gamma_{\bar{z}}^{-1}\psi_{z} - \sqrt{2}\lambda_{\bar{z}z}\psi^{z} - \sqrt{2}\Gamma_{\bar{z}}^{+1}\psi^{z} \\
&\partial\psi^{z} = \sqrt{2}\psi - \chi_{z}\psi^{z} \\
&\bar{\partial}\psi^{z} = -\chi_{\bar{z}}\psi^{z} + \frac{2}{3}\Gamma_{\bar{z}}^{0}\psi^{z} + \sqrt{2}\upsilon_{\bar{z}}^{z}\psi - \sqrt{2}\Gamma_{\bar{z}}^{-1}\psi + 4\Gamma_{\bar{z}}^{-2}\psi_{z}
\end{aligned}
\tag{3.29}
$$

as well as the BRST transformation:

$$
\begin{aligned}
&s\psi_{z} = c\psi_{z} - \sqrt{2}c_{z}\psi - \sqrt{2}c^{+1}\psi + 4c^{+2}\psi^{z} \\
&s\psi = -\frac{4}{3}c^{+1}\psi + \sqrt{2}c^{z}\psi_{z} + \sqrt{2}c^{-1}\psi_{z} - \sqrt{2}c_{z}\psi^{z} - \sqrt{2}c^{+1}\psi^{z} \\
&s\psi^{z} = -c\psi^{z} + \frac{2}{3}c^{0}\psi^{z} + \sqrt{2}c^{z}\psi - \sqrt{2}c^{-1}\psi + 4c^{-2}\psi_{z}
\end{aligned}
\tag{3.30}
$$

Furthermore we define an operator δ (see [14],[15]):

$$\delta c^z = v^z \delta c^{-2} = \Gamma^{-2}$$
$$\delta c = \chi \delta c^{-2} = \Gamma^{-1} \delta c^{+1} = \Gamma^{+1}$$
$$\delta c_z = \lambda_z \delta c^0 = \Gamma^0 \delta c^{+2} = \Gamma^{+2}$$

$$\delta v^z = 0 \delta \Gamma^{-2} = 0$$
$$\delta \chi = 0 \delta \Gamma^{-1} = 0 \delta \Gamma^{+1} = 0$$
$$\delta \lambda_z = 0 \delta \Gamma^0 = 0 \delta \Gamma^{+2} = 0$$

$$\delta \psi^z = 0$$
$$\delta \psi = 0$$
$$\delta \psi_z = 0$$

so that it satisfies the following relations:

$$[\delta, s] = d$$
$$[\delta, d] = 0$$

In conformity with the Sullivan theorem one can decompose the BRST algebra in a minimal subalgebra and a contractive one. Now we must identify this decomposition. Looking to the relations (3.25),(3.26),(3.27), (3.28) and (3.30) it is rather easy to see that $\{c^z, c, c_z, c^{-2}, c^{-1}, c^0, c^{+1}, c^{+2}, \psi^z, \psi, \psi^z\}$ are the generators of the minimal subalgebra. Now, all that we have to do is to search for solutions of eq.(1.1) in the form of linear combinations of the minimal algebra generators of ghost. 3. In order to simplify even more our job we define an new operator

$$\Delta_0 = \left\{ s, \frac{\partial}{\partial c} \right\}$$

It is easy to see from eq.(3.25),(3.26) and (3.30) that all fields are eigenfunctions of the operator Δ_0 which is in fact an even derivative i.e. it obeys the Leibnitz rule:

$$\Delta_0(AB) = \Delta_0(A)B + A\Delta_0(B)$$

The eigenvalues of this operator called the *weight* can be used to filter out the trivial solutions of eq.(1.1). One can prove that a solution ω of the eq.(1.1) which satisfy the relation

$$\Delta_0 \omega = p\omega$$

for $p \neq 0$ is a trivial one, so we have to search for solutions of weight zero. A non trivial solution with weight 0 is:

$$\begin{aligned}\omega = &-c_z cc^z - 4c_z c^{-2}c^{+1} + 2c_z c^{-1}c^0 + 8cc^{-2}c^{+2} - \\ &- cc^{-1}c^{+1} - 4c^z c^{-1}c^{+2} + 2c^z c^0 c^{+1}\end{aligned} \tag{3.31}$$

It is interesting to point out that not all solutions of eq.(1.1) whith weight 0 are non trivial.Indeed one can see that the forms:

$$\begin{aligned}\omega_1 &= c^z c^0 c^{+1} + c_z c^0 c^{-1} \\ \omega_2 &= c^z c^{-1} c^{+2} - c_z c^{-2} c^{+1}\end{aligned}$$

are solutions of eq.(1.1) with weight 0 but they are in fact trivial since

$$\begin{aligned}\omega_1 &= s(2c^{-2}c^{+2} - \frac{1}{2}c^{-1}c^{+1}) \\ \omega_2 &= s(-c^{-2}c^{+2})\end{aligned}$$

The same result with (3.31) can be obtained by using the general method for Y-M cohomology ([14],[15]), i.e.:

$$\omega = \mathrm{tr}(c^3) = c_a c_b c_c \mathrm{tr}(T^a T^b T^c) \tag{3.32}$$

and furthermore it is worth emhasizing that this is the only possible solution of pure ghost 3.

The possible anomaly can be obtained from (3.31) or (3.32) by applying twice the operator δ. Both equations yield:

$$\begin{aligned}A = &-2\lambda_z \chi c^z - 2\lambda_z c v^z - 2c_z \chi v^z - 8\lambda_z \Gamma^{-2}c^{+1} - 8\lambda_z c^{-2}\Gamma^{+1} - 8c_z \Gamma^{-2}\Gamma^{+1} \\ &+4\lambda_z \Gamma^{-1}c^0 + 4\lambda_z c^{-1}\Gamma^0 + 4c_z \Gamma^{-1}\Gamma^0 + 16\chi \Gamma^{-2}c^{+2} + 16\chi c^{-2}\Gamma^{+2} + 16c\Gamma^{-2}\Gamma^{+2} - \\ &-2\chi \Gamma^{-1}c^{+1} - 2\chi c^{-1}\Gamma^{+1} - 2c\Gamma^{-1}\Gamma^{+1} - 8v^z \Gamma^{-1}c^{+2} - 8v^z c^{-1}\Gamma^{+2} - 8c^z \Gamma^{-1}\Gamma^{+2} + \\ &+4v^z \Gamma^0 c^{+1} + 4v^z c^0 \Gamma^{+1} + 4c^z \Gamma^0 \Gamma^{+1}\end{aligned} \tag{3.33}$$

Our purpouse now is to express it in terms of W--currents, W--gauge fields and W--ghost fields. For this we perform the projective parametrization and then we exprime the BRST algebra in function of:

- $W_3 = \Gamma_z^{+2}$ corresponding to the W-currents,
- $v_{\bar{z}}^{zz} = \Gamma_{\bar{z}}^{-2}$ corresponding to the W-gauge fields,
- $c^{zz} = c^{-2}$ corresponding to the W-gauge transformation
- $v_{\bar{z}}^{z}, c^z, \Lambda_{zz}$ which apartain to the SL(2) substructure. We obtain:

$$\chi_{\bar{z}} = \partial v^{z}_{\bar{z}}$$

$$\chi_{z} = 0$$

$$\lambda_{zz} = \frac{1}{2}\Lambda_{zz}$$

$$\lambda_{\bar{z}z} = \frac{1}{2}\partial v^{z}_{\bar{z}} + \frac{1}{2}v^{z}_{\bar{z}}\Lambda_{zz} - 8W_3 v^{zz}_{\bar{z}}$$

$$\bar{\partial}\Lambda_{zz} = \partial^3 v^{z}_{\bar{z}} + 2\Lambda_{zz}\partial v^{z}_{\bar{z}} + v^{z}_{\bar{z}}\partial\Lambda_{zz} - 8(3W_3\partial v^{zz}_{\bar{z}} + 2v^{zz}_{\bar{z}}\partial W_3)$$

$$c = \partial c^{z}$$

$$c_{z} = \frac{1}{2}\partial^2 c^{z} + \frac{1}{2}\Lambda_{zz}c^{z} - 8W_3 c^{zz}$$

$$\Gamma^{-1}_{\bar{z}} = \partial v^{zz}_{\bar{z}}$$

$$\Gamma^{0}_{\bar{z}} = \frac{1}{2}\partial^2 v^{zz}_{\bar{z}} + \Lambda_{zz}v^{zz}_{\bar{z}}$$

$$\Gamma^{+1}_{z} = \frac{1}{2}\partial^3 v^{zz}_{\bar{z}} + \frac{1}{3}\partial\Lambda_{zz}v^{zz}_{\bar{z}} + \frac{5}{6}\Lambda_{zz}\partial v^{zz}_{\bar{z}}$$

$$\Gamma^{+2}_{z} = \frac{1}{24}\partial^4 v^{zz}_{\bar{z}} + \frac{1}{12}\partial^2\Lambda_{zz}v^{zz}_{\bar{z}} + \frac{7}{24}\partial\Lambda_{zz}\partial v^{zz}_{\bar{z}} + \frac{8}{24}\Lambda_{zz}\partial^2 v^{zz}_{\bar{z}} + v^{z}_{\bar{z}}W_3 + \frac{1}{4}\Lambda^2{}_{zz}v^{zz}_{\bar{z}}$$

$$\bar{\partial}W_3 = \frac{1}{24}(\partial^5 v^{zz}_{\bar{z}} + 2\partial^3\Lambda_{zz}v^{zz}_{\bar{z}} + 9\partial^2\Lambda_{zz}\partial v^{zz}_{\bar{z}} + 15\partial\Lambda_{zz}\partial^2 v^{zz}_{\bar{z}} + 10\Lambda_{zz}\partial^3 v^{zz}_{\bar{z}} +$$
$$+16\Lambda_{zz}\partial\Lambda_{zz}v^{zz}_{\bar{z}} + 16\Lambda^2_{zz}\partial v^{zz}_{\bar{z}}) + v^{z}_{\bar{z}}\partial W_3 + 3\partial v_{\bar{z}}W_3$$

$$c^{-1} = \partial c^{zz}$$

$$c^{0} = \frac{1}{2}\partial^2 c^{zz} + \Lambda_{zz}c^{zz}$$

$$c^{+1} = \frac{1}{6}\partial^3 c^{zz} + \frac{1}{3}\partial\Lambda_{zz}c^{zz} + \frac{5}{6}\partial\Lambda_{zz}\partial c^{zz}$$

$$c^{+2} = \frac{1}{24}\partial^4 c^{zz} + \frac{1}{12}\partial^2\Lambda_{zz}$$

$$c^{zz} + \frac{7}{24}\partial\Lambda_{zz}\partial c^{zz} + \frac{8}{24}\Lambda_{zz}\partial^2 c^{zz} + \frac{1}{4}\Lambda^2{}_{zz}c^{zz} + c^{z}W_3$$

Using these relations the consistent anomaly will be:

$$\begin{aligned} A = dz\Lambda d\bar{z}[&\partial v_{\bar{z}}^{z}\partial^2 c^{z} - \partial^2 v_{\bar{z}}^{z}\partial c^{z} - \frac{1}{3}\partial v_{\bar{z}}^{zz}(\partial^4 c^{zz} + 2\partial^2\Lambda_{zz}c^{zz} + \\ &+10\Lambda_{zz}\partial^2 c^{zz}) + \frac{1}{3}(\partial^4 v_{\bar{z}}^{zz} + 2\partial^2\Lambda_{zz}v_{\bar{z}}^{zz} + 10\Lambda_{zz}\partial^2 v_{\bar{z}}^{zz})\partial c^{zz} + \\ &+\frac{1}{3}(\partial^2 v_{\bar{z}}^{zz}\partial^3 c^{zz} - \partial^3 v_{\bar{z}}^{zz}\partial^2 c^{zz} + 2\partial^2 v_{\bar{z}}^{zz}\partial\Lambda_{zz}c^{zz} - 2\partial\Lambda_{zz}v_{\bar{z}}^{zz}\partial^2 c^{zz})] \end{aligned} \tag{3.34}$$

This anomaly could be found out from the general solution (2.12) if one uses the one-form gauge potential (3.13). Thus eq.(2.12) becomes:

$$\omega = \mathrm{tr}(c - \Gamma_z dz - \Gamma_{\bar{z}} d\bar{z})^3 + (d+s)\eta \tag{3.35}$$

and for η=0 the solutions of the descent equation (1.2) are given by:

$$\begin{aligned} A &= 3\mathrm{tr}(c\Gamma_z\Gamma_{\bar{z}} - c\Gamma_{\bar{z}}\Gamma_z)dz\Lambda d\bar{z} \\ Q &= 3\mathrm{tr}(c^2\Gamma_z dz + c^2\Gamma_{\bar{z}}d\bar{z}) \\ Q^1 &= \mathrm{tr}(c^3) \end{aligned} \tag{3.36}$$

We can use the ambiguity of the solution (3.35) to write it down in a most economical way ([10],[16]). If one takes η of the form:

$$\eta = 3\mathrm{tr}(\Gamma_{\bar{z}}\Gamma_z)dz\Lambda[\bar{z} + 3\mathrm{tr}(c\Gamma_z)]dz$$

then the new solution,which is related to (3.36) by some s-exact and d-exact terms, has the form:

$$\begin{aligned} A' &= 3\mathrm{tr}(\Gamma_{\bar{z}}s\Gamma_z - c\bar{\partial}\Gamma_z)dz\Lambda d\bar{z} = 3(\Gamma_{\bar{z}}^{a}s\Gamma_z^{b} - c^{a}\bar{\partial}\Gamma_z^{b})g_{ab}dz\Lambda d\bar{z} \\ Q' &= 3\mathrm{tr}[(-c\partial c + 2c^2\Gamma_z)dz + c^2\Gamma_{\bar{z}}d\bar{z}] \\ Q'' &= \mathrm{tr}(c^3) \end{aligned} \tag{3.37}$$

?From (3.37) one can obtain the compact form of the anomalies given by [10](see also [16]) by using the concret forms of the matrix g_{ab} and the BRST transformations:

$$A = 6[c^{z}\bar{\partial}\Lambda_{zz} - v_{\bar{z}}^{z}s\Lambda_{zz} - 8(c^{zz}\bar{\partial}W_3 - v_{\bar{z}}^{zz}sW_3)]dz\Lambda d\bar{z}$$

Comment

A natural question is the uniquness of the anomalies obtained in this way. In fact the problem of uniquness leads down to the problem of the solution of the equation

$$s\omega_0 = 0 \tag{4.1}$$

for the ghost number three.We shall show that the general solution of (4.1) with the ghost number three has the form

$$\omega = \mathrm{tr}(c^3) \tag{4.2}$$

Indeed if one introduces the operators:

$$i_a = \frac{\partial}{\partial c^a}$$

$$L_a = \{s, i_a\}$$
$$L^2 = L_a L_a$$
$$\Delta = i_a L_a$$

we can write:

$$L^2 = \Delta s + s\Delta$$

This relation shows that a non trivial solution of eq.(4.1) must be G-invariant and it belongs to the hierarchy

$$\begin{aligned} &s(i_a\omega) = 0 \rightarrow i_a\omega = s\omega_a \\ &s(i_a\omega_b) = 0 \rightarrow i_a\omega_b = s\omega_{ab} \\ &s(i_a\omega_b) = 0 \rightarrow i_a\omega_b = d_{abc} \end{aligned} \tag{4.3}$$

where d_{abc} is totaly symmetric G-invariant tensor and {,} means the symmetrization. In our case d_{abc} has an unique form:

$$d_{abc} = str(T_a T_b T_c)$$

with *str* the symmetrized trace and therefore the hierarchy (4.3) has the unique solution (4.2)

REFERENCES

1. A. B. Zamolodchicov, TMP 65(1985)1205 V. A. Fadeev and A. B. Zamolodchicov, *Nucl.Phys*. B 280[FS18] (1987) 644.
2. M. Bershadsky and H. Ooguri, Comm. Math. Phys. 126 (1989) 49.
3. J. Bolog, L. Feher, P. Forgars, L. O'Raiferteigh and A. Wipf, *Phys. Lett.* B227 (1989) 217, Ann. Phys. 203 (1990) 76.
4. L. Feher, L. O'Raiferteigh, P. Ruelle, I. Tsuitsui, A.Wipf, *Phys.Rep*. 222 (1992) 1.
5. A. Bilal J. L. Gernais, *Phys. Lett*. B206 (1988) 412, Nucl.Phys. B314 (1989) 646,Nucl.Phys. B318 (1989) 579.
6. C. M. Hull, *Lectures on W--Gravity, W--Geometry and W--Strings*, given at the Trieste Summer School in High Energy Physics and Cosmology, hep-th/9302110, February 1993.
7. A. Bilal, V. V.Fock, I. I.Kogan, *Nucl.Phys*. B359 (1991) 635.
8. H. Ooguri, K.Schoutens, A.Sewin, P.von Nieuwenhuizen, Comm. Math. Phys. 145 (1992) 515.
9. J.Wess, B.Zumino, *Phys.Lett*. B37 (1971) 95.
10. D. Garajeu, R. Grimm, S. Lazzarini, *W-Gauge Structures and their Anomalies: An Algebraic Approach*, U. of Marseille, preprint.
11. G. Akemann, R. Grimm, *J. Math. Phys*. 34 (1993) 818.
12. M. Polyakov, *Int. J. Math. Phys*. A5 (1990) 833.
13. M. Bershadsky, *Comm. Math. Phys*. 139 (1991) 71.
14. S. P. Sorella, *Algebraic Characterization of the Wess--Zumino Consistency Conditions in Gauge Theory*, UGVA--DPT 1992/08--781, Comm. Math. Phys.
15. S. P. Sorella, L. Tataru, *A Closed Form for Consistent Anomalies in Gauge Theories*, Ref. Tuw. 93-15.
16. M. Abud, J. P.Ader, L. Cappiello, *Consistent Anomalies of the induced W--gravities*, hep-th/9512055.

STUDIA UNIVERSITATIS BABEŞ-BOLYAI, PHYSICA, XLII, 1, 1997

MICROTEACHING EXERCISES IN THE METHODOLOGY TRAINING OF TEACHING APPLICANTS OF PHYSICS

KATALIN BOGDÁN[1]

ABSTRACT. The Physics methodology training at our college includes videotrainings during which teaching applicants perform microteaching activities and demonstration experiments in order to improve skills in teaching Physics. Presentations are discussed on the basis of evaluation sheets. Good points are emphasized, mistakes and the opportunities of further development are pointed out.

INTRODUCTION

The method of microteaching was worked out at Stanford University in the 1963. **[1.]** Since it is applicable in almost all the areas of teacher training **[2.]**, it spread rapidly worldwide. This method combined with the use of video has been applied in more and more teacher training institutions in Hungary since the mid-70s. Experience gained during the application of microteaching are communicated by instructors in videoconferences, periodicals and methodology publications. It is used for different purposes: to practise continuous verbal communication, to develop questioning skills, to improve illustration skills, to prepare, control and monitor students' individual work and evaluate students' achievements. Each microteaching last 15 minutes in a small group of 5 to 10 students. Within the framework of microteaching, teaching applicants teach either primary school students or their own classmates. Presentations are videotaped and after being reviewed they are evaluated by teaching applicants. **[3., 4., 5.]**

It has been used in education classes and in the methodology training of different majors including Physics at Bessenyei György

[1] Department of Physics Bessenyei György Teachers' Training College Nyíregyháza, Hungary

Teachers' Training College since 1979. I will give an account of this training in my essay.

I. The Methodology Training of Teaching Applicants of Physics

Teaching applicants of Physics trained in Hungarian teachers' training colleges will teach students between 12 and 16 years of age. Teaching applicants have to learn physics and methodology in possession of which they will develop the right scientific aspect and way of thinking in students. Methodology subjects link the theoretical and the practical trainings of teaching applicants. We aim at putting subjects in a complex unity, which will contribute to the professional development, provide a firm basis to the teaching practice in primary schools and the teaching profession. Therefore videotrainings are included in the training programme during which teaching applicants give presentations and demonstrate physical experiments. Then teaching applicants present teaching activities individually for the first time.

Standards set up by the curriculum and the experience gained during our visits in primary schools had special importance in planning the programme. Trainees had several problems with motivating students, performing demonstration experiments, the way of asking questions and the continuous verbal communication. These problems rose theoretical and practical issues whose clarification and practice are inevitable for teaching Physics. **[6.]**

1. Introduction to the Methodology Training

Teaching applicants get acquainted with the process of teaching Physics and the principles of methodology in a one-hour lecture in the second semester of the second year. The two-hour seminars running parallel with the lecture include short presentations by students and roundtable discussions. Teaching applicants spend three classes a week in methodology laboratories. They get acquainted with the experiments, the experimental tools and the methodology exercises of teaching Physics. We aim at familiarizing teaching applicants thoroughly with the techniques and the methods of experiments.

2. Exercises for Teaching Physics

Students practise in methodology laboratories for four hours a week in the first semester of the third year. They review primary school physics material in scientific and methodological terms. The purpose of

the applied methods, presentations, discussions, illustrations, carrying out experiments and measuring, is twofold; not only do students revise their knowledge of physics and methodology, but they also have an opportunity of improving their teaching skills. Each class includes two or three presentations by different students. Their subject can be concept building, familiarizing students with the laws of Physics, doing exercises, revision, testing and evaluation supported by experiments carried out either by the teacher or the students. In the absence of real primary school children, classmates act as students. Thus it is not a real-life situation, yet it is useful for practising certain teaching activities. It is also a role play for students in which it comes out to what extent teaching applicants are familiar with the way of thinking, the vocabulary and the level of knowledge of physics of primary school children. For a few years, our teaching applicants have also had the chance of performing teaching activities among primary school children in courses for talented students and summer physics camps.

Teaching applicants receive their tasks, which they have to prepare for on the basis of given guidelines at the beginning of the semester. Their performances are videotaped, which are discussed after being reviewed. The discussion is always started by the teaching applicant. He/she tells the class to what extent he/she managed to realize what he/she had planned, how he/she could correct his/her mistakes. It is followed by the remarks of the classmates. Discussions are finished by the evaluation of the teaching applicant's performance by the instructor.

Discussions are based on *evaluation sheets*. (Each teaching applicant fills in an evaluation sheet while reviewing his/her presentations). The structure of evaluation sheets are similar to the ones in the Appendix; their guidelines always concern the current task. Teaching applicants who do not satisfy any of the guidelines, receive 0 point. Activities well done are evaluated in the positive section, bad ones in the negative. Evaluation sheets do not count in seminar marks. They serve as means of emphasizing the good points, finding the bad ones and examining the opportunities of further development. They are also means of comparing the opinions of the instructors and the teaching applicants. The opinions of people who evaluate the teaching applicant's performance are marked with different lines: the instructor's with a continuous one, the class's with a broken one while the self-evaluation of the teaching applicant who gave the presentation is marked with dot-line-dot. Diagrams show that the

opinions of the class and the instructor are similar, though sometimes the former is less strict. The self-evaluation of the teaching applicants, however, are not always correct.

II. Microteaching Tasks

Exercises for practicing different skills in teaching Physics can be of several kind as regards their content and form. Sometimes all the teaching applicants may work on different topics with similar methods, another time a group of teaching applicants may do together the same exercises with different methods. Thus 4-5 teaching applicants teach a 45-minute class in 10-15 minute shifts. I will give an account of the three most frequent exercises below.

1. Videotaped Demonstration Experiments

Demonstration experiments presented in front of the class show how teaching applicants can carry out and apply them. Each student performs an experiment in class in front of the camera at least three times during the training. We selected to demonstrate the experiments which are not only included in primary school curriculum and contribute to the methodological development of the classmates but also reveal the teaching applicants' theoretical and practical knowledge. Students prepare for the experiments with the help of formerly given guidelines. They have to talk about not only the experiment but also the questions marked with an * in Appendix 1 in order to practise continuous verbal communication. They may prepare the tools and try their experiment before the demonstration. Each teaching applicant has 10 minutes to perform his/her experiment. The order of the formerly given guidelines is free, the teaching applicant has the opportunity of organizing his/her demonstration individually. Although the demonstration experiment is not a classic microteaching exercise, it is useful for practising important teaching activities.

2. Microteaching Exercises for Presenting New Material

Microteaching activities introducing new material are always accompanied by demonstration experiments and illustrations. Teaching applicants prepare for their microteaching by writing lesson plans, preparing illustration tools and practising their experiment before their presentation. They have the opportunity of consulting their instructor and each other. The videotaped performances are discussed after being reviewed on the basis of the evaluation sheet in Appendix 2. Since several guidelines are included on the evaluation sheet, each classmate

observe only one of the guidelines marked with letters A to G. These are the followings:

A: Preparation before introducing new material.
B: Relation between the applied method, the tools and the objective.
C: Requirements of the demonstration experiments.
D: Analysis of the experiment, conclusions.
E: Questions and answers during the microteaching.
F: Professional and general verbal skills.
G: Body language.

3. Microteaching Exercises for Managing Student Experiments

Since we do not have enough time, all the teaching activities cannot be performed by all the teaching applicants. Student experiments, however, should be managed by each teaching applicant. It is a difficult task even for experienced teachers. They required both to focus and divide their attention at the same time. Teaching applicants usually have a lot of difficulties in doing that. Therefore each teaching applicant should have the chance of practising this task at least once during his/her training. The teaching applicant can realize his/her own positive qualities and mistakes on the videotape including the ones that escaped his/her attention while he/she was teaching.

The main objective of managing student experiments is either concept building or explaining laws of physics. Since these are usually measure experiments, *experiment planning*, the selection and the testing of appropriate tools are especially important. Teaching applicants prepare a *worksheet* for the class. The first task of the teaching applicant is to decide *the objective of the experiment* and connecting it with the material already covered. Then the teaching applicant instructs the students to perform the experiment. Students read the instructions in the worksheet and after having understood them they start the experiment. By following the experiment instructions and the observation guidelines, they put down their observances. The teaching applicant has to monitor the students' work and help those who have difficulties in setting up the experiment instruments or performing the experiments. If more than one student make the same mistake, he/she interrupts the work to clear up the problems. Then the experiment may go on. Putting the observances to students, is followed by a discussion during which an explanation is given for the observed phenomenon. For this, teaching applicants are encouraged to apply the Socratic mode of inquiry.

Teaching applicants very often have problems with the technique of asking questions. They do not always manage to ask questions that are exact, clear and appropriate to the age of students. That is why the videotaped presentations are discussed in methodology classes from the point of view of the way of asking questions. The evaluation sheet included in Appendix 3 is used for evaluating student experiments. Since there are several evaluation guidelines, each participant observes only one teaching activity. The evaluation guidelines can be grouped as the followings:

A: Teacher's tasks up to the start of student experiment.
B: Relation between the experiments, the applied tools and the objectives of the experiments.
C: Relation between students' individuality and teacher's help.
D: The factors of confident class management.
E: Teacher's tasks after finishing the experiment.
F: Questions and answers during the experiment.
G: Professional and general communication skills.
H: Body language.

The last two guidelines are always discussed regardless the kind of teaching activity videotaped. The teaching applicants welcome any remark and suggestion which help them correct their mistakes.

The Experience of Applying the Method

We get to the point of applying the above described method after several steps. It has been used in methodology training in our department for ten years. It makes a heavy demand on instructors and teaching applicants as well. Since every teaching applicant participates in every class, they have to prepare for each. One time he/she teaches or manages a student experiment, acts as a student while others teach or participate actively in classroom activities. The following time he/she may give a presentation or leads a discussion. Teaching applicants are only given the tasks; planning and realizing the methods and the use of tools are their responsibility. They spend a lot of time on library research. The analyses of the videotaped presentations do not only give teaching applicants the opportunity of further development, but also improves the classmates' knowledge of methodology. It is impossible for each teaching applicant to perform each experiment or teaching activity in methodology classes. Some shots of the videotaped presentations are often shown as illustrations in seminars. I think teaching applicants

benefit from this work during their teaching practice and later in the teaching profession. The trainees' classes and their closing lessons show good results. Evaluation sheets are also used during the teaching practice. Teaching applicants who participated in the training programme give clearer guidelines, take more care of the way of asking questions, pay more attention to the visibility of teaching tools and they are more confident of managing student experiments than those who did not receive such training.

REFERENCES

1. W. Allen - K. A. Ryan, *Microteaching.* (Addison Wesley, Reading, Mass., 1969).
2. C. Berliner, *Microteaching and the Technical Skills Approach to Teacher Training*. Technical Report (Stanford University, California, USA, 1985).
3. Falus Iván, *Mikrotanítás* (OOK, Budapest, 1976).
4. Sass Attila, *Mikrotanítás az egyetemi tanárképzés gyakorlatában*, Felsőoktatási Szemle, 1982, **2,** 97-102.
5. Gönczi Ákos, Tanítási készségek fejlesztése képmagnó alkalmazásával, *Képmagnetofon alkalmazása a pedagógusképzésben és továbbképzésben III.* (OOK, Budapest, 982).
6. Erlichné Bogdán Katalin, Gyakorlatra orientált fizika módszertani képzés a Bessenyei György Tanárképző Főiskolán, *Isikolakultúra* 1994, **14**, 29-35.

Appendix 1

Evaluation Sheet for Demonstration Experiment

The number of the experiment: .....

Teaching applicant:..... Person evaluating: class instructor TA

		-3	-2	-1	0	+1	+2	+3
1.*	Was the experimenat appropriately placed in the material covered?							
2.*	Did the TA explain well the use of experiment tools?							
3.*	Were the observation guidelines correct?							
4.	Did the TA give the observation guidelines in time?							
5.	Did the TA handle the tools safely?							
6.	Was the experiment clearly visible and audiable?							

7.	Did the TA use special signs to help the observation?							
8.	Was it a successful experiment?							
9.*	Did the TA formulate the experience clearly after the experiment had been performed?							
10.*	Did the TA give a good explanation for the demonstrated penomenon?							
11.*	Did the TA put the physical law demonstrated by the experiment exactly?							
12.*	Did the TA call the attention to the methodological practices needed for performing the experinemt?							
13.*	Did the TA call the attention to the possible mistakes?							
14.*	Did the TA mention the practical aspects of the demonstrated experiment?							
15.*	Did the TA examine whether it is suitable for student experiment?							
16.	Was the TA's presentation well structured?							
17.	Was the TA's style and proficiency good?							
18.	Were the TA's gestures and motion appropriate?							

Appendix 2

Evaluation Sheet for Presenting New Material

Teaching applicant:.....

Person evaluating: class ..... instructor ——— TA -·-·-·-

			-3	-2	-1	0	+1	+2	+3
A	1.	Was the old material needed to understand the new one revised?							
	2.	Did the TA raise the problem appropriately?							
B	3.	Did the TA select an appropriate method to solve the problem?							
	4.	Did the TA select an experiment appropriate to present the new material?							
	5.	Did the TA use the right tools to perform the experiment?							
	6.	Did the TA introduce the experiment tools before starting?							
	7.	Did the TA give appropriate observation guidelines?							
	8.	Did the TA give the guidelines in time?							

C	9.	Did the TA make students involved in the experiment?							
	10.	Did the TA use special signs to make the experiment more visible?							
	11.	Was the experiment clearly visible and audible?							
	12.	Was the experiment successful?							
D	13.	Did the TA formulate the experience after performing the experiment?							
	14.	Was the concept, the law demonstrated by the experiment exactly formulated?							
E	15.	Did the TA ask appropriate questions?							
	16.	Did the TA correct the incorrect answers?							
	17.	Were the TA's explanations clear?							
	18.	Was teacher and student performance properly portioned?							
F	19.	Did the TA use properly the terminology of physics?							
	20.	Were the TA's style and proficiency good?							
G	21.	Were the TA's gestures and motion appropriate?							

Appendix 3

Evaluation Sheet for Managing Student Experiments

Teaching applicant:.....

Person evaluating: class ..... instructor ——— TA -·-·-·-

			-3	-2	-1	0	+1	+2	+3
A	1.	Did the TA set the objective of the experiment correctly?							
	2.	Did the TA related the tasks to the old knowledge properly?							
	3.	Did the TA start and manage the experiment confidently and clearly?							
B	4.	Did the TA select the right experiment to introduce the new material?							
	5.	Did the TA select appropriate tools to carry out the experiment?							
C	6.	Did the TA ensure enough individual student work?							
	7.	Did the TA notice where and when students had needed help?							
	8.	Did the TA give enough help to students who needed it?							

D	9.	Did the TA ensure the necessary work discipline?							
	10.	Did the TA ensure the necessary rhythm of work?							
	11.	Did the TA manage student experiments properly?							
E	12.	Did they give the right explanation to the phenomenon?							
	13.	Did they discuss the practical aspects?							
	14.	Did they discuss the curiosities of the history of physics?							
F	15.	Did the TA ask proper questions?							
	16.	Did the TA correct the incorrect answers?							
	17.	Were the TA's explanations clear?							
	18.	Was teacher and student performance properly portioned?							
G	19.	Did the TA use the terminology of physics appropriately?							
	20.	Are the TA's style and proficiency good?							
H	21.	Were the TA's gestures and motion proper?							